Experimental studies on phase relations in iron-rich peralkaline phonolitic melts

Dissertation

der Mathematisch-Naturwissenschaftlichen Fakultät

der Eberhard Karls Universität Tübingen

zur Erlangung des Grades eines

Doktors der Naturwissenschaften

(Dr. rer. nat.)

vorgelegt von

Dipl. Min. Christopher Giehl

aus Erlangen

Tübingen

2014

Tag der mündlichen Qualifikation:	11.03.2014
Dekan:	Prof. Dr. Wolfgang Rosenstiel
1. Berichterstatter:	Prof. Dr. Marcus Nowak
2. Berichterstatter:	Dr. Michael Marks

Danksagung

Mein besonderer Dank gilt meinen Betreuern Marcus Nowak und Michael Marks für die Vergabe des Themas und die rundum gelungene Betreuung. Ebenso danke ich meinen Prüfern Gregor Markl und Thomas Wenzel. Dagmar Dimitrovice, Beate Fritz und Claudia Jahn danke ich für die immer kompetente Lösung organisatorischer Probleme. Philipp Bellucci, Huy-Tung Nguyen, Matthias Loose, Nanna Mutterer, Rainer Babiel, Stephan Reiche, Christopher Demel, Holger Marxer, Christine Kizler, Philipp Schühle, Nicki Siersch und Andreas Winterhalder haben im Rahmen ihres Studiums an diesem Projekt mitgewirkt, auch dafür vielen Dank. Indra Gill-Kopp und Bertrand Ligouis danke ich für die Präparation der Proben, Norbert Walker und Barbara Maier für die vielen kleinen und großen Basteleien. Für Hilfe im Labor möchte ich mich bei Holger Marxer, Oliver Preuß, Hartmut Schulz, Daniel Russ, Yannick Hemberger und Annette Flicker bedanken. Bei Harald Behrens, Urs Dippon, Christian Schröder und Regina Mertz-Kraus bedanke ich mich für Analysen mit der Karl-Fischer Titration, der Mössbauer-Spektroskopie und der Laser-Ablations Massenspektroskopie. Mein besonderer Dank gilt Thomas Wenzel für die exzellente Unterstützung und den unvermeidlich humorvollen Umgang mit den analytischen Herausforderungen der Elektronenstrahlmikrosonde (15 kV). Für viel zu seltenen Kuchen, viel zu starken Kaffee und flotte Sprüche im Büro und in der Kaffeerunde bedanke ich mich bei Elena Kiemele, Benjamin Walter, Mathias Burisch, Kai Hettmann, Holger Teiber, Richard Brooker, Holger Marxer, Susanne Göb, Tobi Kiemle, Maggi Duchoslav, Kathrin Haßler, Yannick Hemberger, Anselm Loges, Linda Marks, Thomas Wenzel, Sümeyya Eroglu, Mela Keuper, Tobi Fußwinkel, Udo Neumann, Nadja Huber, Oliver Preuß, Marcus Nowak, Katha Pfaff, Julian Schilling und Sara Ladenburger. Allergrößten Dank auch an meine WG-Zeiten, namentlich: Wadde, Johann, Dom, Birk, Jonny, Tobi, Marc, Norma, Uli, Jens, Mischa und Matze, und meiner Heimat, dem Weggental: Wadde, Reinski, Jonas, Aintschie und Johann. Weiterhin gilt mein Dank Tobi Fußwinkel, Jonas Faber, Yannick Hemberger, Caro Schultz, Katha Pfaff, Nadja Huber, Tobi Wichtner, Tobi Neder, Oliver Preuß, Holger Marxer, Victor Nowak, Julia Mielewski, Steffi Lutz, Susanne Kleinert, Christopher Demel, Lena Stark, Mona Baumhoer, Hilde Koch, Gerald Buck, Fabi Setzer, Fabi Bonitz, Dome Köhler, Ully Baranowski, Jan-Erik Gühring und Patrik Schmidt für Spiel und Spaß. Tobias Fußwinkel, Anselm Loges, Sofie Jehle und Julian Schilling gebührt Dank für häufige und gelegentliche Laufrunden (in abnehmender Häufigkeit und zunehmender Herausforderung). Schlussendlich besten Dank an Tobi Fußwinkel und Oliver Preuß für das Korrekturlesen. Von ganzem Herzen danke ich meinen Eltern, Hans und Barbara, und meinen Geschwistern, Hannes und Anna, die mit bedingungsloser Unterstützung immer zur Stelle sind, wenn es nötig ist.
Und natürlich danke Sara, für alles!

Zusammenfassung

Diese Arbeit präsentiert Phasengleichgewichtsexperimente an Eisen-reichen peralkalinen phonolitischen Schmelzen mit unterschiedlichen Fluor- und Chlor-Gehalten. Die Ausgangszusammensetzung entspricht einem Ganggestein, das eine mögliche parentale Schmelze für die peralkalinen Plutonite der Ilímaussaq Intrusion (Südgrönland) darstellt. Diese Zusammensetzung ist ideal zur Durchführung von Phasengleichgewichtsexperimenten, weil sie im Gegensatz zu den plutonischen Ilímaussaq-Gesteinen nicht von Kumulat-bildenden Prozessen beeinflusst ist. Die Experimente wurden beim konstantem Druck (100 MPa) bei 1000 - 650 °C und variablen H_2O (nominell trocken bis H_2O-gesättigt) und variablen Sauerstofffugazitäten durchgeführt (Δ log FMQ -4 bis +1, FMQ entspricht dem Fayalit-Magnetit-Quarz Sauerstoffpuffer). Die Experimente wurden unter Verwendung von Goldkapseln und Gold-Graphit Doppelkapseln in extern beheizten Hydrothermalautoklaven und einer intern beheizten Gasdruckanlage (mit Argon als Druckmedium) durchgeführt. Um das große Temperaturintervall abzudecken wurden neue Ausgangsgläser entsprechend koexistierenden Schmelzen in Experimenten bei 800 °C für Experimente bei niedrigeren Temperaturen synthetisiert.

Die synthetisierten Mineralphasen koexistierend mit Restschmelze sind Titanomagnetit, Fayalit-reicher Olivin, Klinopyroxen, Aenigmatit ($Na_2Fe_5TiSi_6O_{20}$), Alkalifeldspat und Nephelin (± gediegen Eisen). Bei über 1,5 Gew.% F in der koexistierenden Restschmelze wird Klinopyroxen von Fluorit (CaF_2) und Hiortdahlit ($Ca_6Zr_2Si_4O_{16}F_4$) ersetzt. Sodalit ($Na_8Al_6Si_6O_{24}Cl_2$) und Eudialyt ($Na_{15}Ca_6Fe_3Zr_3Si_{26}O_{73}(OH)_3Cl_2$) benötigen, abhängig von der Temperatur, 0,2 - 0,5 Gew.% Cl in der Restschmelze. Außerdem sind Hiortdahlit und Eudialyt nur stabil, wenn die Restschmelzzusammensetzung mindestens 0,7 Gew.% ZrO_2 beinhaltet.

Die frühmagmatischen Phänokristalle des untersuchten Ganggesteins wurden bei 850 - 800 °C und nominell H_2O-freien und reduzierten Bedingungen (Δ log FMQ -2) experimentell reproduziert. Abgesehen von Amphibol konnten die spätmagmatischen Minerale der Grundmasse bei Temperaturen unter 750 °C, einer H_2O-armen koexistierenden Restschmelze und reduzierten Bedingungen (Δ log FMQ -1) reproduziert werden. Folglich können bei fraktionierter Kristallisation sowohl die Phänokristall-Paragenese als auch die Minerale der Grundmasse des Ganggesteins aus einer peralkalinen Schmelze kristallisieren. Das ist ein Hinweis darauf, dass der Ilímaussaq Komplex sich aus einem einzigen Schmelzschub gebildet haben kann.

Geothermometrie in solch hochentwickelten peralkalinen Gesteinen ist häufig durch das Fehlen von Fe-Ti Oxiden, Olivin und Ca-reichem Klinopyroxen erschwert. Verschiedene Thermometer wurden anhand der experimentellen Daten überprüft und erwiesen sich als zur Temperaturabschätzung ungeeignet. Basierend auf dem Verteilungsverhalten von Mn zwischen Klinopyroxen, Aenigmatit, Eudialyt und Schmelze sowie den Na/Ca Verhältnissen zwischen Klinopyroxen und Schmelze wurden neue Thermometer entwickelt. Vorläufige Ergebnisse von Experimenten mit Spurenelement-dotierten Ausgangsgläsern (Nb, La, Ce, Y und Sr) zeigen, dass Phasenstabilitäten und Restschmelzentwicklung ähnlich den Spurenelement-freien Experimenten sind. Diese Beobachtung unterstützt die Aussagekraft von Experimenten mit vereinfachten synthetischen Ausgangszusammensetzungen bezüglich natürlicher Prozesse.

Abstract

The experimental investigation of phase equilibria is a powerful method to study the formation of magmatic rocks. This work presents phase equilibrium experiments investigating an iron-rich peralkaline phonolitic composition with variable fluorine and chlorine contents. The starting composition represents a dyke rock, which is a possible parental melt to the peralkaline Ilímaussaq plutonic complex (South Greenland). The dyke composition is perfectly suited for performing phase equilibrium experiments since, in contrast to the Ilímaussaq plutonic rocks, no major cumulate formation processes occurred. Experiments were performed isobarically (100 MPa) at 1000 - 650 °C with variable H_2O concentrations (nominally dry to H_2O-saturated) and oxygen fugacities (Δ log FMQ -4 to +1, where FMQ represents the fayalite-magnetite-quartz oxygen buffer). Experimental conditions were applied using gold capsules and graphite-lined gold capsules in rapid-quench cold seal pressure vessels and in an internally heated argon pressure vessel . To cover this large *T* interval a two-step fractional crystallization strategy was applied where glasses, representing residual melt compositions at 800 °C, were synthesized as starting material for consecutive experiments at lower *T*.

The observed mineral phases coexisting with residual melt are titanomagnetite, fayalitic olivine, clinopyroxene, aenigmatite ($Na_2Fe_5TiSi_6O_{20}$), alkali feldspar and nepheline (± native iron). Above 1.5 wt% F in the coexisting melt, fluorite (CaF_2) and hiortdahlite ($Ca_6Zr_2Si_4O_{16}F_4$) are stable in favor of clinopyroxene. Sodalite ($Na_8Al_6Si_6O_{24}Cl_2$) and eudialyte ($Na_{15}Ca_6Fe_3Zr_3Si_{26}O_{73}(OH)_3Cl_2$) form at Cl melt concentrations of 0.2 - 0.5 wt% (depending on *T*) and ZrO_2 melt concentrations higher than 0.7 wt%, are additionally needed to stabilize hiortdahlite and eudialyte.

The phenocryst assemblage of the dyke rock was reproduced at 850 - 800 °C, nominally dry conditions and Δ log FMQ -2. Except amphibole, all major mineral phases of the groundmass assemblage were reproduced at < 750 °C in H_2O-poor experiments at Δ log FMQ -1. Therefore, both the phenocryst assemblage and the groundmass assemblage of the dyke rock may crystallize from one peralkaline melt through fractional crystallization. This may indicate that the Ilímaussaq plutonic rocks evolved from one single magma batch.

Geothermometry in such highly evolved peralkaline rocks is often complicated by the absence of Fe-Ti oxides, olivine and clinopyroxene. Erroneous results were obtained when testing several thermometers with experimental data from the present study. Therefore, these experiments were used to calibrate four new geothermometers based on the distribution of Mn between clinopyroxene, aenigmatite, eudialyte and melt, and Na/Ca partitioning between clinoyproxene and melt. Preliminary experiments with REE-doped (Nb, La, Ce, Y and Sr) starting compositions show that phase stabilities and the liquid line of descent are similar to experiments using the same starting composition without trace elements, supporting the significance of the experimental results using simplified starting compositions with respect to nature.

Table of contents

1. Introduction

The cooling history of magmatic rocks is recorded in their textures that distinguish eruptive volcanic rocks, typically with euhedral phenocrysts and a fine-grained groundmass, from medium- to coarse-grained slowly cooled plutonic rocks. In either case, the crystallizing phase assemblage, the crystallization sequence and the crystallization T interval are principally controlled by melt composition, dissolved volatiles (mainly H_2O, CO_2, halogens and sulfur), changes in pressure (P) and oxygen fugacity (fO_2). Further processes influencing the formation of magmatic rocks are fractional crystallization processes, contamination by wall rocks, degassing during ascent, melt-melt immiscibility and fluid exsolution (e. g. Daly 1914; DePaolo 1981; Mohr 1987; Webster 1997; Villemant and Boudon 1999; Markl 2001).

1.1 Phase equilibrium experiments

Pioneering experimental studies by Tuttle and Bowen (1958) for the first time investigated the formation of magmatic rocks experimentally using so-called quench experiments. In this type of experiment, the sample is equilibrated at experimental conditions for a certain dwell time (typically 10^{-1} to 10^3 h) with subsequent rapid cooling. This experimental strategy provides a snapshot of the applied experimental conditions to constrain liquidus and solidus T's and the systematic investigation of mineral stabilities and liquid lines of descent by variation of physico-chemical parameters like P, aH_2O and fO_2. The first studies of this kind determined the phase relations of granites and basalts with focus on the effect of dissolved H_2O (e. g. Tuttle and Bowen 1958; Yoder and Tilley 1962). A fundamental question in investigating mineral-melt equilibria between liquidus and solidus T is whether the experimental sample is cooled or heated towards target experimental T. In so-called melting experiments rock powder is heated from room T towards experimental T. In

contrast, crystallization experiments apply the inverse approach by crystallizing mineral phases from a melt. Crystallization experiments can be done by either cooling of a super-liquidus melt or heating a glass representing the melt composition (synthesized in advance by rapid quench of a super-liquidus melt) to the target experimental T. The main problem of the cooling strategy is compositional zonation of solid-solution minerals that form above target experimental T and adjust composition with decreasing T. This would modify the bulk system composition by precluding mineral phase cores from equilibration with the melt. This problem can be overcome by rapid heating of a glass (an undercooled melt) to the experimental T, as mineral phases then nucleate at the T of interest. To date, numerous experimental studies have been performed and a wide range of starting compositions is covered (Fig. 1). Recent studies systematically investigated the effects of dissolved volatiles (like H_2O, CO_2, halogens and sulfur) and fO_2, although mainly focusing on primitive basaltic and andesitic compositions (e. g. Berndt 2002; Berndt et al. 2005; Feig et al. 2006; Almeev et al. 2007; Botcharnikov et al. 2008a; Botcharnikov et al. 2008b; Freise et al. 2009; Feig et al. 2010; Almeev et al. 2013) and evolved quartz-bearing compositions (e. g. Dall'agnol et al. 1999; Scaillet and Evans 1999; Scaillet and Macdonald 2001; Xiong et al. 2002; Klimm et al. 2003; Holtz et al. 2005; Lukkari and Holtz 2007; Di Carlo et al. 2010; Almeev et al. 2012). Similar studies were performed on evolved SiO_2-undersaturated compositions. However, those are by far underrepresented, with studies on iron-rich peralkaline compositions entirely lacking. In the following section, these studies are briefly summarized.

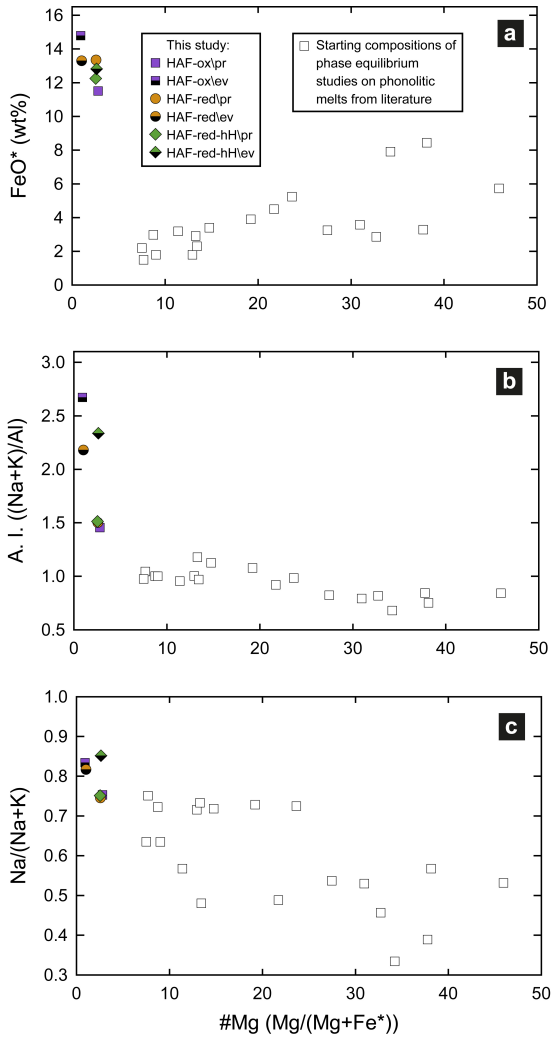

Figure 1: Phonolitic starting compositions used in phase equilibrium experiments from literature (see text) compared with starting compositions used in the present study (Appendix A and B), with #Mg (Mg/(Mg+Fe*)) versus (a) FeO*, (b) (Na+K)/Al and (c) Na/(Na+K)

1.2 Phase relations in phonolites

A number of experimental phase equilibrium studies investigated phase relations of phonolites (Berndt et al. 2001; Freise et al. 2003; Harms et al. 2004; Andújar et al. 2008; Fabbrizio and Carroll 2008; Scaillet et al. 2008; Andújar et al. 2010; Andújar and Scaillet 2012; Moussallam et al. 2013; Masotta et al. 2012; Masotta et al. 2013). The experimental conditions cover a large range of crustal P's (0.1 - 400 MPa), T's (700 - 1050 °C), as well as variable aH_2O (nominally dry to H_2O-saturated) and fO_2 (Δ log FMQ -2 to +4). The starting compositions have #Mg's (the molar Mg/(Mg+Fe) ratio)

Table 1: Mineral phases with abbreviations and simplified formulae, mineral phases *in italics* were not synthesized

Mineral phase	Formula
Titanomagnetite	$Fe_2(Fe,Ti)O_4$
Olivine	Fe_2SiO_4
Clinopyroxene	$(Ca,Na)FeSi_2O_6$
Alkali feldspar	$(Na,K)AlSi_3O_8$
Nepheline	$Na_3KAl_4Si_4O_{16}$
Aenigmatite	$Na_2Fe_5TiSi_6O_{20}$
Biotite	$KAl_3Si_3O_{10}(OH)_2$
Titanite	$CaTiSiO_5$
F-bearing phases	
Fluorite	CaF_2
Hiortdahlite	$Ca_6Zr_2Si_4O_{16}F_4$
Apatite-(F)	$Ca_5(PO_4)_3(OH,F)$
Villiaumite	NaF
Arfvedsonite	$Na_3Fe_5Si_8O_{22}(OH,F)_2$
Cl-bearing phases	
Sodalite	$Na_8Al_6Si_6O_{24}Cl_2$
Eudialyte	$Na_{15}Ca_6Fe_3Zr_3Si_{26}O_{73}(OH)_3(Cl,OH)_2$

between 38 and 8 (Fig. 1a), FeO* contents from 1.5 to 8.4 wt% (Fig. 1a), A. I.'s (the molar (Na+K)/Al ratio) between 0.75 and 1.16 (Fig. 1b), and Na/(Na+K) ratios from 0.33 to 0.75 (Fig. 1c). These studies show that phonolitic melt compositions crystallize alkali feldspar, clinopyroxene, mica and titanomagnetite; alkali feldspar is usually the most abundant mineral phase (for mineral formulae see Tab. 1). Some metaluminous starting compositions (A. I. = 0.75 - 1.0) stabilize plagioclase; those with nepheline typically have an A. I. close to one. Other mineral phases that occur occasionally are amphibole, titanite, apatite, hauyne, leucite, scapolite, garnet, sodalite and ilmenite.

In two studies clinopyroxene is unstable, but mica + alkali feldspar + titanomagnetite (± amphibole, hauyne, titanite, Berndt et al. 2001) or alkali feldspar + amphibole + titanomagnetite are present (Harms et al. 2004). These experiments have the lowest initial FeO* and CaO content and the highest initial Al_2O_3 contents. Clinopyroxene in such rocks is typically dominated by diopside, hedenbergite and aegirine components, therefore low CaO contents may favor Al_2O_3-rich mineral phases over clinopyroxene. Olivine was only reported from the study of Moussallam et al. (2013), likely due

to the combination of a relatively high FeO* content and relatively low fO_2 (Δ log FMQ +0). Berndt et al. (2001) used even higher initial FeO* and MgO content, but these experiments were conducted at conditions that were presumably too oxidized (Δ log FMQ +1 to +3). However, as already mentioned, these studies mainly disregard halogens, despite the effect of halogens on phase equilibria was recognized both from natural observations and experiments (e. g. Manning 1981; Scaillet and Macdonald 2001; Filiberto and Treiman 2009; Filiberto et al. 2012) and current research addresses their potential use a tracers for primary magmatic and secondary alteration processes (Marks et al. 2012; Ballentine et al. 2013; Joachim et al. 2013; Teiber et al. 2014).

1.3 Halogens in magmatic rocks

Fluorine and chlorine concentrations in minerals and F/Cl partitioning between minerals, melts and fluids are promising tools to trace magmatic and post-magmatic processes (e. g. Marks et al. 2012; Zhang et al. 2012). Silicate melts may contain up to several weight percent of F and Cl, whereas Br and I have significantly lower concentration in the ng/g to $\mu g/g$ abundance range (Carroll and Webster 1994; Webster and Duffield 1994; Aiuppa et al. 2009). The timing and the extent of fluid exsolution in magmatic rocks may, for example, strongly influence fO_2 (Markl et al. 2010) and therefore liquid lines of descent, particularly in Fe-rich systems.

Common halogen-bearing minerals in most magmatic rocks are apatite, mica and amphibole, while titanite, fluorite and topaz are subordinate (e. g. Price et al. 1996; Marshall et al. 1998; Frindt et al. 2004; Gioncada et al. 2014). Apatite is a promising tracer reflecting melt compositions of both halogens and trace elements. It is well established that apatite in most magmatic rocks is F-rich and Cl-poor (e. g. Seifert et al. 2000; Rønsbo 2008). Few studies were concerned with Br in apatite (Ionov et al. 1997; O'Reilly and Griffin 2000), but recent analytical advances routinely enable such analyses (Marks et al. 2012). These studies show that Br concentrations vary by orders of magnitude and could therefore be useful tracing magmatic and secondary processes. However, the observed trends are not yet entirely understood (e. g. Marks et al. 2012; Teiber et al. 2014; Wang et al. 2014).

Peralkaline magmatic rocks may contain further halogen-bearing minerals such as sodalite, villiaumite, eudialyte and hiortdahlite (see Tab. 1 for mineral formulae). Peralkaline rocks are subdivided into miaskitic, with titanite and zircon, and agpaitic varieties. The latter are defined by the occurence of complex Na-Ca-Fe-HFSE silicates (see above, Sørensen 1997; Marks et al. 2011). Increasing concentrations of alkalis, H_2O and halogens were identified as crucial factors to transit magma evolution from

miaskitic to agpaitic (Scaillet and Macdonald 2003; Andersen et al. 2010; Marks et al. 2011).

Although conducted in SiO_2-saturated systems, three phase equilibrium studies are mentioned here due to their implications for halogen behavior. However, applicability of the results to phonolites is probably limited (e. g. Appendix B). For example, fluorite saturation was discussed both by an empirical model based on increasing melt alkalinity (Scaillet and Macdonald 2004) and a thermodynamic model predicting fluorite saturation from *T* and the activity product of Ca and F (Dolejš and Baker 2006). Scaillet and Macdonald (2001) investigated peralkaline rhyolites from the Kenya rift valley using starting compositions with 0.2 - 0.5 wt% Cl and 0.4 - 1.0 wt% F. Halogen-bearing mineral phases in their study were fluorite and amphibole. However, rare phase equilibrium studies with phonolitic starting compositions include either F or Cl, but no mixtures were used (Scaillet et al. 2008; Andújar et al. 2008; Andújar et al. 2010).

1.4 Geological background

Peralkaline rocks are interpreted as derivatives from highly fractionated nephelinitic or alkali basaltic magmas (Larsen and Sørensen 1987; Sørensen 1997; Markl et al. 2001; Markl et al. 2010), or mantle-derived partial melts (Macdonald et al. 1987). The evolution of mantle-derived magmas is polybaric with differentiation starting at the crust-mantle boundary (Cox 1980; Lightfoot et al. 1990). Besides contamination through crustal rocks, equilibrium crystallization and fractional crystallization processes operate during ascent and emplacement in shallow crustal levels (Berger et al. 2009; Sha 2012). Furthermore, peralkaline rocks are known to crystallize over a large *T* interval (Sood and Edgar 1970, Appendix B).

The Gardar magmatic province in South Greenland represents a failed rift setting that formed during the Proterozoic (1.35 - 1.14 Ga, Upton et al. 2003). It comprises about twelve large mostly composite intrusive complexes and a large number of dyke rocks (Emeleus and Upton 1976; Upton and Emeleus 1987; Upton et al. 1990; Halama et

al. 2002). While the dyke rocks span a wide compositional range from primitive basaltic to phonolitic, rhyolitic and carbonatitic, intrusive complexes are mostly (nepheline) syenites. Mostly these complexes formed layered cumulates, therefore direct information on melt compositions is unavailable (Upton et al. 1996).

The Ilímaussaq complex is one of the Gardar intrusive complexes and has long been known as an extreme example of a peralkaline intrusion (details on Ilímaussaq can be found in Bailey et al. 2001; Markl et al. 2001; Sørensen 2001; Marks et al. 2004). The depth of emplacement of the plutonic rocks was estimated to 3 - 5 km by fluid-inclusion studies and the sedimentary overburden (Poulsen 1964; Konnerup-Madsen and Rose-Hansen 1984). As typical for intrusive rocks of the Gardar province, the experimental investigation of the Ilímaussaq rocks is complicated as information on suitable melt compositions are lacking due to cumulate formation processes (Sørensen 2001). However, insight into the intrusions‘ parental magma is thought to be provided by the bulk composition of a neighboring dyke rock (Allaart 1969; Larsen and Steenfelt 1974; Marks and Markl 2003). This highly evolved phonolitic dyke was first described by Larsen and Steenfelt (1974) and is located close to Ilímaussaq. It was termed mikrokakortokite due to its petrographic similarities to the layered nepheline syenites (kakortokites) of Ilímaussaq (Allaart 1969). However, field observations provide no clear evidence if the dyke crosscuts the intrusion or vice versa. In direct vicinity to the intrusion, whole-rock analyses of the dyke reveal loss of sodium compared to samples taken at distance of the plutonic Ilímaussaq rocks (Larsen and Steenfelt 1974), implying that the intrusion post-dates dyke formation or is contemporaneous. The dyke is several kilometers long and 10 - 30 m wide, marginally chilled with no or little phenocrysts in the fine-grained matrix. For the calculation of the starting compositions the average of three bulk analyses representing samples from the dykes‘ chilled margin were used (Larsen and Steenfelt 1974).

The petrology of this phonolite was studied in detail by Marks and Markl (2003). The phenocryst assemblage (1) includes titanomagnetite, fayalitic olivine, hedenbergite-

rich clinopyroxene, alkali feldspar and nepheline (± apatite, zircon and titanite); the groundmass assemblage (2) consists of albite and microcline as separate grains, nepheline, sodalite, aegirine-rich clinopyroxene, aenigmatite and arfvedsonite (± Cl-bearing eudialyte and F-bearing fluorite and hiortdahlite); and the (3) late-stage assemblage is represented by analcime and natrolite (for textures of the dyke rock see Figs. 2 and 3 in Marks and Markl 2003). These textures clearly demonstrate disequilibrium between the phenocryst assemblage and the groundmass assemblage, with titanomagnetite and olivine typically rimmed by aegirine-rich clinopyroxene and/or aenigmatite.

In addition, similarities with the neighboring Ilímaussaq plutonic rocks were recognized (Markl et al. 2001; Marks and Markl 2003). The intrusion consists of an early augite syenite phase and an agpaitic main phase, the former mirrored by the dyke's phenocryst assemblage and the latter by the dyke's groundmass assemblage, the late-stage replacement of nepheline, albite and sodalite by analcime and natrolite is also observed both in the Ilímaussaq plutonic rocks and in the investigated dyke rock. Not only the observed mineral phase assemblage is nearly identical but the composition of mineral phases are remarkably similar (Marks and Markl 2003). These similarities offer convincing evidence that the dyke represents a potential parental melt of the Ilímaussaq plutonic rocks.

Furthermore, Marks and Markl (2003) calculated of intensive parameters of crystallization (T, fO_2). Geothermometry using nepheline compositions indicates liquidus T's of at least 900 °C and thermodynamic calculations imply extremely reducing oxygen fugacities of Δ log FMQ -3 to -1.5 during formation of the phenocryst assemblage. The presence of CH_4-rich fluid inclusions in the Ilímausaq plutonic rocks is therefore in agreement with low fO_2's calculated from mineral equilibria (Konnerup-Madsen 2001; Marks and Markl 2001; Markl et al. 2001; Krumrei et al. 2007).

In all, this dyke rock is ideal to investigate the phase relations of an iron-rich peralkaline phonolite experimentally, and might also have some bearing on the plutonic rocks of the Ilímaussaq intrusion. Compared to previous experimental studies on phonolites, the present study extends the range of experimentally investigated phonolitic melts towards extremely evolved (#Mg ~ 3), exceptionally iron-rich (12 wt%) and strongly peralkaline (A. I. ~ 1.5) compositions (Fig. 1) with particular emphasis on the effect of halogens.

1.5 Experimental strategy

As the depth of emplacement is well-constrained for the investigated dyke rock and the Ilímaussaq plutonic rocks, all experiments were conducted isobarically at 100 MPa. Based on the bulk dyke rock composition, three starting compositions with variable Cl and F concentration and ferrous-ferric ratios were synthesized (Tab. 3 in Appendix B). The starting material was mixed from oxide and carbonate powders, homogenized, fused at 1300 - 1600 °C and subsequently quenched to a glass (see methods in Appendix A and B). High *T* glass synthesis is known to involve loss of volatile elements to the vapor phase and is an issue for Cl and F (Lukkari and Holtz 2007, Appendix A and B). Loss of Cl and F to the vapor phase during high *T* glass synthesis was systematically investigated at different *T*'s (1200 - 1600 °C), dwell times (2 - 8 h) and for different initial concentrations (Giehl et al. 2013). Glass synthesis at 1300 °C and 2 h dwell time were found to decrease Cl concentration by approximately 50%. Therefore, initial Cl and F concentrations were doubled to obtain target glass compositions (Appendix B). Au capsules and graphite-lined Au capsules were filled with glass powder (and water in some experiments), welded shut and checked for possible leakage. Therefore, nominally dry, fluid-bearing and fluid-saturated conditions, with either H_2O-dominated or mixed H_2O-CO_2-CH_4 fluids, prevail at experimental conditions. Also, using both Au and graphite-lined Au capsules applies variable oxygen fugacities (Appendix A). Both the coexisting CH_4-bearing fluid and low oxygen fugacities (Δ log FMQ -2 to -1)

closely resemble the conditions prevailing during formation of the dykes‘ phenocryst assemblage (Marks and Markl 2003).

Near-solidus experiments at high degrees of crystallization, which formed separated residual melt pools posed a particular experimental challenge (e. g. Appendix A). Equilibration of such experiments usually failed and increasing run duration (up to 840 h) did not solve this problem (Appendix B). An experimental strategy to follow up the liquid line of descent of the dyke rocks‘ primitive melt is to resynthesize residual melt compositions from nominally dry phase equilibrium experiments at 800 °C and low fO_2. These experiments coexist with the phenocryst assemblage of the dyke rock, but did not encounter the abovementioned equilibration problems and are therefore suited to investigate mineral stabilities of groundmass minerals towards lower *T*‘s. For convenience, starting glasses representing the bulk dyke rock are termed "primitive" and starting glasses representing residual melt compositions of primitive experiments are termed "evolved".

2. Results and discussion

2.1 Phase relations and liquid lines of descent

Adding water to primitive experiments invariably lead to the crystallization of significant amounts of titanomagnetite + clinopyroxene, resulting in high SiO_2-low FeO* liquid lines of descent (Appendix A). However, H_2O-poor experiments (~1.2 wt% H_2O, confirmed by FTIR spectroscopy) stabilize the complete phenocryst assemblage of the investigated dyke rock (titanomagnetite, fayalitic olivine, clinopyroxene, alkali feldspar and nepheline) and follow high FeO*-low SiO_2 liquid lines of descent.

All three H_2O-poor experimental series show decreasing SiO_2, Al_2O_3, K_2O, CaO and increasing Na_2O, MnO and P_2O_5 melt concentrations with falling *T*, resulting in increasing A. I., Na/(Na+K), Na/(Na+Ca) and Na/Fe ratios. Extensive crystallization of alkali feldspar (± nepheline) was found to be responsible for strongly increasing peralkalinity (up to A. I. ~5.5, Appendix A). In contrast, variable liquid lines of descent are observed for TiO_2, ZrO_2, Ti/(Ti+Zr), FeO*, MgO, #Mg, Cl, F and Cl/(Cl+F) (discussed in detail in Appendix B).

2.2 Stability of Cl- and F-bearing mineral phases

To evaluate the stability of halogen-bearing mineral phases it is necessary to distinguish between the solubility of halogens and the saturation of halogen-bearing minerals in melts. In granitic and rhyolitic melts the solubility of F reaches 8 wt% (e. g. Webster 1990; Webster and Holloway 1990). In phonolitic melts the Cl solubility is roughly 0.6 - 0.8 wt% and increases with increasing peralkalinity and FeO content, decreasing SiO_2 content and decreasing *P* (e. g. Metrich and Rutherford 1992; Signorelli and Carroll 2000; Signorelli and Carroll 2002). In the experiments, both Cl and F melt concentrations are significantly lower compared to their estimated solubilities. Perfectly

compatible behavior in favor of the melt and consistent mass-balance calculations indicate that Cl and F do not significantly partition into a fluid phase, therefore saturation of Cl- and F-bearing mineral phases can be interpreted regarding Cl and F melt content (Appendix B).

In the present study it is demonstrated that high F melt content stabilizes fluorite and hiortdahlite inducing both destabilization of clinopyroxene by decreasing CaO melt content and delayed Eud saturation by a prolonged increase of ZrO_2 melt content (Appendix B and C). This facilitates a compositional gap for clinopyroxene and a higher abundance of aenigmatite where clinopyroxene is unstable (Appendix C). These experiments show a trend where both Na/(Na+Ca) in clinopyroxene, towards endmember aegirine, and Na/(Na+Ca) of the melt increase with decreasing *T*. Due to the increase of Na/(Na+Ca) in the melt with decreasing *T*, Na-rich clinopyroxene reoccurs at 650 °C (run 172, Appendix B) confirming that a compositional gap in clinopyroxene may be induced by high F melt content. At low F melt content, clinopyroxene is stable over the entire investigated *T* interval, still its composition jumps from Ca-rich (Na/(Na+Ca) = 0.42) to Na-rich (Na/(Na+Ca) = 0.68) within 750 - 700 °C (Appendix A and B). Although, the compositional jump exists at low F melt content, however, with increasing F melt content clinopyroxene is unstable between 825 and 650 °C.

2.3 Towards new thermometers for peralkaline rocks

Existing geothermometers based on olivine-clinopyroxene-Fe-Ti oxide equilibria (QUILF type, Andersen et al. 1993) and clinopyroxene-melt partitioning (Putirka 2008) were tested using experimental data of the present study. These calculations show that increasing Na-content in clinopyroxene induces increasing misfit with experimental *T*'s (Appendix C). Furthermore, agpaitic rocks often lack olivine and Fe-Ti oxides, complicating the calculation of crystallization *T*'s (Marks et al. 2011). Therefore, we

developed new thermometers based on mineral/mineral and mineral/melt partitioning utilizing Mn concentrations and Na/Ca ratios of clinopyroxene, eudialyte, aenigmatite and melt (see Tab. 1 for mineral formulae). Due to the common occurence of these minerals the thermometers are expected to be applicable to many peralkaline agpaitic rocks.

2.4 Comparison with nature

All evolved experiments presented so far were conducted isobarically (100 MPa), at low fO_2 (Δ log FMQ -1 to -3) and H_2O-poor conditions (<1.4 wt% H_2O melt content). As stated above, all experiments were conducted according to P estimates from fluid-inclusions (Poulsen 1964; Konnerup-Madsen and Rose-Hansen 1984) and fO_2 calculated from phase equilibria (Konnerup-Madsen 2001; Marks and Markl 2001; Krumrei et al. 2007) and primitive experiments indeed demonstrate that H_2O-poor conditions stabilize the phase assemblage observed in the investigated dyke rock (Appendix A). Consecutive evolved experiments also largely reproduced the groundmass assemblage; however, these experiments did not stabilize amphibole (Appendix B). One important conclusion that can be drawn from the present study is that a strongly peralkaline melt (with an A. I. of 1.5) may crystallize a metaluminous phase assemblage closely resembling the early augite syenite phase of Ilímaussaq (Appendix B). This supports the idea that the dyke represents a parental melt of the plutonic complex and principally enables the system to have evolved from one single magma batch (Marks and Markl, in press).

Phase relations in H_2O-saturated systems are strongly affected by changes of P. This is mainly due to the strong P-dependence of H_2O solubility in those melts and the resulting changes in liquidus and solidus T's and modified phase stabilities of both H_2O-bearing and H_2O-free mineral phases (e. g. Holtz et al. 1995). Despite the present study shows that the natural mineral phase assemblage formed at H_2O-poor conditions, it is tempting to study the effect of P on amphibole stability. This effect has been

shown in phase equilibrium studies on phonolites and will be discussed in detail in the following section (e. g. Harms et al. 2004; Moussallam et al. 2013).

Besides amphibole, all major mineral phases present in the dyke rock were synthesized. Bailey (1969) suggested that arfvedsonite is stable below 700 °C at fO_2 lower than Δ log FMQ +0. Coexisting sodic clinopyroxene and arfvedsonite were suggested to be stable below 650 °C and fO_2 more reduced than FMQ (Curtis and Currie 1981). These conditions match the applied experimental parameters (T, fO_2).

Experiments at 200 MPa on F- and Cl-free basaltic compositions show a small but significant increase of amphibole stability to higher T with increasing H_2O melt content. Also, high H_2O melt content is crucial to stabilize amphibole in granitic and dacitic magmas (Dall'agnol et al. 1999; Scaillet and Evans 1999). Nevertheless, amphibole is also stable at H_2O-undersaturated conditions (< 1 wt%, Berndt et al. 2005; Freise et al. 2009; Feig et al. 2010).

In experiments of Freise et al. (2009) on a basaltic composition, increasing H_2O melt content, coupled with increasing fO_2, shifts amphibole stability to lower T, or favors clinopyroxene over amphibole (Helz 1973, 1976). In contrast, a phase equilibrium study on A-type granites implies that lower fO_2 shifts amphibole stability to lower T (Dall'agnol et al. 1999).

Also, phase equilibrium experiments on two phonolitic compositions from the Kerguelen failed to reproduce amphibole, even though this study covers a wide range of experimental conditions and two different starting compositions (100 - 500 MPa, 700 - 900 °C, Δ log FMQ +0.7 to +3 and 2 - 8 wt% H_2O melt content, Freise et al. 2003). To rule out kinetic or nucleation problems, amphibole from natural samples was added to these experimental runs but was, however, completely dissolved or reacted back to clinopyroxene and oxides (Freise et al. 2003). Using a similar phonolitic composition from the Laacher See volcanoe (Berndt et al. 2001), amphibole was synthesized in one experiment at 300 MPa, 760 °C and 4 wt% H_2O, but was unstable at 200 and 400 MPa. A similar "P window" was reported in a study of Scaillet et al. (2008) on phonolites

with amphibole stable within a small *T* interval (830 - 800 °C) at 150 - 200 MPa, but unstable at 100 and 300 MPa.

H_2O-saturated experiments at different *P*'s and *T*'s on a more evolved phonolite from Laacher See volcanoe revealed that amphibole is stable below 770 °C, if *P* is higher than 150 MPa (Harms et al. 2004). Still, lower *P* shifts the stability of amphibole to lower *T*, as was also observed in an experimental study on a dacite from Unzen volcanoe (Holtz et al. 2005). However, amphibole stability in peralkaline F-rich magmas is probably less related to H_2O, as significant amounts of F (and Cl) may substitute for OH (Hawthorne et al. 2012). Amphibole from the investigated dyke rock has indeed up to 2 wt% F, which is roughly 50% of the OH site in amphibole.

Still, Cl- and F-free starting material (intentionally or through loss to the vapor phase during high *T* synthesis of the starting material) is commonly used in experimental studies. If stabilization of amphibole in experiments is unsuccessful, many authors stress the absence of halogens as a possible reason for the lack of amphibole, particularly in favor of clinopyroxene (see references above).

Scaillet and Macdonald (2003) reported F distribution coefficients between amphibole and melt in a study on peralkaline rhyolites (K_d, F = 2.7 - 1). This range of partition coefficients was combined with the maximum F content in amphibole of the dyke rock (2.0 wt%, Marks and Markl 2003) to estimate the F content of the coexisting melt during amphibole crystallization. The calculations yield 0.8 - 2.0 wt% F melt, therefore experiments of this study cover (and exceed) the estimated range of F melt content (0 - 2.7 wt%) required to crystallize amphibole. Hence, amphibole stability is probably not limited by F melt content.

Therefore, it is tempting to presume a *P* dependence of amphibole stability, a parameter not addressed in isobaric experiments of the present study. The amphibole most similar compared to the Ilímaussaq amphiboles, an arfvedsonite-riebeckite, was synthesized at 50 - 150 MPa, 730 - 680 °C and ~Δ log FMQ -1 in an experimental study on a peralkaline rhyolite (Scaillet and Macdonald 2001), in which increasing fO_2 favors clinopyroxene

over amphibole. It is interesting to note that these experiments failed to synthesize aenigmatite, which was expected from the natural rock equivalent. Whereas synthesis of amphibole in experiments on basaltic compositions is successful in most studies (e. g. Freise et al. 2009), amphibole in phonolites (Berndt et al. 2001; Harms et al. 2004; Scaillet et al. 2008; Freise et al. 2009) and (co)-crystallization of compositionally very similar clinopyroxene (and rather similar aenigmatite) is difficult to reproduce. Apparently, particular P, T, $a\mathrm{H_2O}$, $f\mathrm{O_2}$ conditions and melt compositions are required. Even though arfvedsonite + sodic clinopyroxene is a common paragenesis in peralkaline rocks, a detailed petrographical study on the lujavrites from Ilímaussaq demonstrates that the genetic relation between clinopyroxene and amphibole is essentially unclear and may vary strongly even within one rock type. For example, lujavrites may contain clinopyroxene, amphibole or both. Moreover, clinopyroxene may replace amphibole or vice versa (Ratschbacher et al. 2011). The recent review of Marks and Markl (in press) portrays that decades of extensive research elucidated parts of the complex processes that formed the Ilímaussaq plutonic rocks, however, it is equally clear that numerous questions remain unanswered to date.

2.5 Rare Earth Elements in peralkaline rocks

Since the 1960s the rare earth elements experience a growing industrial demand and increasing importance for high-tech consumer products (Chakhmouradian and Zaitsev 2012). In recent years, the increasing demand combined with chinese export-quota lead to unforeseen volatility in the rare earth element market (Hatch 2012). Roughly 50 exploration projects outside China are currently active to meet today‘s challenges in rare earth element supply, of which 33 are related to magmatic rocks and their alteration products. The most promising rare earth element deposits are located in carbonatites and peralkaline silicate rocks (Chakhmouradian and Zaitsev 2012). To date, next to nothing is known about the stabilities of economically important rare earth element-rich minerals and their mineral/melt partitioning of these minerals as

experimental attempts were unsuccesful so far (Chakhmouradian and Zaitsev 2012). Thermodynamic phase stability calculations do not account for complex Na-Ca-Fe-HFSE silicates, which often incorporate Cl and F (including eudialyte and hiortdahlite). However, they do not even account for halogens in general (e. g. MELTS, Ghiorso and Sack 1995; Aiuppa et al. 2009; Rooney et al. 2012).

The global issue of rare earth element supply is linked to the present study by recent exploration activity rating the agpaitic Ilímaussaq plutonic rocks as a world-class rare earth element and U deposit (e. g. Parsons 2012). High concentrations of e. g. Zr, REE's, U and Th are typical for eudialyte and hiortdahlite, and characteristic for the agpaitic rocks they form (Sørensen 1992, 1997; Chakhmouradian and Zaitsev 2012). The economic potential of eudialyte is further emphasized by the fact that eudialyte is already mined in the Lovozero complex (Russia, Kramm and Kogarko 1997; Zakharov et al. 2011). The present study presents first experimental data on stabilities and mineral/melt partitioning of minerals typical for agpaitic rocks (Appendix B) and provides preliminary calibrations to calculate crystallization *T*'s in such rocks (Appendix C). However, simplified synthetic starting compositions were used and rare earth elements were omitted. Hence, the next step was to broaden knowledge on phase stabilities by using starting composition doped with selected trace elements (Winterhalder et al. 2013). Therefore, Nb, La, Ce, Y and Sr were added to the Cl- and F-rich starting composition according to bulk dyke rock concentrations (Larsen and Steenfelt 1974; Appendix B: HAF-hH-red\pr) and the abovementioned two-step fractional crystallization strategy was applied. Preliminary results show that mineral phase stabilities and liquid lines of descent in these experiments are similar compared to undoped starting compositions, supporting the conclusions drawn from experiments with synthetic trace elements-free starting compositions (Larsen and Steenfelt 1974, starting glasses HAF-hH-red and HAF-hH-red\ev, Appendix B). However, hiortdahlite and eudialyte act as a sink for rare earth elements incorporating up to 13 wt% REE_2O_3.

2.6 Open questions and outlook

Experimental phase equilibrium constraints in phonolitic systems suggest that amphibole may be stable at even lower *T*‘s at 100 MPa (e. g. Harms et al. 2004) or *P*‘s exceeding 200 MPa (e. g. Moussallam et al. 2013). In particular such high *P*‘s would question the accepted view that the Ilímaussaq complex and the investigated dyke rock were emplaced at roughly 100 MPa (Konnerup-Madsen and Rose-Hansen 1984; Markl et al. 2001). Fluid-inclusions in sodalite of Ilímaussaq‘s naujaite indicate crystallization *P*‘s of up to 400 MPa, however, crystallization during ascent is contrary to the late magmatic occurrence of amphibole as indicated by textural observations (Marks and Markl 2003). To rule out that low cH_2O and low *P* limit amphibole stability, additional evolved experiments were conducted to investigate the influence of *P*, H_2O melt content and fO_2. These experiments cover H_2O-poor experiments at 150 - 250 MPa, higher H_2O melt concentrations up to H_2O-saturation and a H_2O-saturated experiments at higher fO_2 (Δ log FMQ +0.8). Also, residual melt compositions of experiments at 700 °C (H_2O-poor, 100 MPa) were resynthesized as starting glasses for a second fractionation step. Subsequent H_2O-poor experiments at 650 °C were performed; none of these experiments stabilized amphibole. In summary, higher H_2O melt content and higher *P* did not stabilize amphibole and imply that *T*‘s even lower than 600 °C are are required to do so.

References

Aiuppa A, Baker DR, Webster JD (2009) Halogens in volcanic systems. Chemical Geology 263 (1-4):1-18. doi:10.1016/j.chemgeo.2008.10.005

Allaart JH (1969) The chronology and petrography of the Gardar dykes between Igaliko Fjord and Redekammen, South Greenland. Rapport Grønlands Geologiske Undersøgelse 25: 26 pp

Almeev R, Holtz F, Ariskin A, Kimura J-I (2013) Storage conditions of Bezymianny Volcano parental magmas: results of phase equilibria experiments at 100 and 700 MPa. Contributions to Mineralogy and Petrology 166 (5):1389-1414. doi:10.1007/s00410-013-0934-x

Almeev RR, Bolte T, Nash BP, Holtz F, Erdmann M, Cathey HE (2012) High-temperature, low-H2O Silicic Magmas of the Yellowstone Hotspot: an Experimental Study of Rhyolite from the Bruneau-Jarbidge Eruptive Center, Central Snake River Plain, USA. Journal of Petrology 53 (9):1837-1866. doi:10.1093/petrology/egs035

Almeev RR, Holtz F, Koepke J, Parat F, Botcharnikov RE (2007) The effect of H2O on olivine crystallization in MORB: Experimental calibration at 200 MPa. American Mineralogist 92 (4):670-674. doi:10.2138/am.2007.2484

Andersen DJ, Lindsley DH, Davidson PM (1993) QUILF - A PASCAL program to assess equilibria among Fe-Mg-Mn-Ti Oxides, Pyroxenes, Olivine and Quartz. Computers & Geosciences 19 (9):1333-1350. doi:10.1016/0098-3004(93)90033-2

Andersen T, Erambert M, Larsen AO, Selbekk RS (2010) Petrology of Nepheline Syenite Pegmatites in the Oslo Rift, Norway: Zirconium Silicate Mineral Assemblages as Indicators of Alkalinity and Volatile Fugacity in Mildly Agpaitic Magma. Journal of Petrology 51 (11):2303-2325. doi:10.1093/petrology/egq058

Andújar J, Costa F, Martí J (2010) Magma storage conditions of the last eruption of Teide volcano (Canary Islands, Spain). Bulletin of Volcanology 72 (4):381-395. doi:10.1007/s00445-009-0325-3

Andújar J, Costa F, Marti J, Wolff JA, Carroll MR (2008) Experimental constraints on pre-eruptive conditions of phonolitic magma from the caldera-forming El Abrigo eruption, Tenerife (Canary Islands). Chemical Geology 257 (3-4):173-191. doi:10.1016/j.chemgeo.2008.08.012

References

Andújar J, Scaillet B (2012) Experimental Constraints on Parameters Controlling the Difference in the Eruptive Dynamics of Phonolitic Magmas: the Case of Tenerife (Canary Islands). Journal of Petrology 53 (9):1777-1806. doi:10.1093/petrology/egs033

Bailey DK (1969) The stability of acmite in the presence of H2O. American Journal of Science 267:1-16

Bailey JC, Gwozdz R, Rose-Hansen J, Sørensen H (2001) Geochemical overview of the Ilímaussaq alkaline complex, South Greenland. Geology of Greenland Survey Bulletin 190:35-53

Ballentine CJ, Burgess R, Sumino H, Hilton D, Graham D, Van Keken P, Chavrit D, Ruzie L, Clay P, Joachim B, Moorsom B, Jepson L, Broadley M (2013) Combined Halogen (Cl, Br, I) and Noble Gas Mantle Geochemistry. Mineralogical Magazine 77 (5):648

Berger J, Ennih N, Mercier JCC, Liegeios JP, Demaiffe D (2009) The role of fractional crystallization and late-stage peralkaline melt segregation in the mineralogical evolution of Cenozoic nephelinites/phonolites from Saghro (SE Morocco). Mineralogical Magazine 73 (1):59-82. doi:10.1180/minmag.2009.07

Berndt J (2002) Differentiation of MOR Basalt at 200 MPa: Experimental Techniques and Influence of H2O and fO2 on Phase Relations and Liquid Line of Descent. PhD thesis. Leibniz Universität Hannover, 118 pp

Berndt J, Holtz F, Koepke J (2001) Experimental constraints on storage conditions in the chemically zoned phonolitic magma chamber of the Laacher See volcano. Contributions to Mineralogy and Petrology 140 (4):469-486. doi:10.1007/PL00007674

Berndt J, Koepke J, Holtz F (2005) An Experimental Investigation of the Influence of Water and Oxygen Fugacity on Differentiation of MORB at 200 MPa Journal of Petrology 46 (1):135-167. doi:10.1093/petrology/egh066

Botcharnikov RE, Holtz F, Almeev RR, Sato H, Behrens H (2008a) Storage conditions and evolution of andesitic magma prior to the 1991-95 eruption of Unzen volcano: Constraints from natural samples and phase equilibria experiments. Journal of Volcanology and Geothermal Research 175 (1-2):168-180. doi:10.1016/j.jvolgeores.2008.03.026

Botcharnikov RE, Almeev RR, Koepke J, Holtz F (2008b) Phase Relations and Liquid Lines of Descent in Hydrous Ferrobasalt - Implications for the Skaergaard Intrusion and Columbia River Flood Basalts. Journal of Petrology 49 (9):1687-1727. doi:10.1093/petrology/egn043

Carroll MR, Webster J (1994) Volatiles in magmas: Solubilities of sulfur, noble gases, nitrogen, chlorine, and fluorine in magmas. In: Carroll MJ, Holloway JR (eds) Reviews in Mineralogy, vol 30. Mineralogical Society of America, pp 231-271

References

Chakhmouradian AR, Zaitsev AN (2012) Rare Earth Mineralization in Igneous Rocks: Sources and Processes. Elements 8 (5):347-353. doi:10.2113/gselements.8.5.347

Cox KG (1980) A Model for Flood Basalt Vulcanism. Journal of Petrology 21 (4):629-650. doi:10.1093/petrology/21.4.629

rtis LW, Currie KL (1981) Geology and petrology of the Red Wine alkaline complex, Central Labrador Geological Survey of Canada Bulletin 294:61 pp. doi:10.4095/124257

Dall'agnol R, Scaillet B, Pichavant M (1999) An Experimental Study of a Lower Proterozoic A-type Granite from the Eastern Amazonian Craton, Brazil. Journal of Petrology 40 (11):1673-1698. doi:10.1093/petroj/40.11.1673

DePaolo DJ (1981) Trace element and isotopic effects of combined wallrock assimilation and fractional crystallization. Earth and Planetary Science Letters 53 (2):189-202. doi:10.1016/0012-821X(81)90153-9

Di Carlo I, Rotolo SG, Scaillet B, Buccheri V, Pichavant M (2010) Phase Equilibrium Constraints on Pre-eruptive Conditions of Recent Felsic Explosive Volcanism at Pantelleria Island, Italy. Journal of Petrology 51 (11):2245-2276. doi:10.1093/petrology/egq055

Dolejš D, Baker DR (2006) Fluorite solubility in hydrous haplogranitic melts at 100 MPa. Chemical Geology 225 (1-2):40-60. doi:10.1016/j.chemgeo.2005.08.007

Emeleus CH, Upton BGJ (1976) The Gardar period in southern Greenland. In: Escher A, Watt WS (eds) The Geology of Greenland. Geological Survey of Greenland, Copenhagen, pp 152-181

Fabbrizio A, Carroll MR (2008) Experimental constraints on the differentiation process and pre-eruptive conditions in the magmatic system of Phlegraean Fields (Naples, Italy). Journal of Volcanology and Geothermal Research 171 (1-2):88-102. doi:10.1016/j.jvolgeores.2007.11.002

Feig ST, Koepke J, Snow JE (2006) Effect of water on tholeiitic basalt phase equilibria: an experimental study under oxidizing conditions. Contributions to Mineralogy and Petrology 152 (5):611-638. doi:10.1007/s00410-006-0123-2

Feig ST, Koepke J, Snow JE (2010) Effect of oxygen fugacity and water on phase equilibria of a hydrous tholeiitic basalt. Contributions to Mineralogy and Petrology 160 (4):551-568. doi:10.1007/s00410-010-0493-3

Filiberto J, Treiman AH (2009) The effect of chlorine on the liquidus of basalt: First results and implications for basalt genesis on Mars and Earth. Chemical Geology 263 (1-4):60-68. doi:10.1016/j.chemgeo.2008.08.025

References

Filiberto J, Wood J, Dasgupta R, Shimizu N, Le L, Treiman AH (2012) Effect of fluorine on near-liquidus phase equilibria of an Fe-Mg rich basalt. Chemical Geology 312-313:118-126. doi:10.1016/j.chemgeo.2012.04.015

Freise M, Holtz F, Koepke J, Scoates J, Leyrit H (2003) Experimental constraints on the storage conditions of phonolites from the Kerguelen Archipelago. Contributions to Mineralogy and Petrology 145 (6):659-672. doi:10.1007/s00410-003-0453-2

Freise M, Holtz F, Nowak M, Scoates JS, Strauss H (2009) Differentiation and crystallization conditions of basalts from the Kerguelen large igneous province: an experimental study. Contributions to Mineralogy and Petrology 158 (4):505-527. doi:10.1007/s00410-009-0394-5

Frindt S, Trumbull RB, Romer RL (2004) Petrogenesis of the Gross Spitzkoppe topaz granite, central western Namibia: a geochemical and Nd-Sr-Pb isotope study. Chemical Geology 206 (1-2):43-71. doi:10.1016/j.chemgeo.2004.01.015

Ghiorso MS, Sack RO (1995) Chemical mass transfer in magmatic processes IV. A revised and internally consistent thermodynamic model for the interpolation and extrapolation of liquid-solid equilibria in magmatic systems at elevated temperatures and pressures. Contributions to Mineralogy and Petrology 119 (2):197-212. doi:10.1007/bf00307281

Giehl C, Schröder C, Wenzel T, Nowak M High temperature synthesis of iron-, sodium- and halogen-rich silicate glasses: experimental and analytical challenges. In: GEOFLUIDS: Joint Annual Meeting of the German Mineralogical Society (DMG) and the Geologische Vereinigung (GV), Tübingen, Germany, 16th - 19th September 2013.

Gioncada A, Orlandi P, Vezzoli L, Omarini RH, Mazzuoli R, Lopez-Azarevich V, Sureda R, Azarevich M, Acocella V, Ruch J (2014) Topaz magmatic crystallization in rhyolites of the Central Andes (Chivinar volcanic complex, NW Argentina): Constraints from texture, mineralogy and rock chemistry. Lithos 184-187:62-73. doi:10.1016/j.lithos.2013.10.023

Halama R, Waight T, Markl G (2002) Geochemical and isotopic zoning patterns of plagioclase megacrysts in gabbroic dykes from the Gardar Province, South Greenland: implications for crystallisation processes in anorthositic magmas Contributions to Mineralogy and Petrology 144 (1):109-127

Harms E, Gardner JE, Schmincke HU (2004) Phase equilibria of the Lower Laacher See Tephra (East Eifel, Germany): constraints on pre-eruptive storage conditions of a phonolitic magma reservoir. Journal of Volcanology and Geothermal Research 134 (1-2):125-138. doi:10.1016/j.jvolgeores.2004.01.009

References

Hatch GP (2012) Dynamics in the Global Market for Rare Earths. Elements 8 (5):341-346. doi:10.2113/gselements.8.5.341

Hawthorne FC, Oberti R, Harlow GE, Maresch WV, Martin RF, Schumacher JC, Welch MD (2012) Nomenclature of the amphibole supergroup. American Mineralogist 97 (11-12):2031-2048. doi:10.2138/am.2012.4276

Helz RT (1973) Phase Relations of Basalts in their Melting Range at PH2O = 5 kb as a Function of Oxygen Fugacity: Part I. Mafic Phases. Journal of Petrology 14 (2):249-302. doi:10.1093/petrology/14.2.249

Helz RT (1976) Phase Relations of Basalts in their Melting Ranges at PH2O = 5 kb. Part II. Melt Compositions. Journal of Petrology 17 (2):139-193. doi:10.1093/petrology/17.2.139

Holtz F, Behrens H, Dingwell DB, Johannes W (1995) H2O Solubility in Haplogranitic Melts - Compositional, Pressure, and Temperature-Dependence. American Mineralogist 80 (1-2):94-108

Holtz F, Sato H, Lewis J, Behrens H, Nakada S (2005) Experimental Petrology of the 1991-1995 Unzen Dacite, Japan. Part I: Phase Relations, Phase Composition and Pre-eruptive Conditions. Journal of Petrology 46 (2):319-337. doi:10.1093/petrology/egh077

Ionov DA, Griffin WL, O'Reilly SY (1997) Volatile-bearing minerals and lithophile trace elements in the upper mantle. Chemical Geology 141 (3-4):153-184. doi:10.1016/S0009-2541(97)00061-2

Joachim B, Lyon I, Pawley A, Henkel T, Ruzie L, Clay P, Burgess R, Ballentine CJ (2013) Halogen Partitioning Behavior at Earth's Mantle Conditions. Mineralogical Magazine 77 (5):1393

Klimm K, Holtz F, Johannes W, King PL (2003) Fractionation of metaluminous A-type granites: an experimental study of the Wangrah Suite, Lachlan Fold Belt, Australia. Precambrian Research 124 (2-4):327-341. doi:10.1016/S0301-9268(03)00092-5

Konnerup-Madsen J (2001) A review of the composition and evolution of hydrocarbon gases during solidification of the Ilímaussaq alkaline complex, South Greenland Geology of Greenland Survey Bulletin 190:159-166

Konnerup-Madsen J, Rose-Hansen J (1984) Composition and significance of fluid inclusions in the Ilímaussaq peralkaline granite, South Greenland. Bulletin de Minéralogie 107 (2):317-326

Krumrei TV, Pernicka E, Kaliwoda M, Markl G (2007) Volatiles in a peralkaline system: Abiogenic hydrocarbons and F-Cl-Br systematics in the naujaite of the Ilímaussaq intrusion, South Greenland. Lithos 95 (3-4):298-314. doi:10.1016/j.lithos.2006.08.003

References

Larsen LM, Sørensen H (1987) The Ilímaussaq intrusion - progressive crystallization and formation of layering in an agpaitic magma. Geological Society, London, Special Publications 30:473-488. doi:10.1144/GSL.SP.1987.030.01.23

Larsen LM, Steenfelt A (1974) Alkali loss and retention in an iron-rich peralkaline phonolite dyke from the Gardar province, south Greenland. Lithos 7 (2):81-90. doi:10.1016/0024-4937(74)90021-8

Lightfoot PC, Hawkesworth CJ, Devey CW, Roger NW, van Calsteren PWC (1990) Source and Differentiation of Deccan Trap Lavas: Implications of Geochemical and Mineral Chemical Variations. Journal of Petrology 31 (5):1165-1200. doi:10.1093/petrology/31.5.1165

Lukkari S, Holtz F (2007) Phase relations of a F-enriched peraluminous granite: an experimental study of the Kymi topaz granite stock, southern Finland. Contributions to Mineralogy and Petrology 153 (3):273-288. doi:10.1007/s00410-006-0146-8

Macdonald R, Davies GR, Bliss CM, Leat PT, Bailey DK, Smith RL (1987) Geochemistry of High-silica Peralkaline Rhyolites, Naivasha, Kenya Rift Valley. Journal of Petrology 28 (6):979-1008

Manning DAC (1981) The effect of fluorine on liquidus phase relationships in the system Qz-Ab-Or with excess water at 1 kb. Contributions to Mineralogy and Petrology 76 (2):206-215. doi:10.1007/bf00371960

Markl G (2001) A new type of silicate liquid immiscibility in peralkaline nepheline syenites (lujavrites) of the Ilímaussaq complex, South Greenland. Contributions to Mineralogy and Petrology 141 (4):458-472

Markl G, Marks M, Schwinn G, Sommer H (2001) Phase equilibrium constraints on intensive crystallization parameters of the Ilímaussaq complex, South Greenland. Journal of Petrology 42 (12):2231-2258. doi:10.1093/petrology/42.12.2231

Markl G, Marks MAW, Frost BR (2010) On the Controls of Oxygen Fugacity in the Generation and Crystallization of Peralkaline Melts. Journal of Petrology 51 (9):1831-1847. doi:10.1093/petrology/egq040

Marks M, Markl G (2001) Fractionation and assimilation processes in the alkaline augite syenite unit of the Ilímaussaq intrusion, South Greenland, as deduced from phase equilibria. Journal of Petrology 42 (10):1947-1969. doi:10.1093/petrology/42.10.1947

Marks M, Markl G (2003) Ilímaussaq 'en miniature': closed-system fractionation in an agpaitic dyke rock from the Gardar Province, South Greenland (contribution to the mineralogy of Ilímaussaq no. 117) Mineralogical Magazine 67 (5):893-919. doi:10.1180/0026461036750150

References

Marks M, Markl G (2013) The Ilímaussaq alkaline complex (South Greenland). In: Charlier B, Namur O, Latypov R, Tegner C (eds) Layered Intrusions. Springer, Dordrecht, in press

Marks MAW, Hettmann K, Schilling J, Frost BR, Markl G (2011) The Mineralogical Diversity of Alkaline Igneous Rocks: Critical Factors for the Transition from Miaskitic to Agpaitic Phase Assemblages. Journal of Petrology 52 (3):439-455. doi:10.1093/petrology/egq086

Marks MAW, Vennemann T, Siebel W, Markl G (2004) Nd-, O-, and H-isotopic evidence for complex, closed-system fluid evolution of the peralkaline Ilímaussaq intrusion, south Greenland. Geochimica et Cosmochimica Acta 68 (16):3379-3395. doi:10.1016/j.gca.2003.12.008

Marks MAW, Wenzel T, Whitehouse MJ, Loose M, Zack T, Barth M, Worgard L, Krasz V, Eby GN, Stosnach H, Markl G (2012) The volatile inventory (F, Cl, Br, S, C) of magmatic apatite: An integrated analytical approach. Chemical Geology 291:241-255. doi:10.1016/j.chemgeo.2011.10.026

Marshall AS, Hinton RW, Macdonald R (1998) Phenocrystic fluorite in peralkaline rhyolites, Olkaria, Kenya Rift Valley. Mineralogical Magazine 62 (4):477-486

Masotta M, Freda C, Gaeta M (2012) Origin of crystal-poor, differentiated magmas: insights from thermal gradient experiments. Contributions to Mineralogy and Petrology 163 (1):49-65. doi:10.1007/s00410-011-0658-8

Masotta M, Mollo S, Freda C, Gaeta M, Moore G (2013) Clinopyroxene-liquid thermometers and barometers specific to alkaline differentiated magmas. Contributions to Mineralogy and Petrology 166 (6):1545-1561. doi:10.1007/s00410-013-0927-9

Metrich N, Rutherford MJ (1992) Experimental study of chlorine behavior in hydrous silicic melts. Geochimica et Cosmochimica Acta 56:607-616. doi:10.1016/0016-7037(92)90085-W

Mohr PA (1987) Crustal Contamination in Mafic Sheets: a summary. In: Halls HC, Fahrig WC (eds) Mafic Dyke Swarms, vol 34. Special Publication - Geological Association of Canada, pp 75-80

Moussallam Y, Oppenheimer C, Scaillet B, Kyle PR (2013) Experimental Phase-equilibrium Constraints on the Phonolite Magmatic System of Erebus Volcano, Antarctica. Journal of Petrology 54 (7):1285-1307. doi:10.1093/petrology/egt012

O'Reilly SY, Griffin WL (2000) Apatite in the mantle: implications for metasomatic processes and high heat production in Phanerozoic mantle. Lithos 53 (3-4):217-232. doi:10.1016/S0024-4937(00)00026-8

References

Poulsen V (1964) The sandstones of the Precambrian Eriksfjord formation in South Greenland. Rapport Grønlands Geologiske Undersøgelse 2:16 pp

Price JD, Hogan JP, Gilbert MC (1996) Rapakivi texture in the Mount Scott Granite, Wichita Mountains, Oklahoma. European Journal of Mineralogy 8 (2):435-451

Putirka K (2008) Thermometers and barometers for volcanic systems. In: Putirka K, Tepley F (eds) Reviews in Mineralogy and Geochemistry: Minerals, inclusions and volcanic processes, vol 69. Mineralogical Society of America, pp 61-120

Ratschbacher B, Marks MAW, Pfaff K, Markl G Mineral Compositions Indicate Magma Recharge Processes in the Ilímaussaq Complex, Greenland. In: Goldschmidt, Prague, Czech Republic, 14th - 19th August 2011. Mineralogical Magazine 75(3), p 1698

Rønsbo JG (2008) Apatite in the Ilímaussaq alkaline complex: Occurrence, zonation and compositional variation. Lithos 106 (1-2):71-82. doi:10.1016/j.lithos.2008.06.006

Rooney T, Hart W, Hall C, Ayalew D, Ghiorso M, Hidalgo P, Yirgu G (2012) Peralkaline magma evolution and the tephra record in the Ethiopian Rift. Contributions to Mineralogy and Petrology 164 (3):407-426. doi:10.1007/s00410-012-0744-6

Scaillet B, Evans BW (1999) The 15 June 1991 Eruption of Mount Pinatubo. I. Phase Equilibria and Pre-eruption P-T-fO2-fH2O Conditions of the Dacite Magma. Journal of Petrology 40 (3):381-411. doi:10.1093/petroj/40.3.381

Scaillet B, Macdonald R (2001) Phase relations of peralkaline silicic magmas and petrogenetic implications. Journal of Petrology 42 (4):825-845. doi:10.1093/petrology/42.4.825

Scaillet B, Macdonald R (2003) Experimental Constraints on the Relationships between Peralkaline Rhyolites of the Kenya Rift Valley. Journal of Petrology 44 (10):1867-1894. doi:10.1093/petrology/egg062

Scaillet B, Macdonald R (2004) Fluorite stability in silicic magmas. Contributions to Mineralogy and Petrology 147 (3):319-329. doi:10.1007/s00410-004-0559-1

Scaillet B, Pichavant M, Cioni R (2008) Upward migration of Vesuvius magma chamber over the past 20,000 years. Nature 455:216-219. doi:10.1038/nature07232

Seifert W, Kämpf H, Wasternack J (2000) Compositional variation in apatite, phlogopite and other accessory minerals of the ultramafic Delitzsch complex, Germany: implication for cooling history of carbonatites. Lithos 53 (2):81-100. doi:10.1016/S0024-4937(00)00010-4

Sha LK (2012) Concurrent fractional and equilibrium crystallisation. Geochimica et Cosmochimica Acta 86:52-75. doi:10.1016/j.gca.2012.02.027

References

Signorelli S, Carroll M (2002) Experimental study of Cl solubility in hydrous alkaline melts: constraints on the theoretical maximum amount of Cl in trachytic and phonolitic melts. Contributions to Mineralogy and Petrology 143 (2):209-218. doi:10.1007/s00410-001-0320-y

Signorelli S, Carroll MR (2000) Solubility and fluid-melt partitioning of Cl in hydrous phonolitic melts. Geochimica et Cosmochimica Acta 64 (16):2851-2862. doi:10.1016/s0016-7037(00)00386-0

Sood MK, Edgar AD (1970) Melting relations of undersaturated alkaline rocks from the Ilímaussaq intrusion and Grønnedal-Ika Complex South Greenland, under Water Vapour and controlled Partial Oxygen Pressure. Meddelelser om Grønland 181 (12):41

Sørensen H (1997) The agpaitic rocks - an overview. Mineralogical Magazine 61 (4):485-498. doi:10.1180/minmag.1997.061.407.02

Sørensen H (2001) The Ilímaussaq alkaline complex, South Greenland: status of mineralogical research with new results. Geology of Greenland Survey Bulletin 190:167 pp

Teiber H, Marks MAW, Wenzel T, Siebel W, Altherr R, Markl G (2014) The distribution of halogens (F, Cl, Br) in granitoid rocks. Chemical Geology 374-375:92-109. doi:10.1016/j.chemgeo.2014.03.006

Tuttle OF, Bowen NL (1958) Origin of granite in the light of experimental studies in the system NaAlSi3O8-KAlSi3O8-SiO2-H2O. Geological Society of America Memoirs 74:153 pp.

Upton BGJ, Emeleus CH (1987) Mid-Proterozoic alkaline magmatism in southern Greenland: the Gardar province. In: Fitton JG, Upton BGJ (eds) Alkaline igneous rocks, vol 30. Geological Society Special Publication, London, pp 449-471

Upton BGJ, Emeleus CH, Heaman LM, Goodenough KM, Finch AA (2003) Magmatism of the mid-Proterozoic Gardar Province, South Greenland: chronology, petrogenesis and geological setting. Lithos 68 (1-2):43-65. doi:10.1016/S0024-4937(03)00030-6

Upton BGJ, Martin AR, Stephenson D (1990) Evolution of the Tugtutôq Central Complex, South Greenland: a high-level, rift-axial, late Gardar centre. Journal of Volcanology and Geothermal Research 43 (1-4):195-214

Upton BGJ, Parsons I, Emeleus CH (1996) Layered Alkaline Igneous Rocks of the Gardar Province, South Greenland. In: Cawthorn RG (ed) Layered intrusions. Elsevier Science Ltd., pp 331-364

Villemant B, Boudon G (1999) H2O and halogen (F, Cl, Br) behaviour during shallow magma degassing processes. Earth and Planetary Science Letters 168 (3-4):271-286. doi:10.1016/S0012-821X(99)00058-8

Wang L-X, Marks MAW, Wenzel T, Von Der Handt A, Keller J, Teiber H, Markl G (2014) Apatites from the Kaiserstuhl Volcanic Complex, Germany: new constraints on the relationship between carbonatite and associated silicate rocks. European Journal of Mineralogy. doi:10.1127/0935-1221/2014/0026-2377

Webster JD (1990) Partitioning of F between H2O and CO2 fluids and topaz rhyolite melt. Contributions to Mineralogy and Petrology 104 (4):424-438. doi:10.1007/bf01575620

Webster JD (1997) Exsolution of magmatic volatile phases from Cl-enriched mineralizing granitic magmas and implications for ore metal transport. Geochimica et Cosmochimica Acta 61 (5):1017-1029. doi:10.1016/s0016-7037(96)00395-x

Webster JD, Duffield WA (1994) Extreme halogen abundances in tin-rich magma of the Taylor Creek Rhyolite, New Mexico. Economic Geology 89 (4):840-850. doi:10.2113/gsecongeo.89.4.840

Webster JD, Holloway JR (1990) Partitioning of F and Cl between magmatic hydrothermal fluids and highly evolved granitic magmas. Geological Society of America Special Papers 246:21-34. doi:10.1130/SPE246-p21

Winterhalder A, Giehl C, Marks M, Nowak M Trace element partitioning in peralkaline iron-rich melts. In: GEOFLUIDS: Joint Annual Meeting of the German Mineralogical Society (DMG) and the Geologische Vereinigung (GV), Tübingen, Germany, 16th - 19th September 2013

Xiong X-L, Rao B, Chen F-R, Zhu J-C, Zhao Z-H (2002) Crystallization and melting experiments of a fluorine-rich leucogranite from the Xianghualing Pluton, South China, at 150 MPa and H2O-saturated conditions. Journal of Asian Earth Sciences 21 (2):175-188

Yoder HS, Tilley CE (1962) Origin of Basalt Magmas: An Experimental Study of Natural and Synthetic Rock Systems. Journal of Petrology 3 (3):342-532. doi:10.1093/petrology/3.3.342

Zhang C, Holtz F, Ma C, Wolff PE, Li X (2012) Tracing the evolution and distribution of F and Cl in plutonic systems from volatile-bearing minerals: a case study from the Liujiawa pluton (Dabie orogen, China). Contributions to Mineralogy and Petrology 164 (5):859-879. doi:10.1007/s00410-012-0778-9

A. Appendix

Title
Phase relations and liquid lines of descent of an iron-rich peralkaline phonolitic melt: an experimental study

Authors
Christopher Giehl, Michael Marks and Marcus Nowak

Status
Published in *Contributions to Mineralogy and Petrology* 165 (2): 283-304
(doi: 10.1007/s00410-012-0809-6)

Associate Editor
Jochen Hoefs

Reviewer
Renat Almeev, Bruno Scaillet and an anonymous reviewer

Contributions of the candidate

Scientific ideas	50 %
Experimental work	90 %
Analytical work	90 %
Analysis and interpretation	80 %
Preparation of manuscript	90 %

Contrib Mineral Petrol (2013) 165:283–304
DOI 10.1007/s00410-012-0809-6

ORIGINAL PAPER

Phase relations and liquid lines of descent of an iron-rich peralkaline phonolitic melt: an experimental study

Christopher Giehl · Michael Marks · Marcus Nowak

Received: 2 May 2012 / Accepted: 30 August 2012 / Published online: 9 October 2012

Abstract We experimentally investigated the phase relations of a peralkaline phonolitic dyke rock associated with the Ilímaussaq plutonic complex (South Greenland). The extremely evolved and iron-rich composition (magnesium number = 2, alkalinity index = 1.44, FeO* = 12 wt%) may represent the parental magma of the Ilímaussaq complex. This dyke rock is therefore perfectly suited for performing phase-equilibrium experiments, since in contrast to the plutonic rocks of the complex, no major cumulate formation processes complicate defining a reasonable starting composition. Experiments were carried out in hydrothermal rapid-quench cold-seal pressure vessels at $P = 100$ MPa and $T = 950$–750 °C. H_2O contents ranging from anhydrous to H_2O saturated ($\sim$5 wt% H_2O) and varying fO_2 ($\sim\Delta$logFMQ -3 to $+1$; where FMQ represents the fayalite–magnetite–quartz oxygen buffer) were applied. Reduced and dry conditions lead to substantial crystallization of alkali feldspar, nepheline, hedenbergite-rich clinopyroxene, fayalite-rich olivine and minor amounts of ulvøspinel-rich magnetite, which represent the phenocryst assemblage of the natural dyke rock. Oxidized and H_2O-rich conditions, however, suppress the crystallization of olivine in favor of magnetite and clinopyroxene with less or no alkali feldspar and nepheline formation. Accordingly, combined low fO_2 and aH_2O force the evolution of the residual melt toward decreasing SiO_2, increasing FeO* and alkalinity index (up to 3.55). On the contrary, high fO_2 and aH_2O produce residual melts with relatively low FeO*, high SiO_2 and a relatively constant alkalinity index. We show that variations of aH_2O and fO_2 lead to contrasting trends regarding the liquid lines of descent of iron-rich silica-undersaturated peralkaline compositions. Moreover, the increase in FeO* and alkalinity index (reduced and dry conditions) in the residual melt is an important prerequisite to stabilize late-magmatic minerals of the dyke rock, for example, aenigmatite ($Na_2Fe_5TiSi_6O_{20}$), coexisting with the most evolved melts at 750 °C. Contrary to what might be expected, experiments with high aH_2O and interlinked high fO_2 exhibit higher liquidus T's compared with experiments performed at low aH_2O and fO_2 for experiments where magnetite is liquidus phase. This is because ulvøspinel-poor magnetite crystallizes at higher fO_2 and has a higher melting point than ulvøspinel-rich magnetite, which is favored at lower fO_2.

Keywords Crystallization experiments · Phase relations · Liquid line of descent · Peralkaline · Phonolite · Ilímaussaq

Introduction

The investigation of phase equilibria is a powerful method to elucidate crystallization, differentiation and fractionation processes in magmatic systems. Previous experimental work on phase relations in igneous systems covers a range of whole-rock compositions like granites (Tuttle and Bowen 1958), alkali and tholeiitic basalts (Villiger et al. 2004; Berndt et al. 2005; Freise et al. 2009), ferro basalts (Toplis and Carroll 1995; Botcharnikov et al. 2008),

Communicated by J. Hoefs.

Electronic supplementary material The online version of this article (doi:10.1007/s00410-012-0809-6) contains supplementary material, which is available to authorized users.

C. Giehl (✉) · M. Marks · M. Nowak
Eberhard Karls Universität Tübingen,
Wilhelmstr. 56, 72074 Tübingen, Germany
e-mail: christopher.giehl@uni-tuebingen.de
URL: http://www.geo.uni-tuebingen.de/index.php?id=2179

gabbros (Feig et al. 2010), phonolites (Berndt et al. 2001; Freise et al. 2003; Andújar et al. 2008; Scaillet et al. 2008) and peralkaline rhyolites (Scaillet and MacDonald 2001, 2006; Di Carlo et al. 2010). Besides bulk chemistry, these studies emphasize a strong influence of P, aH_2O, fO_2 and halogens (Cl, F) on the phase relations and the evolution of the coexisting residual melt ("liquid line of descent").

Peralkaline igneous rocks are interpreted to be derived from highly fractionated alkali basaltic or nephelinitic magmas (e.g., Sørensen 1997; Larsen and Sørensen 1987; Markl et al. 2010, 2011) or from partial mantle melting (e.g., MacDonald et al. 1987). In such rocks, typical indicators of fractionation like Mg/(Mg + Fe) or Ca/(Na + K) approach zero documenting the extremely evolved character of such compositions (e.g., Bailey et al. 2001).

The liquid line of descent of peralkaline magmas covers an unusually large T interval, which is attributed to the retention of network modifiers like alkalis and volatiles in the melt (e.g., Piotrowski and Edgar 1970; Sood and Edgar 1970; Edgar and Parker 1974; Kogarko and Romanchev 1977). The interval between liquidus and solidus T is suggested to exceed 500 °C with several crystallizing phases, many of them being solid solutions. Peralkaline magmas are therefore highly suitable for the detailed experimental investigation concerning the crystallization sequence and the evolution of mineral–melt equilibria during cooling.

Geological background

The Ilímaussaq plutonic complex (South Greenland) represents an extreme example of a peralkaline intrusion and is part of the Proterozoic Gardar province, which is thought to be a failed rift setting (Upton et al. 2003). Details on the geology, petrology and geochemistry of the Ilímaussaq complex can be found in Bailey et al. (2001), Markl et al. (2001), Sørensen (2001) and Marks et al. (2004). The experimental investigation of the melt evolution of such a plutonic complex is challenging, because it is problematic to find a reasonable starting composition, since most rock units are affected by cumulate formation processes (Sørensen 2001). However, based on petrography, mineral chemistry and geochemistry, an iron-rich and peralkaline phonolitic dyke rock associated with the Ilímaussaq plutonic complex is suggested to represent an early separation of the intrusions' parental magma (Allaart 1969; Larsen and Steenfelt 1974; Marks and Markl 2003) and is therefore perfectly suited as a starting composition for phase-equilibrium experiments. The dyke has a length of several kilometers and a width of 10–30 m, is marginally chilled with no or little phenocrysts in the fine-grained matrix and is the focus of this study.

Petrographically, three phase assemblages can be distinguished in the dyke: (1) an early magmatic phenocryst assemblage with titano magnetite (Mag), fayalitic olivine (Ol), hedenbergite-rich clinopyroxene (Cpx), alkali feldspar (Afs), and nepheline (Nph) ± fluorite (Fl), apatite (Ap), zircon and titanite (Spn); (2) a late-magmatic groundmass, represented by albite (Ab) and microcline (Mc) as separate grains, Nph, sodalite (Sdl), aegirine-rich clinopyroxene, aenigmatite (Ae, $Na_2Fe_5TiSi_6O_{20}$) and arfvedsonite ± eudialyte (Eud) and hjordahlite (Hjo); and (3) a late-stage assemblage with analcime and natrolite. For textures of the dyke rock, see Figs. 2 and 3 in Marks and Markl (2003). These three stages of crystallization parallel those found in the Ilímaussaq plutonic rock sequences: the phenocryst dyke assemblage parallels with the early plutonic augite syenite phase, the dyke groundmass with the plutonic agpaitic main phase and the late-stage hydrothermal alterations are similar (with Anl and Ntr replacing Nph, Ab and Sdl) both in the dyke and the plutonic rocks of the intrusion. The composition of the early magmatic phenocrysts is remarkably similar to their plutonic counterparts (see Marks and Markl 2003 for details).

The depth of dyke emplacement was estimated to 3–5 km, roughly corresponding to $P = 100$ MPa (Poulsen 1964; Konnerup-Madsen and Rose-Hansen 1984). Nph thermometry indicates liquidus T's of at least 900 °C, and thermodynamic calculations imply extremely reducing conditions of ΔlogFMQ −3 to −1.5 during the formation of the phenocryst assemblage (Marks and Markl 2003). The presence of CH_4-rich fluid inclusions in the Ilímaussaq intrusion itself is in agreement with the low oxygen fugacity (fO_2) calculated from mineral phase equilibria (Konnerup-Madsen 2001; Marks and Markl 2001; Markl et al. 2001; Krumrei et al. 2007).

The aim of this study is to investigate the influence of coexisting fluid phases (cH_2O) and fO_2 on the phase relations and the liquid lines of descent of iron-rich silica-undersaturated peralkaline melts. We therefore conducted nominally dry experiments as well as fluid-bearing experiments with pure H_2O or H_2O–CO_2–CH_4 mixtures. Our experimental results elucidate the crystallization sequence and the evolution of the residual melt in such compositions. The results are compared with the observed phase assemblages in the dyke rock itself and the estimated T–cH_2O–fO_2 conditions of formation.

Starting material and experimental methods

Starting glasses for phase-equilibrium experiments were synthesized by mixing oxide and carbonate powders, diammonium phosphate, sodium chloride and fluorite (sources for P, Cl and F) according to the chilled margin

composition of the dyke rock (Table 1; Larsen and Steenfelt 1974). This composition is termed high alkali facies (HAF, Larsen and Steenfelt 1974) and resembles a low #Mg of 2 (the molar $Mg/(Mg + Fe^{2+})$ ratio), a high FeO* content of 11.86 wt% and a high alkalinity index of 1.44 (the molar $(Na_2O + K_2O)/Al_2O_3$ ratio, labeled A. I. in the following). It is compared with whole-rock compositions from previous experimental work in Fig. 1 (#Mg = 1–76; FeO* = 1.3–14.6; A. I. = 0.2–2.0) showing the lack of experimental data for iron-rich silica-undersaturated peralkaline compositions. It is worth mentioning that the investigated phonolites are, with one exception, not strongly peralkaline.

The powders were homogenized in a zirconia ball mill and fused at 1,600 °C (1 atm, 6 h) in an iron-saturated $Pt_{90}Rh_{10}$ crucible covered with a Pt lid, which was subsequently rapidly quenched in water. The glass pieces were ground to a grain size <300 µm, re-melted (1,600 °C, 1 atm, 1 h) to improve homogeneity and ground again (<300 µm). This glass will be referred to as oxidized starting glass (HAF ox). Half of the glass powder was re-melted in a graphite crucible jacketed with a corundum crucible at 1,200 °C (1 atm, 4 h) and quenched in air to a glass bead. During glass synthesis, the melt is in direct contact with the graphite crucible. To overcome possible zonation of XFe^{3+}, the surface was removed by cutting several millimeters roundly. Afterward, the bead was ground to the same grain size (<300 µm) and will be referred to as reduced starting glass (HAF red). Glass powder was used to promote nucleation of crystal phases in phase-equilibrium experiments. The relatively large grain size helps to minimize adsorbed H_2O, which is important for nominally dry experiments.

For the experiments, two types of capsules were used. The starting glasses dried at 120 °C were filled in gold (Au) capsules (length (*l*): 20 mm; outer diameter (od): 3 mm; wall thickness (wt): 0.25 mm), in large Au capsules for prehydration experiments (*l*: 30 mm; od: 5 mm; wt: 0.25 mm) and in graphite capsules (*l*: 20 mm; od: 4.5 mm; wt: 1.25 mm) encapsulated in Au capsules (*l*: 22 mm, od: 5 mm, wt: 0.25 mm), referred to as graphite (C) capsules in the following. This type of capsule is appropriate to avoid iron loss in high-*P* and high-*T* experiments (e.g., Kesson and Lindsley 1976; Holloway et al. 1992). Both types of capsules were filled with 50 mg glass powder (300 mg in

Table 1 Bulk composition of the dyke rock and composition of the starting glasses in wt%

Method	Ø Dyke rock[a] WC	HAF ox XRF	HAF ox EMP	HAF red EMP
n	3		18	6
#Mg	2	4	3	3
A. I.	1.44	1.40	1.45	1.50
SiO_2	52.91	53.70 (14)	54.72 (64)	53.91 (24)
TiO_2	0.54	0.56 (02)	0.52 (02)	0.53 (02)
ZrO_2	0.67	na	0.65 (09)	0.69 (05)
Al_2O_3	14.36	14.30 (06)	14.12 (21)	13.90 (18)
FeO*	11.86[b]	11.53[c] (06)	11.51[d] (29)	12.23[d] (48)
XFe^{3+}	0.63[e]	0.61[f] (01)	0.61[f] (01)	0.45[f] (01)
FeO	4.39	4.50	4.49	6.73
Fe_2O_3	8.30	7.81	7.80	6.11
MnO	0.44	0.44 (01)	0.46 (03)	0.50 (02)
MgO	0.17	0.25 (14)	0.19 (02)	0.20 (04)
CaO	2.79	2.91 (10)	2.84 (08)	3.01 (20)
Na_2O	9.25	9.01 (07)	9.40 (27)	9.45 (32)
K_2O	5.03	4.75 (04)	4.69 (11)	4.92 (25)
P_2O_5	0.13	0.21 (01)	0.13 (03)	0.11 (04)
Cl	0.31	na	0.06 (01)	0.05 (01)
F	0.91	na	0.17 (05)	0.16 (06)
Total	100.00	98.69	99.53 (92)	100.35 (38)
LOI		−0.30		

HAF ox oxidized starting glass, *HAF red* reduced starting glass, *WC* wet chemical analysis, *EMP* electron microprobe analysis ($\pm 1\sigma$), *n* number of analysis, *na* not analyzed, *FeO** total iron oxide, $XFe^{3+} = Fe^{3+}/(Fe^{2+}+Fe^{3+})$

[a] Average from three whole-rock analysis from the chilled margin of the dyke rock (Larsen and Steenfelt 1974; normalized to 100 wt%); [b] calculated from $FeO + Fe_2O_3$; [c] calculated from Fe_2O_3 and XFe^{3+}; [d] analyzed with EMP; [e] calculated from $FeO + Fe_2O_3$; [f] determined by Mössbauer spectroscopy

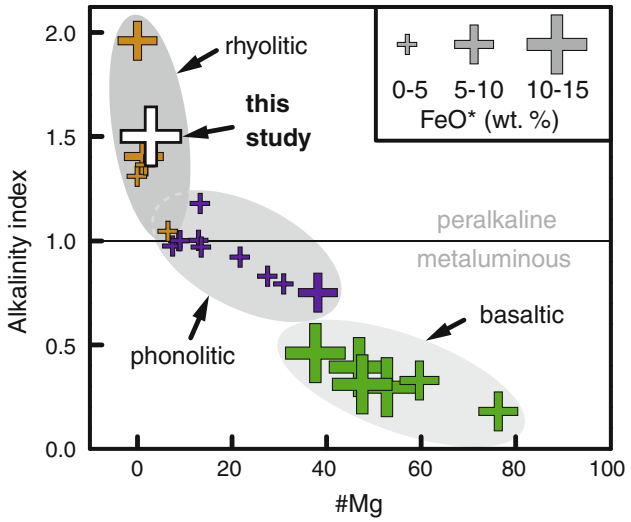

Fig. 1 Experimentally investigated bulk compositions compared in terms of #Mg and A. I. (Toplis and Carroll 1995; Berndt et al. 2001; Scaillet and MacDonald 2001; Freise et al. 2003; Villiger et al. 2004; Scaillet and MacDonald 2006; Andújar et al. 2008; Botcharnikov et al. 2008; Scaillet et al. 2008; Freise et al. 2009; Di Carlo et al. 2010; Feig et al. 2010). The size of the *symbols* represents the FeO* content (wt%) of the investigated composition, subdivided into three groups

prehydration experiments) and welded shut. Possible leakage was gravimetrically checked by (1) heating H_2O-bearing capsules at 120 °C for 4 h or (2) placing nominally dry capsules in an ultrasonic bath for 2 min, subsequently controlled for loss or gain of H_2O, respectively.

We performed seven series of experiments using three types of starting glasses (Table 2). As mentioned by Feig et al. (2006), nominally dry experiments may contain up to 0.5 wt% H_2O and the presence of even small amounts of H_2O can strongly lower the liquidus T (see also Almeev et al. 2007; Médard and Grove 2008). In the following, we will distinguish between H_2O-bearing (run 30–69) and nominally dry (run 70–95) experiments (denoted dry in the following for convenience).

Experiments in Au capsules are labeled oxidized, and those in C capsules are labeled reduced, respectively. H_2O-bearing experiments at 950 °C were prepared with dried glass powder (HAF ox) and different amounts of H_2O (1–8 wt%). For lower T (850 and 750 °C), hydrated glass from 950 °C experiments was used as starting glass, and an additional fluid phase (1 wt% H_2O) was added. Dry experiments were prepared using anhydrous glass powder (HAF ox and HAF red) without adding H_2O. To check reproducibility and sufficient experiment duration, we repeated dry experiments and varied the experiment duration from 168 to 504 h.

Experiments were conducted in vertically mounted cold-seal pressure vessels (CSPV) made of a nickel–chromium alloy (Inconel 713LC) pressurized by water. We performed experiments at $P = 100$ MPa and $T =$ 750–950 °C in 50 °C steps. T was measured with a K-type thermocouple outside the vessel close to the sample position and found to be constant during the experiments within an uncertainty of ±5 °C. The experiments were stopped by isobaric rapid quenching (ca. 200 °C/s; e.g., Berndt et al. 2002) controlled with an increase in pressure due to the dropped hot capsule expanding H_2O in the cold part of the autoclave.

After the experiments, capsules were reweighed to confirm closed-system behavior during the experiments. Subsequently, capsules were opened and several sample pieces from different parts of the capsule were mounted in epoxy resin, polished and carbon-coated for electron microprobe (EMP) analysis. Whenever possible, cross sections of glass cylinders were prepared to check the experimental products for homogeneity.

Interrelation of capsule material, cH_2O and fO_2

Oxidizing conditions were adjusted in Au capsules at H_2O-saturated conditions close to NNO ($\sim\Delta$logFMQ +0.8 for the investigated T interval; where NNO is the nickel–nickel oxide oxygen buffer and FMQ is the fayalite–magnetite–quartz oxygen buffer; Schwab and Kuestner 1981; O'Neill 1987a, b). The intrinsic fO_2 ($\sim\Delta$logFMQ +0.8) and fH_2 are superimposed by the autoclave alloy in equilibrium

Table 2 Experiment series

	H_2O bearing			Dry			
Starting glass	HAF ox	Hydrated glass ox		HAF ox	HAF ox	HAF red	HAF red
cH_2O (wt%) of the starting glass	Dry	1.6–4.7		Dry			
Redox conditions	Oxidized	Oxidized	Reduced	Oxidized	Reduced	Oxidized	Reduced
T (°C)	950	850, 750		950, 900, 850, 800, 750			
H_2O added (wt%)	1–8	1	1	–	–	–	–
Experiment duration (h)	24	4		168–504			
n	8	13	12	5	5	7	6

HAF ox oxidized starting glass, *HAF red* reduced starting glass, n number of experiments, *Hydrated glass ox* material from run 30, 31, 33, 34, 35, 36, 37, 39; see Table 3

Contrib Mineral Petrol (2013) 165:283–304 287

with the pressure medium H_2O. As H_2 diffuses through Au, fO_2 is imposed in the capsule for H_2O-saturated conditions.

Experiments with aH_2O <1 are usually conducted using fluid-saturated conditions with mixed H_2O–CO_2 fluids (with $Ag_2C_2O_4$ as CO_2 source; e.g., Freise et al. 2009; Di Carlo et al. 2010). We established H_2O undersaturation by adjusting cH_2O in the starting fluid assuming the solubility of H_2O ($aH_2O = 1$) at $P = 100$ MPa. As demonstrated in other studies, fH_2O decreases with decreasing XH_2O and leads, based on the dissociation reaction of H_2O, to an exponential decrease in fO_2 (Scaillet et al. 1995; Freise et al. 2009; Feig et al. 2010). We can presume a relatively constant fO_2 within one log unit for XH_2O >0.5 but a strong decrease in several log units for XH_2O <0.2 in Au capsules (Webster et al. 1987).

Reduced conditions in C capsules were assessed for both dry and H_2O-bearing experiments. The fO_2 in dry experiments can be, given the absence of hydrogen, described with the carbon–carbon oxide oxygen buffer (CCO, French and Eugster 1965; Jakobsson and Oskarsson 1994) and define fO_2 to $\sim\Delta$logFMQ -1 to -2 for the T interval applied in the experiments. In Au capsules, the coexisting fluid is H_2O dominated ($\pm H_2$ and O_2), but in H_2O-bearing C capsule experiments, H_2O and C (available in excess: $aC = 1$) form a COH fluid which consists mainly of H_2O, CO_2 and CH_4, if internally buffered (eFig. 1). The speciation of the fluid can be calculated assuming a fixed atomic H/O ratio; thus, for the experiments, we used pure water. This is, however, a simplification as a hydrothermal experimental setup is a system not closed to hydrogen and H_2O fugacity coefficients may vary through the influence of Cl (Aranovich and Newton 1996). The aH_2O and fO_2 are decreased and fH_2 is increased in these experiments. This coincides with generally lower cH_2O of the residual melt in C capsules with equal amounts of H_2O added as fluid (Table 3). When C and the COH fluid are in equilibrium, they buffer fO_2 to about ΔlogFMQ $= -2$ to -2.5 for the investigated T interval (eFig. 1, French 1966; Ohmoto and Kerrick 1977; Huizenga 2001). Reduced H_2O-bearing experiments therefore feature the requested fluid speciation (H_2O, CO_2 and CH_4) and prevailing fO_2 in contrast to oxidized conditions with a H_2O fluid. However, dry and reduced experiments will not be thoroughly hydrogen-free and the COH fluid in H_2O-bearing C capsule experiments will equilibrate toward the intrinsic fH_2 by means of losing H_2 through outward diffusion. Even though the quantification of fluid speciation cannot be the aim of this study, the CCO and the COH buffer roughly border the prevailing fO_2 in C capsule experiments. H_2O-bearing C capsule experiments conducted in an internally heated pressure vessel were recently found to run dry. This might be explained by higher experimental T and fO_2 compared with this study resulting in fast outward diffusion of H_2 through the capsule material and consecutive fluid re-equilibration at the expense of H_2O or the speciation of the COH fluid being CO_2 rich and H_2O poor (Husen et al. 2012). In those experiments, T (>1,000 °C) and the intrinsic fO_2 are significantly higher ($\sim\Delta$logFMQ +4.2 in IHPV; Berndt et al. 2002; compared to $\sim\Delta$logFMQ +0.8 in CSPV; O'Neill 1987a, b), resulting in a lower intrinsic fH_2. We suggest that outward diffusion of H_2 is more effective at higher T and an increased fH_2 gradient between capsule and pressure medium. To minimize this problem, run durations of H_2O-bearing C capsule experiments were kept short (4 h), and in order to rapidly establish a coexisting COH fluid, 1 wt% H_2O was added in experiments with hydrated glass as starting material.

Analytical methods

For XRF analysis of the starting glass HAF ox, the glass powder was ground with an agate mill for 10 min. Loss on ignition (LOI) was determined at 1,000 °C. For the fused beads, 1.5 g of dried glass powder (at 105 °C) was mixed with 7.5 g MERCK spectromelt A12 (mixture of 66 % Li-tetraborate and 34 % Li-metaborate) and melted at 1,200 °C to fused beads using an Oxiflux system from CBR analytical service. Major and trace elements were analyzed with a Bruker AXS S4 Pioneer (Rh-tube at 4 kW).

The XFe^{3+}'s of both starting glasses (ground to <125 µm) were determined with ^{57}Fe-Mössbauer spectroscopy using a ^{57}Co source in Rh matrix operated at room T. The spectra were calibrated against α-Fe(0) foil and interpreted with the RECOIL software package (University of Ottawa, Canada).

Starting glasses, residual glasses and crystal phases of the experimental products were analyzed using a JEOL 8900 electron microprobe. The emission current was 20 nA for Mag, Cpx and Ol; 8 nA for Afs and Nph; and 4 nA for glasses. We used an acceleration voltage of 15 kV; some small Mag crystals were analyzed with 10 kV. For calibration, natural and synthetic standard materials were used. The counting times were 16 s for major elements and 30–60 s for trace elements. A focused beam was used for Mag, Cpx and Ol. In order to minimize sodium migration, counting times were kept short and a defocused beam was used for Afs, Nph (8 s, 2 µm) and glasses (10 s, 20–10 µm). The sodium signal was monitored during analysis and found to be stable for the applied conditions. Similar to other experimental studies (e.g., Freise et al. 2003; Scaillet and MacDonald 2003, 2006; Feig et al. 2006; Freise et al. 2009), the size of the crystal phases is too small for EMP analysis in many cases, leading to contamination from the surrounding residual

Table 3 Experimental conditions, run products and phase proportions of the experiments

Run	Run time (h)	T (°C)	aH_2O[a] (a.u.)	fO_2[a] (ΔlogFMQ)	H_2O added (wt%)	H_2O_{melt}[b] (wt%)	Capsule	Phase proportions[c]
H_2O-bearing experiments (with oxidized starting glass: HAF ox)								
30	24	950	0.1	−0.9	1	1.3	Au	Gl(96) Mag(4)
31	24	950	0.4	−0.1	2	2.3	Au	Gl(96) Mag(4)
34	24	950	0.4	0.1	4	2.7	Au	Gl(97) Mag(3)
33	24	950	0.4	0.1	3	2.7	Au	Gl(96) Mag(4)
39	24	950	0.7	0.4	8	3.6	Au	Gl(97) Mag(3)
36	24	950	0.9	0.7	6	3.9	Au	Gl(96) Mag(4)
35	24	950	0.8	0.6	5	4.1	Au	Gl(97) Mag(3)
37	24	950	0.9	0.7	7	4.5	Au	Gl(96) Mag(4)
H_2O-bearing experiments (with hydrated or saturated starting glass: run 30–37)								
54^{R34}	4	850	0.2	−0.7	1	1.5	Au	Gl(83) Mag(5) Cpx(12)
52^{R31}	4	850	0.3	−0.4	1	2.0	Au	Gl(71) Mag(5) Cpx^{na}(24)
51^{R30}	4	850	0.3	−0.3	1	2.0	Au	Gl(65) Mag(4) Cpx^{na}(31)
53^{R33}	4	850	0.3	−0.3	1	2.0	Au	Gl(83) Mag(6) Cpx(11)
55^{R35}	4	850	0.4	−0.2	1	2.0	Au	Gl(75) Mag(4) Cpx^{na}(21)
57^{R37}	4	850	0.5	0.2	1	3.0	Au	Gl(74) Mag(5) Cpx^{na}(21)
56^{R36}	4	850	0.5	0.3	1	3.0	Au	Gl(84) Mag(5) Cpx(11)
48^{R36}	4	750	0.9	0.7	1	4.5	Au	Gl(86) Mag(6) Cpx^{na}(8)
47^{R35}	4	750	0.9	0.7	1	5.0	Au	Gl(86) Mag(5) Cpx^{na}(9)
49^{R37}	4	750	1.0	0.8	1	5.5	Au	Gl(87) Mag(6) Cpx^{na}(7)
44^{R31}	4	750	1.1[d]	0.9[d]	1	6.0	Au	Gl(65) Mag(6) Cpx^{na}(29)
45^{R33}	4	750	1.2[d]	0.9[d]	1	6.0	Au	Gl(89) Mag(6) Cpx^{na}(5)
46^{R34}	4	750	1.2[d]	1.0[d]	1	6.0	Au	Gl(87) Mag(4) Cpx^{na}(9)
64^{R30}	4	850	–	−2.3	1	0.0	C	Gl(78) Mag(2) Cpx^{na}(19) Afs(1)
65^{R31}	4	850	–	−2.3	1	0.5	C	Gl(82) Mag^{na}(3) Cpx^{na}(14) Afs(1)
69^{R37}	4	850	–	−2.3	1	0.5	C	Gl(85) Mag^{na}(5) Cpx^{na}(10)
68^{R36}	4	850	–	−2.3	1	0.5	C	Gl(85) Mag^{na}(5) Cpx^{na}(10)
67^{R35}	4	850	–	−2.3	1	1.0	C	Gl(83) Mag^{na}(4) Cpx^{na}(13)
66^{R34}	4	850	–	−2.3	1	1.5	C	Gl(85) Mag(4) Cpx^{na}(11)
58^{R30}	4	750	–	−2.0	1	–	C	Gl(64) Mag(5) Cpx(5) Afs(26)
61^{R34}	4	750	–	−2.0	1	0.5	C	Gl(71) Mag(3) Cpx^{na}(13) Afs(13)
59^{R31}	4	750	–	−2.0	1	0.5	C	Gl(69) Mag(4) Cpx(8) Afs(19)
60^{R33}	4	750	–	−2.0	1	1.0	C	Gl(65) Mag(3) Cpx^{na}(9) Afs(23)
62^{R37}	4	750	–	−2.0	1	1.5	C	Gl(72) Mag(5) Cpx^{na}(23)
Dry experiments (with oxidized starting glass: HAF ox)								
72*	504	950	0.4	−0.1	–	2.5	Au	Gl(100)[c]iron loss: 66 %
90*	504	900	0.0	−3.1	–	0.5	Au	Gl(99) Mag^{na}(<1) Cpx(1)
71	504	850	0.1	−1.5[f]	–	1.0	Au	Gl(87) Mag(<1) Cpx(4) Afs(6) Ol(3)
86	504	800	0.1	−1.8	–	0.5	Au	Gl(48) Mag(2) Cpx(24) Afs^{na}(24) Nph(2)
70	504	750	–	–	–	nc	Au	Gl(28) Mag(4) Cpx^{na}(22) Afs(34) Nph(12)
92	504	900	–	−1.9[e]	–	0.5	C	Gl(81) Cpx(4) Afs(12) Ol(3)
74	504	850	–	−1.8[e]	–	0.0	C	Gl(60) Mag^{na}(<1) Cpx(9) Afs(22) Ol(4) Nph(5)
88	504	800	–	−1.7[e]	–	0.0	C	Gl(38) Mag^{na}(<1) Cpx(11) Afs(32) Ol(4) Nph(15)
94	504	800	–	−1.7[e]	–	0.0	C	Gl(37) Mag^{na}(<1) Cpx(10) Afs(35) Ol(5) Nph(13)
73	504	750	–	−1.5[e]	–	na	C	Gl^{na}(20) Mag(4) Cpx(24) Afs(41) Nph(11)

Table 3 Experimental conditions, run products and phase proportions of the experiments

Run	Run time (h)	T (°C)	aH_2O[a] (a.u.)	fO_2[a] (ΔlogFMQ)	H_2O added (wt%)	H_2O_{melt}[b] (wt%)	Capsule	Phase proportions[c]
Dry experiments (with reduced starting glass: HAF red)								
79*	504	950	0.8	0.6	–	4.5	Au	Gl(100)[c]iron loss: 69 %
91*	504	900	0.0	−4.6	–	0.0	Au	Gl(99) Mag[na](< 1) Cpx[na](1)
78	504	850	0.0	−2.0	–	0.5	Au	Gl(66) Mag(4) Cpx(12) Afs(18)
87	504	800	0.0	−4.3	–	0.0	Au	Gl(31) Mag[na](<1) Cpx(27) Afs[na](33) Ol(2) Nph(7)
83	168	750	–	–	–	na	Au	Gl[na](37) Mag(1) Cpx[na](9) Afs(47) Nph(6) Ae(< 1)
84	336	750	–	–	–	na	Au	Gl[na](42) Mag(1) Cpx[na](6) Afs(45) Nph(5) Ae(1)
77	504	750	–	−0.8[f]	–	na	Au	Gl[na](25) Mag(1) Cpx(27) Afs[na](34) Ol(1) Nph(10) Ae(2)
82	504	950	–	−2.0[e]	–	1.5	C	Gl(100)[c]iron loss: 0 %
93	504	900	–	−1.9[e]	–	0.5	C	Gl(98) Mag(2)
81	504	850	–	−1.8[e]	–	0.0	C	Gl(38) Mag[na](<1) Cpx(14) Afs(37) Ol(6) Nph(5)
95	504	800	–	−2.9[f]	–	0.0	C	Gl(45) Mag(<1) Cpx(10) Afs(29) Ol(5) Nph(12)
85	168	750	–	−1.5[e]	–	1.5	C	Gl(33) Mag[na](<1) Cpx[na](9) Afs(40) Ol(3) Nph(13) Ae(2)
80	504	750	–	−1.5[e]	–	nc	C	Gl(32) Mag[na](<1) Cpx[na](5) Afs(51) Ol(4) Nph(5) Ae(3)

The experimental pressure is $P = 100$ MPa in all experiments; *Abbreviations Gl glass*, *Mag* titano magnetite, *Cpx* clinopyroxene, *Afs* alkali feldspar, *Ol* olivine, *Nph* nepheline, *Ae* aenigmatite

[a] H_2O activity (aH_2O) and oxygen fugacity (fO_2) in Au capsules are roughly estimated from the solubility model of Burnham (1979), estimations for C capsules can be found in eFig. 1 for aH_2O and in Fig. 10 for fO_2 (see also experimental methods)

[b] H_2O content analyzed with the by-difference method, except run 30–39 (analyzed with KFT)

[c] Phase proportions (wt%) calculated from image analysis or mass balance

[d] aH_2O is higher than 1 due to the error of the by-difference method (±0.5 wt%)

[e] fO_2 estimated as average between COH and CCO oxygen buffers

[f] fO_2 estimated from QUILF95 calculations

na H_2O content not analyzed successfully; *nc* H_2O content not considered

* Iron loss to the capsule material was calculated by ($FeO^*_{melt}/FeO^*_{starting\ glass}$) * 100 for superliquidus experiments

^{RXX} indicates that material from run XX was used as starting glass

glass. To ensure high quality data, we only used EMP data (eTab. 1) that fulfilled the requirements listed in eTab. 2 and gave reasonable structural formulas (eTab. 3–8).

Relatively high Fe_2O_3 contents of up to 3.3 wt% (eTab. 5) in Afs can be explained by the incorporation of an iron-orthoclase component ($KFeSi_3O_8$, e.g., Ackermann et al. 2004) or by contamination with the surrounding iron-rich residual glass. We compared the concentrations of Fe_2O_3 (<0.1 wt% in Afs of the dyke rock) and TiO_2 (as contaminant) analyzed in Afs analyses relative to the surrounding glass and suggest that the linear correlation between the ratios implies contamination of Afs with the surrounding glass of up to 25 % and a maximum "true" Fe_2O_3 content of 1 wt% (eFig. 2). This is similarly observed for Nph considering an iron-nepheline component, respectively ($NaFeSiO_4$, e.g., Bailey and Schairer 1966); some Nph show even higher contamination than Afs. This and frequently observed Afs inclusions may explain the relatively high SiO_2 content of some Nph analyses.

To estimate the phase proportions, back-scattered electron (BSE) images of all experiments were analyzed quantitatively with the software ImageJ (ver. 1.42q, Abramoff et al. 2004). Where EMP analysis was not possible (crystal size <2 μm), Mag, Cpx and Afs were identified qualitatively. As BSE image analysis only provides two-dimensional surface intersections of the sample, the observed crystal sizes should be considered minimum estimates. Compared with spherical or near-spherical crystal phases, the quantification of non-spherical crystal phases comprises a larger error. For simplicity, the analyzed

area was assumed to be equal with volume relations. Mineral phase densities (Deer et al. 1992) and glass densities (Kloess 2000) were used to calculate weight percent phase proportions. The uncertainty of image analysis was not quantified in detail, but shows deviations up to 5 wt% quantifying different images of the same experiment. Whenever the complete mineral phase assemblage and the residual glass were successfully analyzed, we performed mass balance multiple linear regression analysis (least squares fit) using starting glass data (normalized to 100 wt%) to estimate phase proportions. The standard error of mass balance calculations is always <1 wt%. Image analysis and mass balance calculations of phase proportions were compared and found to be similar (eFig. 3). Still, deviations are smaller for near-spherical crystal phases (Mag, Ol, Nph and Ae) compared with non-spherical crystal phases (Cpx, Afs) being overestimated by image analysis. On account of the smaller error, mass balance is favored over image analysis, whenever the calculation is possible. Trends in the evolution of phase proportions are not significantly affected by the use of the two different methods.

H_2O contents of the starting and residual glasses were determined with the by-difference method by calculating the difference between the sum of the element oxides based on EMP analysis and 100 wt% (Devine et al. 1995). To check whether the by-difference method is reliable, bulk H_2O contents of HAF ox and experiments 30–37 were determined by Karl Fischer titration (KFT, Behrens 1995). For the latter method, H_2O contents were corrected for small amounts of Mag (<4.5 wt%, calculated with mass balance) present in these experiments.

Starting glasses, hydrated glasses and H_2O contents

Both starting glasses (HAF ox and HAF red) are bubble- and crystal-free and homogeneous. Similar compositions analyzed with XRF and EMP underline large-scale and small-scale homogeneity and indicate that no significant sodium migration during EMP analysis occurred (Table 1). Chlorine (Cl) and fluorine (F) contents are significantly lower (decreased by 80 % relative) compared with the average dyke rock. This is attributed to their volatility during high-T glass synthesis, similarly reported by Lukkari and Holtz (2007) for F. The decrease should only have a minor effect on the phase relations and phase compositions of the halogen-free phenocrysts. However, liquidus and solidus T might be increased by some tens of degrees in the experiments as it was found for granitic systems (Manning 1981). Furthermore, saturation of Cl- and F-bearing accessories (e.g., Ap, Fl) could be missed. Thus, the remaining element oxides are relatively increased, but remain within error except for SiO_2 (increased by ~2 wt%). The ferric–ferrous ratio of iron is roughly 2:1 in the oxidized and 1:1 in the reduced starting glass (Table 1).

Pre-hydrated glasses contain 1.6–4.7 wt% H_2O analyzed with KFT, recalculated for small amounts of Mag. The H_2O content calculated based on the by-difference method reveals similar concentrations. However, the large scatter of 1–2 wt% H_2O is due to the combined effects of the estimated $X\mathrm{Fe}^{3+}$ (up to ±0.5 wt% H_2O) and potentially analyzing microcrysts below the BSE detected surface (eFig. 4). Some experiments show apparently negative H_2O contents (run 58, 70 and 80; eTab. 2), which might be due to the relatively large statistical standard deviation (>±1 wt%) calculated from multiple data points (n = 3–13). An explanation for total values >101 wt% could be crystal phases in the interaction volume below the surface, especially in small residual melt pockets. Indeed, these totals correlate with highly crystallized experiments at ≤800 °C with 28–64 wt% residual melt. These by-difference H_2O contents observed in four experiments are highly uncertain and thus not considered in the following.

Iron loss to the capsule material

Iron loss to the capsule material in high-P/T experiments is a well-known problem, especially when using Pt or $Au_{80}Pd_{20}$ capsules (e.g., Green and Ringwood 1967). In comparable experimental work, iron loss is prevented by pre-saturation of the capsule material with iron (e.g., Ford 1978; Freise et al. 2009). In contrast, Au was found to be less problematic for iron loss (e.g., Botcharnikov et al. 2008). However, for high T, low fO_2 and especially low sample/capsule mass ratios, iron loss to Au capsules was suggested to be significant (Ratajeski and Sisson 1999). Our sample/capsules mass ratio for Au capsule experiments is <0.1, which is thought to result in significant iron loss for ΔlogFMQ <+1 (Ratajeski and Sisson 1999). Au capsules of experiments with the highest T (950 °C) and different H_2O contents (run 30–37) were analyzed for iron with the EMP and persistently found to be <240 ppm Fe. We attribute this to the oxidizing effect of H_2O and the almost one order of magnitude higher FeO* content of our starting composition, resulting in higher apparent sample/capsule mass ratios. Some dry experiments in Au capsules at ≥900 °C show a significant decrease in FeO* (900 °C, run 90 and 91: ~33 %; 950 °C, run 72 and 79: ~55 %) and unusually increased #Mg of up to 9 in the residual melt that cannot be explained by coexisting crystal phases. For super-liquidus experiments, iron loss was directly calculated by comparing FeO* of the starting glass with FeO* of the melt (run 72, 79, 82; Table 3). An attending effect of iron loss is the production of oxygen (Eq. 1) and the consecutive production of H_2O through the reaction with hydrogen provided from the pressure medium (Eq. 2).

$$2FeO_{(melt)} \leftrightarrow 2Fe^{0}_{(capsule)} + O_{2(melt)} \quad (1)$$

$$2H_2O_{(melt)} \leftrightarrow 2H_{2(membrane)} + O_{2(melt)} \quad (2)$$

Initially dry experiments with the highest iron loss therefore show H_2O contents of 2.5 and 4.5 wt%, respectively, that can only be explained with the aforementioned mechanism. For $T \leq 850$ °C, the FeO* content of the residual melt in Au capsules is comparable to experiments in C capsules, #Mg is ≤3, and mass balance uncertainties are low.

In C capsules, this problem is less severe while there is no direct contact between Au capsules and melt. Even though we have no indication for iron loss in C capsules (run 82; Table 3), iron might permeate through C capsules by means of a fluid phase. Iron loss is suggested to be negligible for our experiments in C capsules, for H_2O-bearing experiments in Au capsules and for dry experiments in Au capsules at $T \leq 850$ °C.

Attainment of equilibrium

Near-equilibrium conditions were confirmed by euhedral to subhedral equally distributed and chemically homogeneous crystal phases (Fig. 2), multiple EMP analysis of crystal phases and residual glasses, and the error of mass balance calculation residuals (eTab. 2). Only highly crystallized experiments show residual melt pockets surrounded by crystals, still chemical homogeneity of the coexisting phases is maintained.

Repeated experiments (800 °C, HAF ox, dry, reduced) were found to yield similar phase assemblages, proportions and compositions. Varying the experimental duration from 168 to 504 h did not show significant differences when we examined run 85 and 80 (750 °C, HAF red, dry, reduced). Nevertheless, the variation form 168 to 504 h in run 84, 83 and 77 showed a significant increase in crystal size, and in the 504 h experiment, Ol as additional crystal phase is observed (750 °C, HAF red, dry, reduced). Due to its low abundance (<1 wt%), small crystal size, similarity to Mag in BSE images and the high crystallinity of dry runs at 750 °C (>58 wt%), Ol may have been overlooked or was simply not intersected during preparation in the experiments with shorter run durations.

The variability of #Mg mentioned above for Mag and Cpx may be pulled up to argue for disequilibrium. For Mag, it can simply be explained by analytical limitations as MgO is <0.2 wt% in Mag, and therefore, the analytical error exceeds the observed variability. For Cpx, this is not the case, but $X\mathrm{Fe}^{3+}$ shows large variations and this affects #Mg, as it is calculated from $\mathrm{Mg}/(\mathrm{Mg} + \mathrm{Fe}^{2+})$. Unusually high #Mg were also reported for iron-rich peralkaline rocks of the Katzenbuckel volcano and accounted to severe changes in $X\mathrm{Fe}^{3+}$ (Mann et al. 2006).

In preliminary oxidized H_2O-bearing experiments, the run duration was varied from 1 h to 168 h. Neither the size of crystal phases nor their compositions were observed to be significantly different for runs with 4 h or longer. H_2O-bearing experiments were therefore stopped after 4 h.

For reduced H_2O-bearing experiments, redox equilibration needs to be evaluated separately. The use of pre-hydrated starting material allows for fast equilibration with the fluid, but small amounts of Mag are inherited from pre-hydration experiments. The experimental fO_2 in reduced H_2O-bearing runs should be some 3 log units lower than for the pre-hydration experiments. XUsp in Mag is prone to indicate changes in fO_2, but remains unchanged compared with the pre-hydrated runs. To conclude, restricted to reduced H_2O-bearing runs, maybe equilibrium was not fully obtained. We recommend considering these runs critical.

Results

Most of the experiments are located within the supersolidus-subliquidus T interval, and few are located above the liquidus. Run conditions, run products, the H_2O content of the residual glasses and phase proportions of the experiments are listed in Table 3.

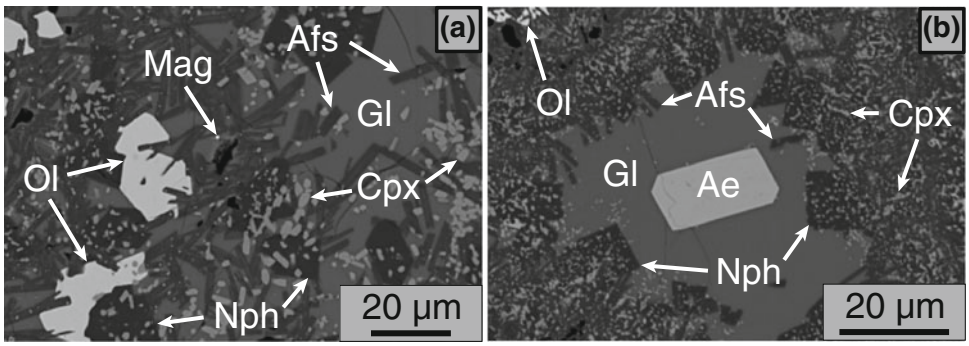

Fig. 2 BSE images of dry and reduced experiments. **a** Run 95, 800 °C, with the complete phenocryst phase assemblage of the dyke rock, and **b** run 85, 750 °C, with aenigmatite. Crystal phases are abbreviated as Mag *titano magnetite*, Cpx *clinopyroxene*, Afs *alkali feldspar*, Ol *olivine*, Nph *nepheline* and Ae *aenigmatite*

Phase compositions

Detailed phase proportions and compositions (eTab. 1), as well as formula calculations (eTab. 3–8) and residual glass data (eTab. 9) of the various experiments are given in the electronic appendix. For the illustration of crystal and residual melt compositions, we used the average values of multiple EMP analyses (n = 1–20; eTab. 1). The observed crystal phases mimic the phenocryst assemblage of the dyke rock (Fig. 2a; run 95), and a run with stable Ae (Fig. 2b; run 85) is shown in BSE images.

Isometric Mag (1–10 μm) is present throughout the H_2O-bearing experiments and is observed in dry experiments at $T \leq 900$ °C. It represents nearly pure magnetite–ulvøspinel (Fe_3O_4-Fe_2TiO_4, Mag–Usp) solid solutions (Fig. 3a) with minor amounts of Al_2O_3, MnO and MgO (<1 wt%). The #Mg roughly decreases with decreasing T, but the trend is not well defined (Fig. 4). In H_2O-bearing experiments, XUsp is <0.15. In contrast, dry experiments contain Mag with XUsp up to 0.82, and XUsp decreases with decreasing T. Comparing H_2O-bearing and dry experiments, Al_2O_3 is lower and MnO is higher in dry experiments. In reduced H_2O-bearing experiments, Mag is slightly rounded (see below).

Cpx is prismatic (1–10 × 5–50 μm) and occurs in all experiments below 950 °C except run 93. In H_2O-bearing experiments, Cpx is in most cases too small for EMP analysis; in dry experiments Cpx is generally larger. It represents nearly pure hedenbergite–aegirine ($CaFeSi_2O_6$ $NaFeSi_2O_6$, Hd–Aeg) solid solutions (Fig. 3b). MgO is below 2.2 wt% and #Mg is positively correlated with T (Fig. 4), and still this trend shows considerable scatter, even more pronounced than for Mag. XAeg increases with decreasing T from 0.1 at 900 °C to 0.4 at 750 °C. ZrO_2 content is increasing up to 1.7 wt% with decreasing T.

Isometric Ol (5–20 μm, Fig. 3c) occurs only in dry experiments between 900 and 750 °C and approaches fayalitic end member composition (XFa >0.9). The #Mg (2–4) is positively correlated with T, and the tephroite content (XTe = 0.05–0.07) is relatively constant (Fig. 4).

Ae is present in 750 °C experiments using the reduced starting glass. Isometric crystals are up to 20 μm in diameter. It can be described as aenigmatite–wilkinsonite solid solution with minor amounts of rhönite (Fig. 3d; Kunzmann 1999). Ae is found in residual melt pockets in experiments with less than 50 wt% residual melt with an A. I. >2.9 (Fig. 2b).

Afs is tabular (1–10 × 10 – 50 μm) and therefore shows similar analytical problems as Cpx (see above). In dry experiments, Afs occurs at $T \leq 850$ °C, in one experiment (run 92) even at 900 °C. The occurrence of Afs is restricted to low cH_2O for $T \leq 850$ °C. It represents an intermediate Ab–Or solid solution (Fig. 3e). XAn (0.05–0) and XAb (0.64–0.56) decrease and XOr (0.33–0.43) increases with decreasing T (900–750 °C).

Isometric Nph (10–30 μm) is only present at $T \leq 850$ °C in dry experiments. Nph composition can be characterized as nearly pure Nph with minor amounts of kalsilite (Kls) and excess SiO_2 (Fig. 3f). Small inclusions of Cpx and/or Afs in Nph are common.

Residual glass compositions

Residual glass is present in all experiments; therefore, the solidus T is <750 °C. Dry experiments comprise at least 20 wt% residual melt (Table 3). As the H_2O content and the interlinked fO_2 have a strong influence on the amount of residual melt at a certain T, the experiments are compared best in terms of the amount of residual melt (wt%). In contrast to other experimental work, #Mg as a common indicator of differentiation is not as useful, since #Mg is as low as 3–4 for the starting composition (Table 1).

The observed crystal phase assemblages do not contain H_2O-bearing phases, thus H_2O is enriched in the residual melt. H_2O contents in dry experiments determined with the by-difference method are <1.5 wt%. Totals of reduced H_2O-bearing experiments are usually lower than in oxidized runs. This is in agreement regarding saturation with fluid having other species than H_2O, namely CO_2, CH_4 or CO with solubilities <0.1 wt% at 100 MPa.

The H_2O solubility of the melt and the reliability of the by-difference method were confirmed with KFT analyses (eFig. 3). For 100 MPa, the composition shows a H_2O solubility of approximately 4.5 wt%, similar to phonolites (Carroll and Blank 1997; Schmidt and Behrens 2008) and peralkaline rhyolites (Di Carlo et al. 2010). Based on the H_2O concentrations and the composition of the quenched residual glasses, the solubility model of Burnham (1979) was applied to calculate aH_2O. As this model underestimates H_2O solubility, it is necessary to apply a correction factor that calculates from the ratio between the computed solubility of the Burnham model and the analyzed solubility (Holtz et al. 1995). The solubility is affected by the changing composition of the residual melt and changing T. As analyzed with the by-difference method, residual glasses contain up to 6.0 wt% H_2O. However, for the calculations, we fixed the solubility to 5.5 wt% for all experiments. With this assumption, aH_2O does not exceed 1 within error of the by-difference method. The prevailing fO_2 was then calculated using the dissociation reaction of H_2O; for a detailed description of the procedure, see Freise et al. (2009) and references therein. The error estimates based on the uncertainty of the by-difference method increase with decreasing cH_2O. Typical errors are ±0.1 for aH_2O and ±0.5 for ΔlogFMQ close to H_2O saturation, still errors increase with decreasing cH_2O.

Contrib Mineral Petrol (2013) 165:283–304 293

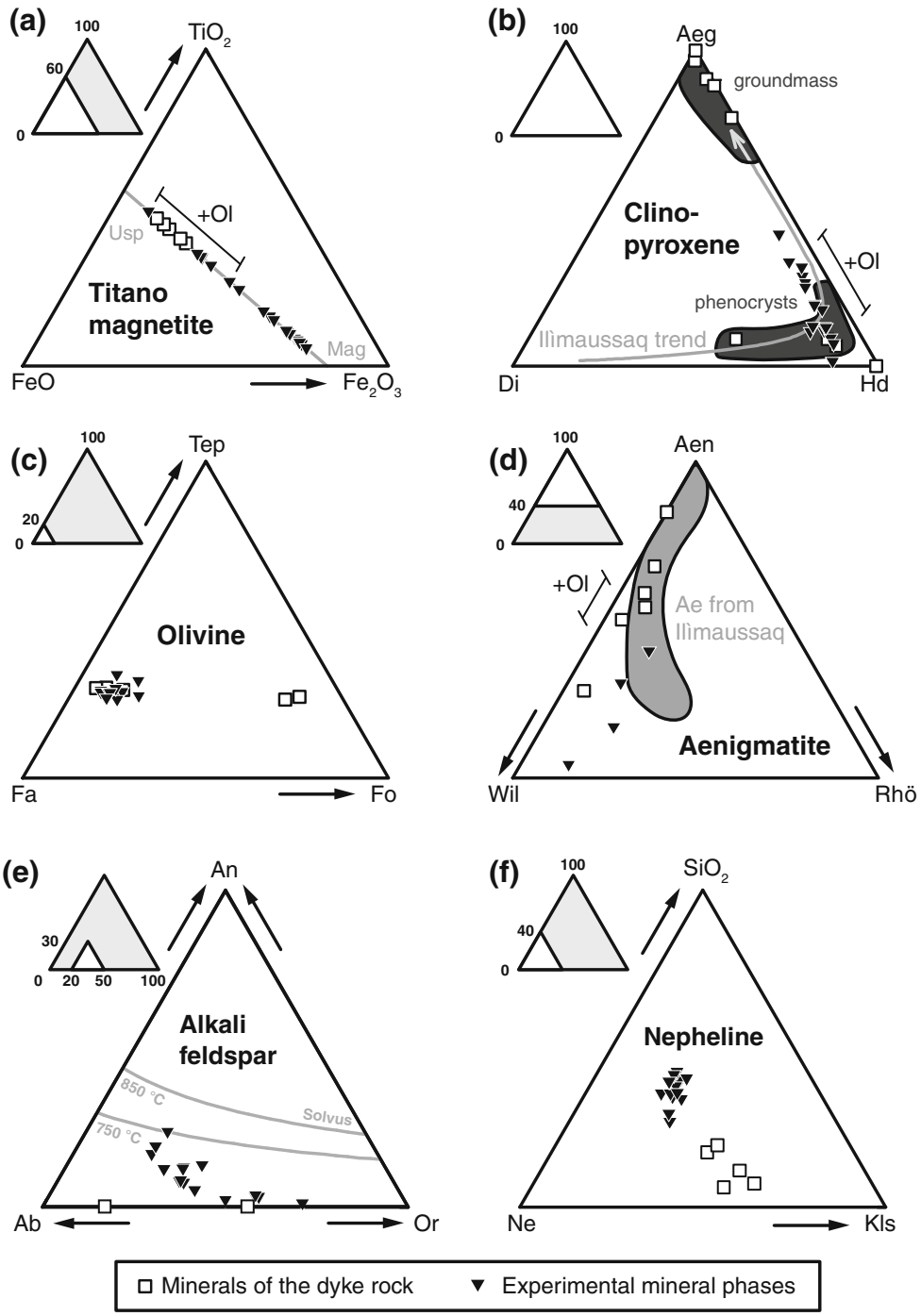

Fig. 3 Crystal composition of mafic phases: **a** Mag (magnetite–ulvøspinel, Mag–Usp), **b** Cpx (diopside–hedenbergite–aegirine, Di–Hd–Aeg), **c** Ol (forsterite–fayalite–tephroite, Fo–Fa–Tep) and **d** Ae (aenigmatite ($Na_2(Fe^{2+})_5Ti^{4+}Si_6O_{20}$)–wilkinsonite ($Na_2(Fe^{2+})_4(Fe^{3+})_2Si_6O_{20}$)–rhönite ($Ca_2(Mg,Fe^{2+})_4Fe^{3+}Ti^{4+}Si_3Al_3O_{20}$), Aen–Wil–Rhö). +Ol indicates the range of *X*Usp (for Mag), *X*Hd (for Cpx) and *X*Aen (for Ae) with coexisting Ol. The Ilímaussaq trend for Cpx is after Larsen (1976). Crystal composition of felsic phases: **e** Afs (anorthite–orthoclase–albite, An–Or–Ab) and **f** Nph (nepheline–kalsilite–SiO_2, Ne–Kls–SiO_2). Solvus data for Afs are calculated for 100 MPa after Nekvasil and Burnham (1987). Representative data points from the dyke rock are from Marks and Markl (2003)

Cl and F are known to show contrasting partitioning behavior in silicate melts. Whereas Cl partitions preferentially into the aqueous fluid, F favors staying in the melt (e.g., Carroll and Webster 1994). However, Stelling et al. (2008) showed that the fluid/melt partitioning coefficient in basaltic systems decreases with increasing Cl concentration in the melt. Most basaltic rocks contain <0.1 wt% Cl and F, but alkaline rocks

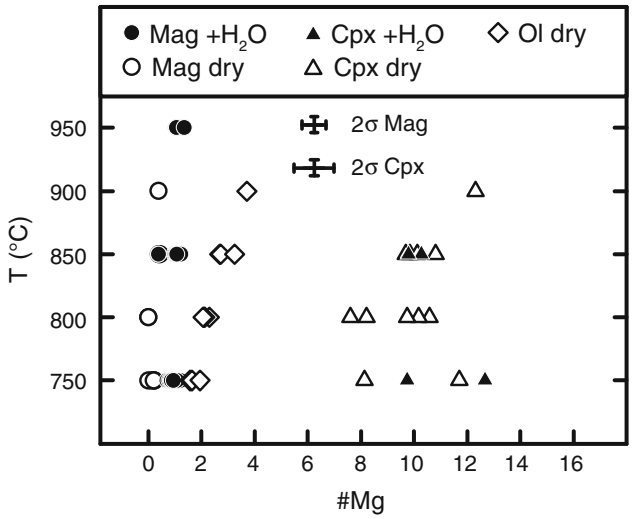

Fig. 4 The #Mg of experimental crystal phases decreases with falling *T*. Shown for Mag, Cpx and Ol

may exhibits significantly higher solubilities of up to 0.5 wt% Cl and 5 wt% F dissolved (Allman and Koritnig 1974; Michael and Schilling 1989). Furthermore, increasing FeO* content and A. I. show a positive effect on Cl solubility (Metrich and Rutherford 1992). In our experiments, we do not observe Cl- or F-bearing crystal phases. In spite of a coexisting fluid phase in H_2O-bearing experiments, Cl and F increase in the residual melt with decreasing amount of residual melt. Thus, Rayleigh fractionation (Rayleigh 1896) was calculated for Cl and F, and the calculations nicely trace the analyzed concentrations (bold lines in Fig. 5a). A similar behavior of Cl and F was observed in an experimental study on peralkaline rhyolites with a high FeO* content (6.9 wt%) and a high A. I. of 2.0 (Scaillet and MacDonald 2006). ZrO_2 shows a similar behavior as Cl and F, but deviates significantly from the modeled fractionation curve, which can be explained by significant incorporation of ZrO_2 (up to 1.8 wt%; eTab. 4) in Cpx.

The behavior of Na_2O, K_2O and Al_2O_3 is of special interest as their relative concentrations define the A. I. (Fig. 5b). K_2O slightly decreases, Na_2O increases, and Al_2O_3 first slightly increases followed by a significant decrease. These trends result in large differences of the A. I. with ratios from 1.35 to 3.55 (Fig. 5c). In contrast, the concentration of CaO in the residual melt decreases in all experiments (eTab. 9).

The major differences in the stable crystal phase assemblage between dry and H_2O-bearing experiments lead to trends in the evolution of the residual melt characterized by changing SiO_2 and FeO* content (Fig. 6). On the one hand, a strong FeO* decrease with strong SiO_2 increase for H_2O-bearing conditions is observed. This trend is similar, yet less pronounced, for dry and oxidized conditions. The influence of redox conditions is clearly observed, as dry and reduced experiments force the opposite evolution toward FeO* increase and SiO_2 decrease. The experimental results show that the investigated composition is extremely sensitive to cH_2O with different phase assemblages for dry (Mag, Cpx, Ol, Afs, Nph, Ae) compared with H_2O-bearing (Mag, Cpx) conditions at the same *T* (Figs. 7, 8). Mag (*X*Usp ≤0.15) is stable in all subliquidus H_2O-bearing experiments, inhibiting FeO* increase in the residual melt.

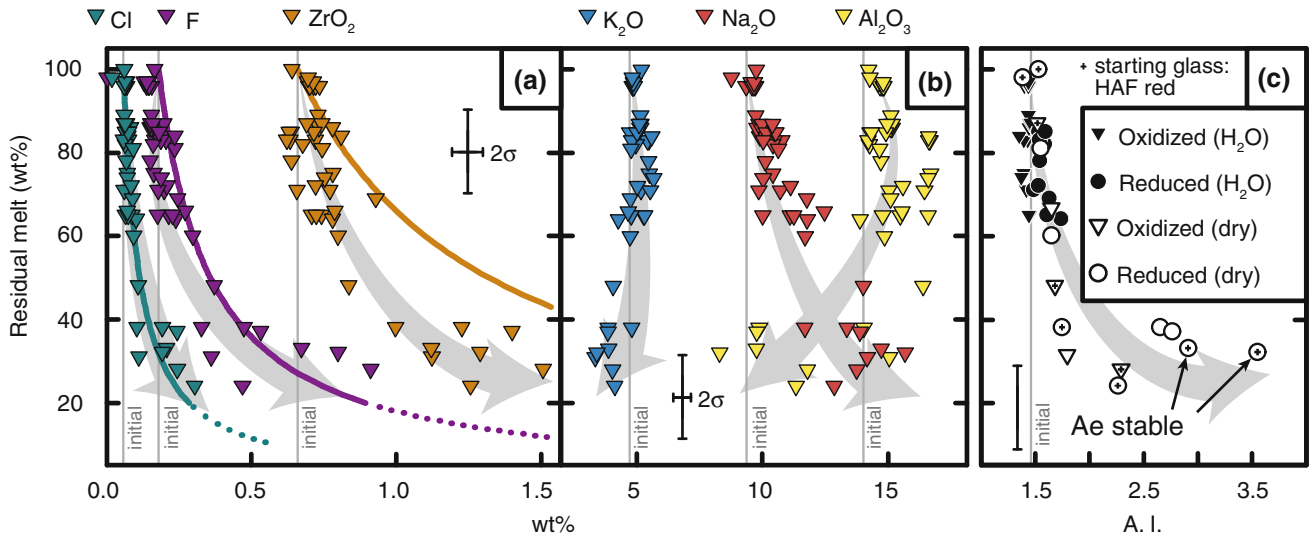

Fig. 5 Compositional evolution of **a** Cl, F and ZrO_2, **b** K_2O, Na_2O and Al_2O_3, (**c**) and the A. I. with decreasing amount of residual melt (wt%). Rayleigh fractionation (no partitioning into the fluid phase, no incorporation in crystal phases) in the residual melt is shown for Cl, F and ZrO_2 (*bold lines*). Since up to 1.7 wt% ZrO_2 are incorporated in Cpx, the increase in the residual melt is significantly reduced

Contrib Mineral Petrol (2013) 165:283–304 295

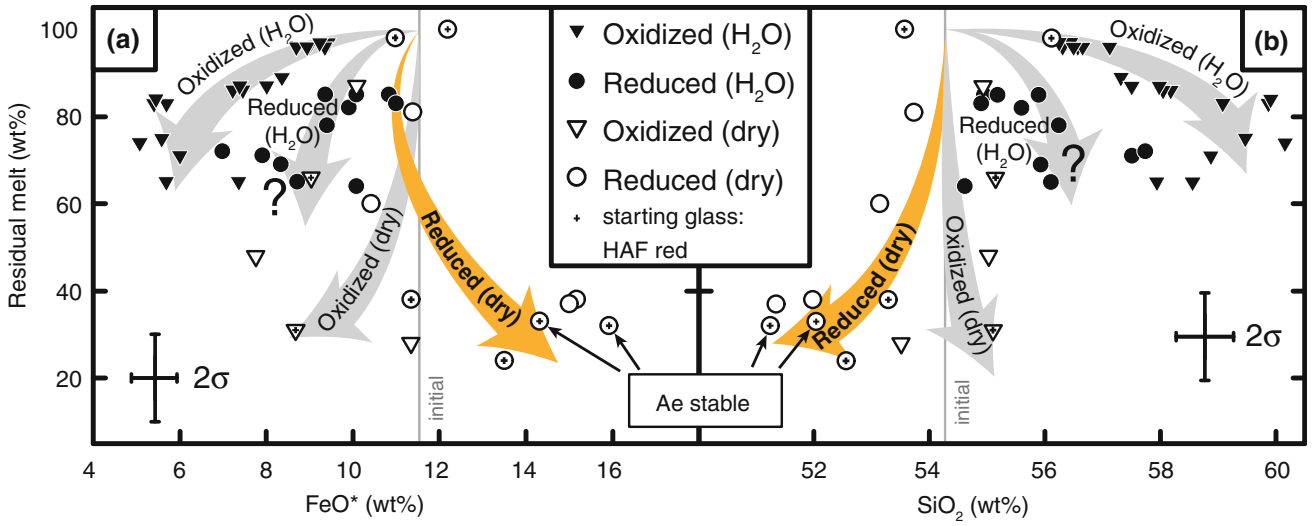

Fig. 6 Compositional evolution of **a** FeO* and **b** SiO_2 in the residual melt shows distinct trends for oxidized and reduced conditions and for variation of the H_2O content. The residual melt of dry and reduced experiments follows, speaking in basaltic terminology, a "Fenner-like" trend; whereas H_2O-bearing experiments follow a "Bowen-like" trend. The residual melt of oxidized dry experiments shows an intermediate behavior

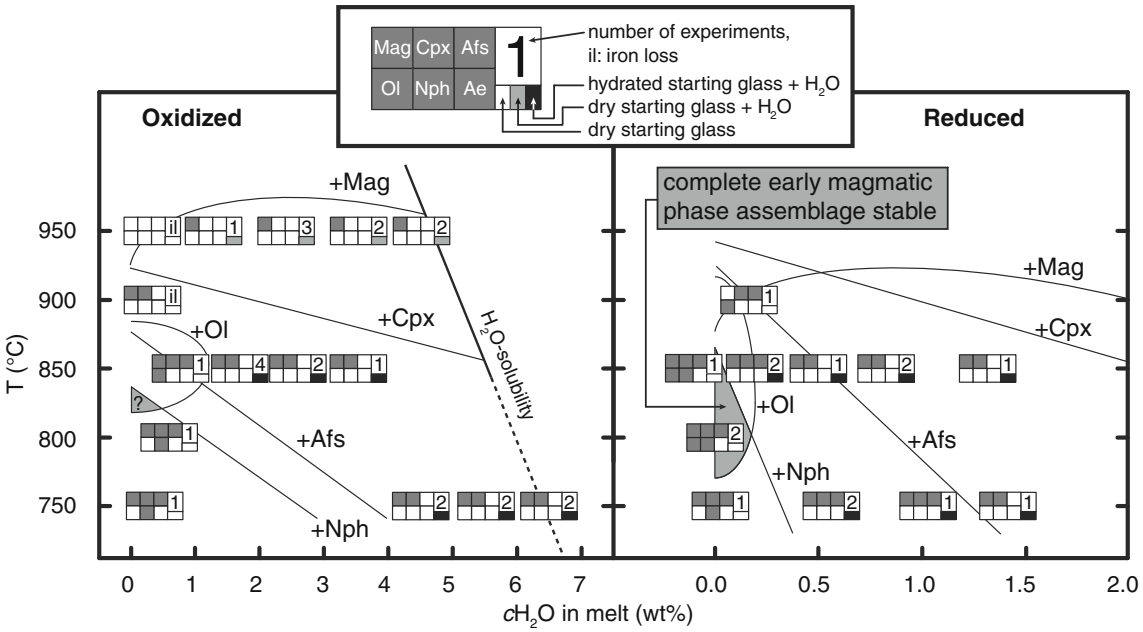

Fig. 7 Phase relations on the T versus cH_2O (melt) plot. The x-axis is extended to negative values due to the large uncertainty of the by-difference method (±0.5 wt%). Crystal phases are abbreviated as *Mag* titano magnetite, *Cpx* clinopyroxene, *Afs* alkali feldspar, *Ol* olivine, *Nph* nepheline and *Ae* aenigmatite. In all experiments a coexisting residual melt is present

Adjusting dry conditions is difficult and prone to inherit adsorbed H_2O through capsule preparation (see also experimental methods). Both adsorbing H_2O and generation of secondary H_2O through Fe loss (Eqs. 1, 2) may then affect phase relations and compositions.

Phase relations and melt evolution

Phase stabilities dependent on T and cH_2O are illustrated in Fig. 7. The stability of Ol and Usp-rich Mag is restricted to dry conditions, and the stability field of Afs extends to

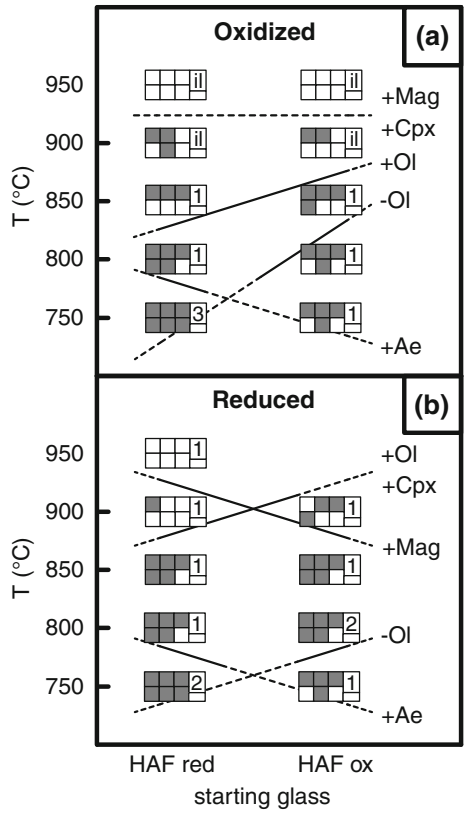

Fig. 8 Phase relations on the *T* versus starting glass plot. Phase boundaries for Afs and Nph are not shown. For *abbreviations* and *symbols,* see Fig. 7

higher H_2O content for lower *T*. H_2O-bearing experiments invariably contain Mag and Cpx. Experiments with the reduced starting glass were only conducted applying dry conditions. The phase relations are compared with the corresponding experiments with the oxidized starting glass in terms of *T* (Fig. 8). For the reduced starting glass, the Ol stability field is increased and shifted to lower *T* for oxidizing conditions. If the reduced starting glass is used, Ae is observed at 750 °C, and Cpx crystallizes at higher *T* and Mag at lower *T* for reduced conditions (Fig. 8).

Discussion

General interpretations

XFe^{3+} of the starting glass

The pre-equilibration of starting glasses regarding XFe^{3+} at conditions close to the experimental fO_2 is helpful to minimize the time necessary for attaining equilibrium redox conditions (Botcharnikov et al. 2008; Freise et al. 2009). Still, in dry and H_2O-bearing experiments, a range of several log units is covered due to different H_2O contents (e.g., Feig et al. 2006; Andújar et al. 2008; Freise et al. 2009; Feig et al. 2010). According to Holloway et al. (1992) C capsules encapsulated in noble metal capsules place constraints on the fO_2 in fluid-absent super-liquidus piston–cylinder experiments. The maximum fO_2 can here be modified by XFe^{3+} variations of the starting material. In a hydrothermal experimental setup, we expect equilibration toward the intrinsic fH_2, which may, in dry experiments, reduce Fe_2O_3, leading to an even lower fO_2 and secondary production of H_2O (Eq. 3).

$$Fe_2O_{3(melt)} + H_{2(membrane)} \leftrightarrow H_2O_{(melt)} + 2FeO_{(melt)} \quad (3)$$

Gaillard et al. (2001) showed that Fe^{2+} is dominant over Fe^{3+} in metaluminous and peralkaline glasses for $\sim\Delta$logFMQ $<+3$. Furthermore, XFe^{3+} decreases with decreasing *T*, and still the presence of H_2O was found to increase XFe^{3+} for $\sim\Delta$logFMQ $<+2.5$. Following the procedure of Kress and Carmichael (1991), XFe^{3+}'s of residual glasses were calculated. Values are invariantly below 0.4 although the initial XFe^{3+} adjusted by the starting glass is 0.45 (for HAF red) and 0.61 (for HAF ox), respectively. Thus, according to equation 3, in dry experiments using starting glass HAF ox, up to 0.17 wt% more secondary H_2O is produced compared with HAF red.

Most striking are the oxidized runs 71 and 79 where significant iron loss to the capsule material occurred. In addition to the reduction of Fe_2O_3 to FeO, alloying with the capsule material (Eqs. 1, 2) liberates more oxygen with the consecutive production of 2.5 and 4.5 wt% H_2O.

Although not closed to hydrogen, the oxygen content of dry experiments in the capsule is therefore fixed and differs for variation of initial XFe^{3+}. Although we used dried glass powder with relatively large grain size (<300 μm), some H_2O may be adsorbed. As all capsules were prepared in the same manner, we expect the amount of adsorbed H_2O to be low and similar.

The presence of anhydrous crystal phases, regardless of composition, concentrates dissolved H_2O in the residual melt attended by increasing fO_2 and fH_2. The effect of variations in secondary H_2O production can be seen comparing the crystallinity of the four dry experiment series (Fig. 9). The effect of increasing cH_2O is decreasing the crystallization *T* of crystal phases (Hamilton et al. 1964). This effect is not linear, most effective for low cH_2O <1 wt% and diminishes for high crystallinity and therefore higher cH_2O.

Both the use of reduced conditions in C capsules and the use of the reduced starting glass contribute to decreasing cH_2O and, as a consequence, to higher crystallinity at a given *T*. At 850 °C, crystallinity varies from 13 % (HAF ox, dry, oxidized) to 62 % (HAF red, dry, reduced). At 750 °C, cH_2O is higher and differences become less

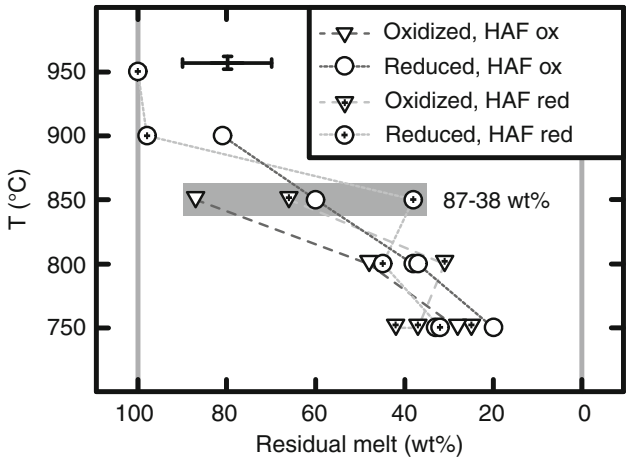

Fig. 9 Comparison of dry experimental series on the *T* versus residual melt (wt%) plot showing different grades of crystallinity for different redox conditions and starting glasses

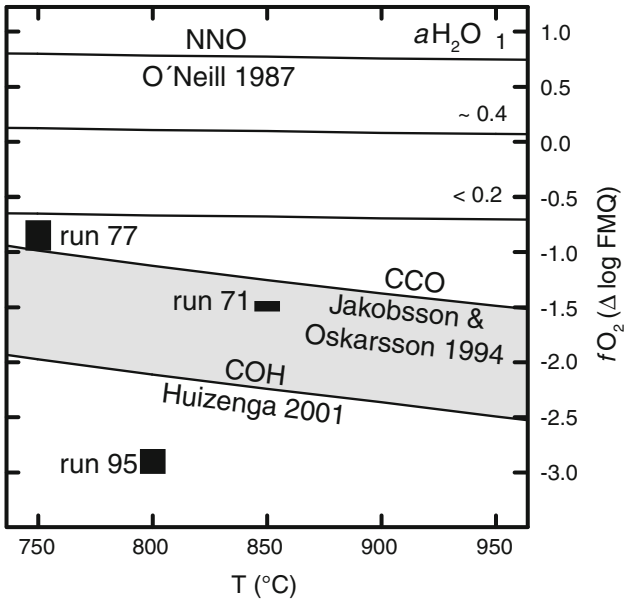

Fig. 10 *T*–fO_2 diagram showing the intrinsic fO_2 at H_2O-saturated conditions ($aH_2O = 1$, NNO oxygen buffer), fO_2 estimations for aH_2O <1, calculations of the CCO and COH oxygen buffers and QUILF95 calculations for run 71, 77 and 95

pronounced concerning crystallinity. This results in similar crystallinity for all dry experimental series at 750 °C. For H_2O-bearing experiments, the effect of producing secondary H_2O (<0.3 wt%) is negligible since masked by abundant H_2O added by choice.

Calculation of fO_2 and $aSiO_2$

For oxidized H_2O-saturated experiments, the intrinsic fO_2 ($\sim\Delta$logFMQ +0.8) is known. Estimations of fO_2 were calculated for aH_2O <1 ($\sim\Delta$logFMQ −0.9 to +0.8) using the solubility model of Burnham (1979) and for dry and fluid-bearing reduced experiments using the CCO (French and Eugster 1965; Jakobsson and Oskarsson 1994) and the COH (French 1966; Ohmoto and Kerrick 1977; Huizenga 2001) oxygen buffer (ΔlogFMQ = −1 to −2.5; Fig. 10).

Additionally, fO_2 can be determined from the composition of coexisting crystal phases bordered by the following limitations: (1) Mag, Cpx and Ol are only stable in dry experiments; and (2) given all crystal phases are stable, they might be too small for quantitative EMP analysis. In three dry experiments (run 71, 77, 95), we were able to calculate fO_2 from the composition of coexisting Mag, Cpx and Ol using the QUILF95 software (version 6.42, Andersen et al. 1993). This method was used before to calculate fO_2 for natural (e.g., Marks and Markl 2003; MacDonald et al. 2011) and experimental phase assemblages (e.g., Nekvasil et al. 2004). We calculated values ranging from ΔlogFMQ −0.8 to −2.9 (Fig. 10; Table 4). As these represent oxidized and reduced experiments and different *T* (750–850 °C), it can be derived that low fO_2 was successfully adjusted in dry experiments in contrast to more oxidized H_2O-bearing experiments.

We observe a rough negative correlation between *X*Usp with the abundance of Mag (eFig. 5a) and between *X*Usp and prevailing fO_2 (eFig. 5b). Also, the crystal size of Mag correlates negatively with *X*Usp in Mag, and the low TiO_2 content of the starting glass is here suggested to be the limiting factor. Fe–Ti oxides are known to re-equilibrate with changing fO_2 (Evans and Scaillet 1997) and are therefore a sensitive indicator for redox equilibrium in reduced H_2O-bearing experiments. Inherited Mag from pre-hydrated starting glasses did not significantly change composition, is slightly rounded and therefore did not fully equilibrate with the coexisting COH fluid in terms of redox conditions. Still, in reduced H_2O-bearing experiments, the stability field of Cpx in the *T*–cH_2O diagram is consistent with oxidized experiments. The stability field of Afs shows the same topology as in oxidized experiments, but is shifted to lower cH_2O. In Fig. 10 *T*–fO_2 conditions are summarized.

The experimental $aSiO_2$ was calculated using the QUILF95 software from coexisting Mag, Cpx and Ol ($aSiO_2$ = 0.40–0.70; Table 4) or in Mag-absent experiments from coexisting Cpx and Ol only ($aSiO_2$ = 0.60–0.91). Except for two experiments, these calculations comprise unacceptable large errors of up to ±0.28 (Table 4), which we attribute to partly imperfect EMP analyses due to contamination (see above). These results are thus problematic and are not considered further. The experiments with an acceptable error (±0.02) gave the lowest values for $aSiO_2$ of 0.40 and 0.51, which is considered to be reliable and matches the $aSiO_2$ values calculated for the natural phase assemblage (0.25–0.5; Marks

and Markl 2003). Consistently, EMP analyses for these experiments are of a much better quality.

Using equilibria between coexisting Afs (activity model of Holland and Powell 2003) and Nph (ideal mixing on sites), the calculated $a\mathrm{SiO_2}$ values are nearly invariant at 0.36 ± 0.02, values similar to the most reliable QUILF95 calculations and those given by Marks and Markl (2003). It would be tempting to apply AUNILF-type equilibria among Afs, Nph, Mag, Ilm, Cpx and Ol (Schilling et al. 2011), but this is not possible due to the absence of either Nph or Ilm. We conclude that the calculation of $a\mathrm{SiO_2}$ with QUILF95 from Cpx and Ol only is prone to be erroneous. Still, calculations with Mag, Cpx and Ol require EMP analyses of extremely high quality. Both QUILF95 calculations from Cpx and Ol only and poor EMP analyses are likely to overestimate $a\mathrm{SiO_2}$.

Phase relations and liquid line of descent

A crucial step during differentiation of more primitive basaltic and andesitic systems is whether Mag precipitates or not, which is controlled by the prevailing $f\mathrm{O_2}$. This feature was observed in basaltic systems (Osborn 1959) and confirmed experimentally (Berndt et al. 2005; Botcharnikov et al. 2008; Freise et al. 2009). It results in two opposing evolutionary trends of the coexisting residual melt: Mag precipitation at high $f\mathrm{O_2}$ will lead to a (speaking in basaltic terminology) calc-alkaline trend with low FeO, high $\mathrm{SiO_2}$ and a constant FeO/MgO ratio (e.g., Bowen 1928), whereas suppression of Mag crystallization and/or co-crystallization of Ol at low $f\mathrm{O_2}$ will result in a tholeiitic trend with high FeO, low $\mathrm{SiO_2}$ and an increasing FeO/MgO ratio (e.g., Fenner 1929). High FeO/low $\mathrm{SiO_2}$ trends were observed in nature, for example for Skaergaard melts (Wager and Deer 1939), and reported from experimental studies (Toplis and Carroll 1995; Botcharnikov et al. 2008).

Even though not directly comparable with basaltic systems, similar opposing trends are observed in our study and in an experimental study on peralkaline rhyolites conducted at relatively reducing conditions ($\sim\Delta$logFMQ -1 to -1.5; $\mathrm{FeO^*_{initial}} = 7$ wt%; Scaillet and MacDonald 2006). The high FeO and low $\mathrm{SiO_2}$ trend appears at relatively low $f\mathrm{O_2}$, meaning $\sim\Delta$logFMQ <-1 and iron-rich systems (Fig. 6). From existing experimental findings, we cannot rule out that this may also happen in iron-poor systems, although the effect on the liquid line of descent would be smaller.

Comparing $\mathrm{H_2O}$-bearing experiments at 950 °C, we observe Mag as liquidus phase for a wide range of $\mathrm{H_2O}$ contents in the residual melt (1.3–4.5 wt%). In contrast, reduced dry experiments are above the liquidus at 950 °C. This means, in turn, that the absence of $\mathrm{H_2O}$, combined with low $f\mathrm{O_2}$, may decrease the liquidus T (run 82) or change (run 92) the liquidus phase, whereas the absence of $\mathrm{H_2O}$ is usually known to increase the liquidus T.

Whenever Mag is successfully analyzed and coexists with Ol, XUsp is always >0.40. From Eq. 4, it can be derived that coexisting Mag and Ol indicate relatively lower $f\mathrm{O_2}$ compared with Ol-free experiments.

$$3\mathrm{Fe_2SiO_4} + \mathrm{O_2} \leftrightarrow 2\mathrm{Fe_3O_4} + 3\mathrm{SiO_2} \quad (4)$$

For dry experiments, Mag and Cpx show an increase in $X\mathrm{Fe^{3+}}$ with decreasing T expressed as XUsp from 0.55 to 0.20 and as XAeg from 0.02 to 0.42 (eFig. 6a & b). This increase in $X\mathrm{Fe^{3+}}$ parallels increasing $\mathrm{Na_2O}$ content and

Table 4 Calculation of $f\mathrm{O_2}$ and $a\mathrm{SiO_2}$

Run	71	95	77	74	87	88	94	81	92
T (°C)	850	800	750	850	800	800	800	850	900
Capsule	Au	C	Au	C	Au	C	C	C	C
Starting glass	HAF ox	HAF red	HAF red	HAF ox	HAF red	HAF ox	HAF ox	HAF red	HAF ox
Observed crystal phases	**Mag**	**Mag**	**Mag**	Mag	Mag	Mag	Mag	Mag	**Cpx**
	Cpx	**Cpx**	**Cpx**	**Cpx**	**Cpx**	**Cpx**	**Cpx**	**Cpx**	Afs
	Afs	Afs	Afs	Afs	Afs	Afs	Afs	Afs	**Ol**
	Ol	**Ol**	**Ol**	**Ol**	**Ol**	**Ol**	**Ol**	**Ol**	
		Nph	Nph	Nph	Nph	Nph	Nph	Nph	
			Ae						
ΔlogFMQ QUILF95	−1.5 (1)	−2.9 (1)	−0.8 (2)	–	–	–	–	–	–
$a\mathrm{SiO_2}$ QUILF95	0.51 (01)	0.40 (02)	0.70 (07)	0.91 (27)	0.70 (21)	0.62 (13)	0.60 (22)	0.68 (17)	0.85 (28)
$a\mathrm{SiO_2}$ Afs-Nph	–	0.35	0.38	0.35	0.35	–	0.34	0.35	–

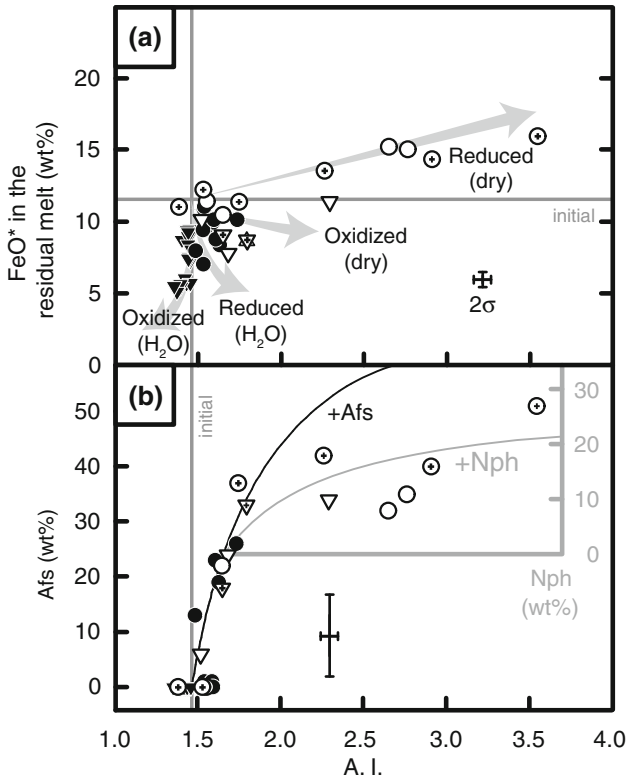

Fig. 11 **a** Systematics of FeO* compared with the A. I. of the residual melt. The uncertainty is smaller than the symbol size. **b** Changes in the A. I. were modeled exclusively influenced by Afs crystallization (+Afs, *black line*). The extended model additionally takes into account Nph crystallization, starting from the minimum amount Afs (24 wt%) where coexisting Nph is observed (+Nph, *gray line*). For symbols, see Figs. 5 and 6

increasing A. I. of the residual melt (eFig. 6c & d). In contrast, H_2O-bearing experiments do not show such a correlation and no strong increase in Na_2O and A.I. is observed. $X\mathrm{Fe}^{3+}$ in Mag is always higher in H_2O-bearing experiments compared with dry runs. The most straightforward explanation would be that higher H_2O contents (through the decreasing amount of residual melt) are responsible for higher fO_2 values, with different amounts of secondary H_2O produced depending on the $X\mathrm{Fe}^{3+}$ of the staring glass (Eq. 3, see above). On the other hand, increasing alkalinity is known to increase the solubility of HFSE elements like Ti^{4+} and Zr^{4+} (Watson 1979; Dickenson and Hess 1986) and the $X\mathrm{Fe}^{3+}$ in melts even at constant oxygen fugacity (Giuli et al. 2012). We observe an increase in $X\mathrm{Fe}^{3+}$ in Cpx with increasing Na_2O and A.I. of the coexisting residual melt for both oxidized and reduced conditions and both starting glasses. Markl et al. (2010) suggested that Aeg crystallization reduces the coexisting melt/fluid by the coupled incorporation of Na^{+} and Fe^{3+} in Cpx, which might be an alternative explanation for the correlation of Na_2O, A.I. and $X\mathrm{Fe}^{3+}$ with falling T and increasing amount of residual melt in our experiments.

Aenigmatite represents a mineral phase of the late-magmatic groundmass of the dyke rock. In our experiments, Ae is observed at 750 °C, but only if the reduced starting glass was used. Ae coexists with a residual melt with a high A. I. >2.9 (Fig. 5c). The extended T stability field of Ol and the stabilization of Ae at 750 °C underline the effect of the reduced starting glass (Fig. 8). For oxidized experiments, $X\mathrm{Fe}^{3+}$ in Ae (expressed as XWil) is higher compared with reduced experiments, confirming the lower fO_2 (Fig. 3d).

Evolution of the residual melt

As shown above, FeO* and SiO_2 are beneficial to distinguish between different evolution trends for the residual melt. Precipitation of Mag is prevented involving a fractionating assemblage dominated by Afs and Ol. This leads to the fundamental difference for the liquid line of descent regarding FeO* and SiO_2 content. Whereas in oxidized experiments the decrease in FeO* (crystallization of Mag) does not change the A. I. significantly, in reduced experiments, the increase in FeO* is linked to a strong increase in the A. I. (Fig. 11a). The A. I. of the residual melt was modeled for the simplified case of exclusively crystallizing Afs. If Afs is not stable, the A. I. roughly exhibits the initial value (±0.1). Removing equal molar amounts of Na+K and Al from the melt with an initial value higher than 1 by crystallizing Afs, the A. I. increases in terms of an exponential function tracing the analyzed residual melt compositions of our experiments (Fig. 11b). This effect is intensified by the onset of Nph crystallization (max. 15 wt%) observed with at least 24 wt% coexisting Afs. From this point, the A. I. of the residual melt was additionally calculated for simultaneously crystallizing equal amounts of Nph (Fig. 11b). Even though other stable crystal phases are not considered in this calculation, both curves roughly parallel the A. I. of our residual melt compositions.

In summary, we state that only under dry and reduced conditions, a FeO* increase and SiO_2 decrease can be realized. The crystallization of Afs and Nph controls the A. I. of the residual melt and is necessary to reach extreme peralkalinity.

Comparison with previous experimental work

We chose three experimental studies representing basaltic (Botcharnikov et al. 2008), rhyolitic (Di Carlo et al. 2010) and phonolitic compositions (Andújar et al. 2008) for comparison, each having distinct similarities to the starting composition of this study. The basaltic composition has a similar FeO* content, the rhyolite holds similar #Mg and

A. I., and the phonolite is identical in terms of the TAS classification (total alkalis vs. silica; Le Bas et al. 1986).

The correlation of fO_2 with liquidus T of Mag ($\sim$200 °C for 5 log units lower fO_2) is known for more primitive, iron-rich basaltic systems, whereas the T stability field for Mag is only slightly decreased for increasing XH_2O. Whereas Mag is liquidus phase for oxidizing conditions (ΔlogFMQ $>+1.5$) and XH_2O >0.2, Ol replaces Mag as liquidus phase at constant XH_2O and more reducing conditions (ΔlogFMQ $<+1.5$). It was also noted that, for oxidizing conditions (ΔlogFMQ $>+2$), increasing fO_2 interlinked with increasing aH_2O may increase the liquidus T, which is contrary to the well-known decrease in liquidus T in the presence of H_2O. However, these conditions are expected to be rare or absent in nature, particularly regarding basaltic systems (Botcharnikov et al. 2008). For lower fO_2 and aH_2O, the liquidus phases change to Ol, Cpx (with #Mg >70) and plagioclase (Pl, XAn >60).

Similarly, in this study, crystallization T of Mag increases with increasing cH_2O and fO_2 (see run 82 compared to runs 30–39, Fig. 7). As our composition is extremely evolved, Ol (#Mg <4), Cpx (#Mg <12) and Afs (analogous to Pl) crystallize at 200–300 °C lower T and take the place of Mag as liquidus phases (run 92). The decrease in liquidus T is also observed in experiments with the reduced starting glass (run 82), but here Mag is again liquidus phase, and Ol, Cpx and Afs crystallize at even lower T. As fO_2 is more than three log units lower in our study (the intrinsic value is ΔlogFMQ $+0.8$ compared with $+4.2$), this effect is likely to be more relevant in more evolved natural systems comparable to this study.

A study on peralkaline rhyolites by Di Carlo et al. (2010) is comparable to our starting composition in terms of #Mg and A. I. (Fig. 1), but with lower FeO* and higher SiO_2 content. Mag is absent, which we attribute to the lower FeO* content. Stability of quartz and absence of Nph are explained by the silica saturation, amphibole is stabilized only below 700 °C, and again Ol is not observed. The extensive crystallization of Afs was stressed likewise to reach extreme peralkalinity (up to A. I. = 3.5). However, at 100 MPa, $T \leq 750$ °C and ΔlogFMQ ≤ 0, Ae coexists with a melt having a relatively low A. I. (1.3–1.5), Afs and sodic Cpx ($\pm$sodic Amph). Previous work suggests that Ti is crucial to stabilize Ae at pressures above 90 MPa and Ti-bearing Ae is not stable for ΔlogFMQ $>+1$ (Ernst 1962; Thompson and Chisholm 1969). Maximum T stability at 750 °C and low fO_2 are in agreement with our results. Mag and Ae were proposed not to coexist having a peritectic relation with each other, resulting in a no-oxide field in T–fO_2 space (Nicholls and Carmichael 1969). This is in agreement with experimental data (Di Carlo et al. 2010). In contrast, we observe coexisting Mag and Ae and suggest that a no-oxide field might be intersected at lower T owing to the low fO_2 in experiments of this study (ΔlogFMQ <-1).

A relatively evolved phonolitic composition was experimentally investigated by Andújar et al. (2008). However, their starting composition is still lower in CaO, FeO* and A. I. and higher in Al_2O_3 and SiO_2 compared with our study. Additional phases found in their experiments are Spn, hauyne (Hyn) and biotite, but Ol, Nph and Ae are absent. Spn might be stabilized due to the higher fO_2, and Hyn is probably a result of abundant S in the system. The A. I. is remarkably constant in all residual glasses (0.9–1.2) similar to other phonolites (Berndt et al. 2001: 0.7–1.0; and Freise et al. 2003: 0.6–1.2) with an initial A. I. $\sim$1.

Even though our studied composition is extremely evolved, basaltic features are preserved by the high FeO* content accompanied by Mag and Ol stability with strong influence of fO_2. Alkali feldspar is, as for peralkaline rhyolites and phonolites, the most abundant crystal phase. Liquidus T's of felsic phases are depressed with increasing aH_2O in all three studies, which is also observed in our experiments. However, if the starting composition has an A. I. close to 1, Afs ($\pm$Nph) crystallization is not able to direct the liquid line of descent toward extreme peralkalinity.

Comparison with the dyke rock

The extreme fractionation trend found in the Ilímaussaq complex is believed to be governed by low $aSiO_2$, low aH_2O, low fO_2 and a principally closed-system evolution (Larsen 1976; Markl 2001; Markl et al. 2001; Marks and Markl 2001). Our experimental results confirm this regarding phase stabilities and phase compositions (Figs. 3, 7, 8).

Cpx and Ol phenocrysts of the dyke rock can be divided into two groups with relatively high (XDi = 0.35; XFo = 0.12–0.13) and relatively low #Mg (XDi = 0.08–0.10; XFo = 0.01–0.03; Marks and Markl 2003; Fig. 3b, c). Our synthetic Cpx and Ol nicely match the low #Mg type. Cpx and Ol with higher #Mg as found in the dyke rock may well be crystallized and transported at an earlier stage of differentiation and/or significantly higher T than in our experiments. The phase diagram shows that the Ol stability field is limited in terms of T and fO_2, and another explanation for the absence of Ol would be slightly higher aH_2O and/or fO_2 following a crystallization path not intersecting the Ol stability field (Fig. 7). Mag, Cpx and Ol phenocrysts in the dyke rock itself are absent in samples close to the wall rock (<1 m), and the complete early magmatic phenocryst assemblage is observed at a minimum distance of 1.5 m (Marks and Markl 2003). This might simply be explained by different flow rates close to the wall rock given the phenocrysts were probably already crystallized during emplacement.

Large amounts of Afs, Nph and Sdl are typical for evolved alkaline igneous rocks (Marks et al. 2011). Our study emphasizes the importance of Afs and Nph crystallization coupled with an initial A. I. >1 for the evolution toward extreme peralkalinity (Fig. 11b). In the dyke Ap, Fl, Sdl and Eud are observed, but our experiments did not produce any Cl- or F-bearing crystal phases. As Cl and F are decreased by 80 % relative to our starting glass, a larger proportion of crystal phases will be required to saturate Cl and F in the residual melt to stabilize the aforementioned crystal phases. The absence of distinct Zr phases in our experiments is in contrast to the abundant Eud and Hjo in the natural dyke rock (Larsen and Steenfelt 1974; Marks and Markl 2003). This might explain the distinctively higher ZrO_2 contents in our synthetic Cpx (0.37–1.72 wt% ZrO_2) compared to Cpx found in the natural dyke rocks (≤0.31 wt%; Marks and Markl 2003). Thus, the incompatible behavior of ZrO_2 and the absence of a Zr phase cause an increase in ZrO_2 in Cpx with decreasing experimental T (eTab. 4),

Conclusions

Our experimental study showed that a dyke rock linked to the Ilímaussaq intrusion formed from a melt with low fO_2 and probably low cH_2O. H_2O-bearing and dry experiments represent two differentiation trends for oxidized H_2O-bearing and for reduced dry experiments. This is because for reduced conditions Ol dominates over Mag, contrary to what is observed for oxidized conditions. The increase in FeO and interlinked decrease in SiO_2 can only be realized for reduced and dry experiments using the reduced starting glass. In contrast to the usually observed effect of decreasing the liquidus T, the presence of H_2O and interlinked higher fO_2 seems to increase the liquidus T in our experiments, at least for low H_2O concentrations (cH_2O <1 wt%).

In a model calculation, we showed that extensive Afs and Nph crystallization controls the A. I. and is therefore, coupled with an initial A. I. ≫1, necessary to reach extreme peralkalinity as indicated from the late-magmatic mineral assemblage. The use of a starting glass with lower XFe^{3+} reduces the secondary production of H_2O, influencing phase relations for initially dry experiments. Most remarkabe are the expansion of the Ol stability field in terms of T and the stabilization of Ae at 750 °C.

The detailed comparison of phase relations, main and trace elements in natural and synthetic crystal phases, reveals similarities as follows: all mineral phases of the early magmatic assemblage were successfully reproduced in dry experiments at 850–800 °C (run 74, 88, 94, 87, 81 and 95). The phase compositions matching best are observed in run 95 at 800 °C at dry and reduced conditions ($fO_2 \sim \Delta$logFMQ −2.9) using the reduced starting glass. The increase in fO_2 with decreasing T in the dyke rock is exemplified by early Hd-rich Cpx followed by increasing XAeg in Cpx, also observable in dry experiments. The observation of Ae at 750 °C in residual melt pockets with high A. I. indicates the transition to late-magmatic dyke rock conditions.

Outlook

Ongoing studies will simulate fractional crystallization processes by using the residual melt composition of experiments with the complete coexisting early magmatic phase assemblage. By applying a lower synthesis T, we will try to minimize the loss of Cl and F during glass synthesis. Additionally, the halogen loss will be compensated by adding more halogens than the target composition.

Reduced H_2O-rich probably did not fully equilibrate in terms of fO_2; therefore, either further time-dependent experiments or the use of a different experimental setup is necessary to assure near-equilibrium conditions in those experiments.

An analytical challenge will be a more precise determination of the H_2O content in the residual glasses with micro FT-IR spectroscopy calibrated with KFT.

Acknowledgments We thank Indra Gill-Kopp for the careful sample preparation. Norbert Walker and Barbara Maier kindly assembled gold and graphite capsules. Philipp Bellucci, Huy-Tung Nguyen, Stephan Reiche and Rainer Babiel are thanked for support with the experimental work. XRF analyses of the starting glasses were done by Heiner Taubald, Urs Dippon performed Mössbauer spectroscopy on the starting glasses, and Harald Behrens analyzed our samples with KFT. Special thanks go to Thomas Wenzel for invaluable support with challenging EMP analyses. We thank Renat Almeev, Bruno Scaillet and an anonymous reviewer for constructive and helpful comments. Financial support of the Deutsche Forschungsgemeinschaft (grants MA 2563/4-1 and NO 378/7-1) is gratefully acknowledged.

References

Abramoff MD, Magelhaes PJ, Ram SJ (2004) Image processing with ImageJ. Biophotonics Int 11:36–42

Ackermann S, Kunz M, Armbruster T, Schefer J, Hänni H (2004) Cation distribution in a Fe-bearing K-feldspar from Itrongay, Madagascar: a combined neutron- and X-ray single-crystal diffraction study. Schweizer Mineralogische und Petrographische Mitteilungen 84:345–354. doi:10.5169/seals-63754

Allaart JH (1969) The chronology and petrography of the Gardar dykes between Igaliko Fjord and Redekammen, South Greenland. Rapp Grønl Geol Unders 25:20

Allman R, Koritnig S (1974) Fluorine. In: Wedepohl KH (ed) Handbook of geochemistry. Springer, Berlin

Almeev RR, Holtz F, Koepke J, Parat F, Botcharnikov RE (2007) The effect of H_2O on olivine crystallization in MORB: experimental calibration at 200 MPa. Am Mineral 92:670–674. doi:10.2138/am.2007.2484

Andersen DJ, Lindsley DH, Davidson PM (1993) QUILF—a PASCAL program to assess equilibria among Fe–Mg–Mn–Ti oxides, pyroxenes, olivine and quartz. Comput Geosci 19:1333–1350. doi:10.1016/0098-3004(93)90033-2

Andújar J, Costa F, Marti J, Wolff JA, Carroll MR (2008) Experimental constraints on pre-eruptive conditions of phonolitic magma from the caldera-forming El Abrigo eruption, Tenerife (Canary Islands). Chem Geol 257:173–191. doi:10.1016/j.chemgeo.2008.08.012

Aranovich LY, Newton RC (1996) H_2O activity in concentrated NaCl solutions at high pressures and temperatures measured by the brucite–periclase equilibrium. Contrib Miner Petrol 125:200–212. doi:10.1007/s004100050216

Bailey DK, Schairer JF (1966) The system Na_2O-Al_2O_3-Fe_2O_3-SiO_2 at 1 atmosphere, and the petrogenesis of alkaline rocks. J Petrol 7:114–170. doi:10.1093/petrology/7.1.114

Bailey JC, Gwozdz R, Rose-Hansen J, Sørensen H (2001) Geochemical overview of the Ilimaussaq alkaline complex, South Greenland. Geol Greenl Surv Bull 190:35–53

Behrens H (1995) Determination of water solubilities in high-viscosity silicate glasses. An experimental study on $NaAlSi_3O_8$ and $KAlSi_3O_8$ melts. Eur J Mineral 7:905–920

Berndt J, Holtz F, Koepke J (2001) Experimental constraints on storage conditions in the chemically zoned phonolitic magma chamber of the Laacher See volcano. Contrib Miner Petrol 140:469–486. doi:10.1007/PL00007674

Berndt J, Liebske C, Holtz F, Freise M, Nowak M, Ziegenbein D, Hurkuck W, Koepke J (2002) A combined rapid-quench and H_2-membrane setup for internally heated pressure vessels: description and application for water solubility in basaltic melts. Am Mineral 87:1717–1726

Berndt J, Koepke J, Holtz F (2005) An experimental investigation of the influence of water and oxygen fugacity on differentiation of MORB at 200 MPa. J Petrol 46:135–167. doi:10.1093/petrology/egh066

Botcharnikov RE, Almeev RR, Koepke J, Holtz F (2008) Phase relations and liquid lines of descent in hydrous ferrobasalt—implications for the Skaergaard intrusion and Columbia river flood basalts. J Petrol 49:1687–1727. doi:10.1093/petrology/egn043

Bowen NL (1928) The evolution of the igneous rocks. Princeton University Press, Princeton

Burnham CW (1979) The importance of volatile constituents. In: Yoder HS (ed) The evolution of the igneous rocks: fiftieth anniversary perspectives. Princeton University Press, Princeton, pp 439–482

Carroll MR, Blank JG (1997) The solubility of H_2O in phonolitic melts. Am Mineral 82:549–556

Carroll MJ, Webster J (1994) Volatiles in magmas: solubilities of sulfur, noble gases, nitrogen, chlorine, and fluorine in magmas. In: Carroll MR, Holloway JR (eds) Reviews in mineralogy, vol 30. Mineralogical Society of America, pp 231–271

Deer WA, Howie RA, Zussman J (1992) An introduction to the rock forming minerals, 2nd edn. Prentice Hall, Harlow, England

Devine JD, Gardner JE, Brack HP, Layne GD, Rutherford MJ (1995) Comparison of microanalytical methods for estimating H_2O contents of silicic volcanic glasses. Am Mineral 80:319–328

Di Carlo I, Rotolo SG, Scaillet B, Buccheri V, Pichavant M (2010) Phase equilibrium constraints on pre-eruptive conditions of recent felsic explosive volcanism at Pantelleria Island, Italy. J Petrol 51:2245–2276. doi:10.1093/petrology/egq055

Dickenson MP, Hess PC (1986) The structural role and homogeneous redox equilibria of iron in peraluminous, metaluminous and peralkaline silicate melts. Contrib Miner Petrol 92:207–217. doi:10.1007/BF00375294

Edgar AD, Parker LM (1974) Comparison of melting relationships of some plutonic and volcanic undersaturated alkaline rocks. Lithos 7:263–273. doi:10.1016/0024-4937(74)90047-4

Ernst WG (1962) Synthesis, stability relations, and occurrence of riebeckite and riebeckite–arfvedsonite solid-solutions. J Geol 70:689–736

Evans BW, Scaillet B (1997) The redox state of Pinatubo dacite and the ilmenite–hematite solvus. Am Mineral 82:625–629

Feig ST, Koepke J, Snow JE (2006) Effect of water on tholeiitic basalt phase equilibria: an experimental study under oxidizing conditions. Contrib Miner Petrol 152:611–638. doi:10.1007/s00410-006-0123-2

Feig ST, Koepke J, Snow JE (2010) Effect of oxygen fugacity and water on phase equilibria of a hydrous tholeiitic basalt. Contrib Miner Petrol 160:551–568. doi:10.1007/s00410-010-0493-3

Fenner CN (1929) The crystallization of basalts. Am J Sci 18:225–253. doi:10.2475/ajs.s5-18.105.225

Ford CE (1978) Platinum-iron alloy sample containers for melting experiments on iron-bearing rocks, minerals, and related systems. Mineral Mag 42:271–275

Freise M, Holtz F, Koepke J, Scoates J, Leyrit H (2003) Experimental constraints on the storage conditions of phonolites from the Kerguelen archipelago. Contrib Miner Petrol 145:659–672. doi:10.1007/s00410-003-0453-2

Freise M, Holtz F, Nowak M, Scoates JS, Strauss H (2009) Differentiation and crystallization conditions of basalts from the Kerguelen large igneous province: an experimental study. Contrib Miner Petrol 158:505–527. doi:10.1007/s00410-009-0394-5

French BM (1966) Some geological implications of equilibrium between graphite and a C–H–O gas phase at high temperatures and pressures. Rev Geophys 4:223–253. doi:10.1029/RG004i002p00223

French BM, Eugster HP (1965) Experimental control of oxygen fugacities by graphite-gas equilibriums. J Geophys Res 70:1529–1539. doi:10.1029/JZ070i006p01529

Gaillard F, Scaillet B, Pichavant H, Bény JM (2001) The effect of water and fO_2 on the ferric–ferrous ratio of silicic melts. Chem Geol 174:255–273. doi:10.1016/S0009-2541(00)00319-3

Giuli G, Alonso-Mori R, Cicconi MR, Paris E, Glatzel P, Eeckhout SG, Scaillet B (2012) Effect of alkalis on the Fe oxidation state and local environment in peralkaline rhyolitic glasses. Am Mineral 97:468–475. doi:10.2138/am.2012.3888

Green DH, Ringwood AE (1967) The genesis of basaltic magmas. Contrib Miner Petrol 15:103–190. doi:10.1007/bf00372052

Hamilton DL, Burnham CW, Osborn EF (1964) The solubility of water and effects of oxygen fugacity and water content on crystallization in Mafic Magmas. J Petrol 5:21–39. doi:10.1093/petrology/5.1.21

Holland T, Powell R (2003) Activity-composition relations for phases in petrological calculations: an asymmetric multicomponent formulation. Contrib Miner Petrol 145:492–501. doi:10.1007/s00410-003-0464-z

Holloway JR, Pan V, Gudmundsson G (1992) High-pressure fluid-absent melting experiments in the presence of graphite: oxygen fugacity, ferric/ferrous ratio and dissolved CO_2. Eur J Mineral 4:105–114

Holtz F, Behrens H, Dingwell DB, Johannes W (1995) H_2O solubility in haplogranitic melts—compositional, pressure, and temperature-dependence. Am Mineral 80:94–108

Huizenga JM (2001) Thermodynamic modelling of C–O–H fluids. Lithos 55:101–114. doi:10.1016/S0024-4937(00)00040-2

Husen A, Almeev RR, Koepke J, Holtz F (2012) Conducting absolutely H_2O-free high pressure experiments: method and

implications to Shatsky Rise Oceanic Plateau Basalts. In: Experimental mineralogy petrology geochemistry. Kiel, Germany, p 78
Jakobsson S, Oskarsson N (1994) The system C–O in equilibrium with graphite at high pressure and temperature: an experimental study. Geochim Cosmochim Acta 58:9–17. doi:10.1016/0016-7037(94)90442-1
Kesson SE, Lindsley DH (1976) Mare basalt petrogenesis—a review of experimental studies. Rev Geophys 14:361–373. doi:10.1029/RG014i003p00361
Kloess G (2000) Dichtefluktuationen natürlicher Gläser, Habil Thesis. Universität Jena
Kogarko LN, Romanchev BP (1977) Temperature, pressure, redox conditions, and mineral equilibria in agpaitic nepheline syenites and apatite-nepheline rocks. Geochem Int 14:113–128
Konnerup-Madsen J (2001) A review of the composition and evolution of hydrocarbon gases during solidification of the Ilímaussaq alkaline complex. South Greenl Geol Greenl Surv Bull 190:159–166
Konnerup-Madsen J, Rose-Hansen J (1984) Composition and significance of fluid inclusions in the Ilímaussaq peralkaline granite, South Greenland. Bulletin de Mineralogie 107:317–326
Kress VC, Carmichael ISE (1991) The compressibility of silicate liquids containing Fe_2O_3 and the effect of composition, temperature, oxygen fugacity and pressure on their redox states. Contrib Miner Petrol 108:82–92. doi:10.1007/BF00307328
Krumrei TV, Pernicka E, Kaliwoda M, Markl G (2007) Volatiles in a peralkaline system: abiogenic hydrocarbons and F–Cl–Br systematics in the naujaite of the Ilímaussaq intrusion, South Greenland. Lithos 95:298–314. doi:10.1016/j.lithos.2006.08.003
Kunzmann T (1999) The aenigmatite–rhönite mineral group. Eur J Mineral 11:743–756
Larsen LM (1976) Clinopyroxenes and coexisting mafic minerals from the alkaline Ilímaussaq intrusion, South Greenland. J Petrol 17:258–290. doi:10.1093/petrology/17.2.258
Larsen LM, Sørensen H (1987) The Ilímaussaq intrusion—progressive crystallization and formation of layering in an agpaitic magma. Geol Soc Lond Special Publ 30:473–488. doi:10.1144/GSL.SP.1987.030.01.23
Larsen LM, Steenfelt A (1974) Alkali loss and retention in an iron-rich peralkaline phonolite dyke from the Gardar province, south Greenland. Lithos 7:81–90. doi:10.1016/0024-4937(74)90021-8
Le Bas MJ, Maitre RWL, Streckeisen A, Zanettin B, IUGS Subcommission on the Systematics of Igneous Rocks (1986) A chemical classification of volcanic rocks based on the total alkali-silica diagram. J Petrol 27:745–750. doi:10.1093/petrology/27.3.745
Lukkari S, Holtz F (2007) Phase relations of a F-enriched peraluminous granite: an experimental study of the Kymi topaz granite stock, southern Finland. Contrib Miner Petrol 153:273–288. doi:10.1007/s00410-006-0146-8
MacDonald R, Davies GR, Bliss CM, Leat PT, Bailey DK, Smith RL (1987) Geochemistry of high-silica peralkaline rhyolites, Naivasha, Kenya Rift Valley. J Petrol 28:979–1008. doi:10.1093/petrology/28.6.979
MacDonald R, Baginski B, Leat PT, White JC, Dzierzanowski P (2011) Mineral stability in peralkaline silicic rocks: information from trachytes of the Menengai volcano, Kenya. Lithos 125:553–568. doi:10.1016/j.lithos.2011.03.011
Mann U, Marks M, Markl G (2006) Influence of the oxygen fugacity on mineral compositions in peralkaline melts: the Katzenbuckel volcano, Southwest Germany. Lithos 91:262–285. doi:10.1016/j.lithos.2005.09.004
Manning DAC (1981) The effect of fluorine on liquidus phase relationships in the system Qz–Ab–Or with excess water at 1 kb. Contrib Miner Petrol 76:206–215. doi:10.1007/bf00371960
Markl G (2001) Stability of Na–Be minerals in late-magmatic fluids of the Ilímaussaq alkaline complex, South Greenland. Geol Greenl Surv Bull 190:145–158
Markl G, Marks M, Schwinn G, Sommer H (2001) Phase equilibrium constraints on intensive crystallization parameters of the Ilimaussaq complex, South Greenland. J Petrol 42:2231–2258. doi:10.1093/petrology/42.12.2231
Markl G, Marks MAW, Frost BR (2010) On the controls of oxygen fugacity in the generation and crystallization of peralkaline melts. J Petrol 51:1831–1847. doi:10.1093/petrology/egq040
Marks M, Markl G (2001) Fractionation and assimilation processes in the alkaline augite syenite unit of the Ilimaussaq intrusion, South Greenland, as deduced from phase equilibria. J Petrol 42:1947–1969. doi:10.1093/petrology/42.10.1947
Marks M, Markl G (2003) Ilímaussaq 'en miniature': closed-system fractionation in an agpaitic dyke rock from the Gardar Province, South Greenland (contribution to the mineralogy of Ilímaussaq no. 117). Mineral Mag 67:893–919. doi:10.1180/0026461036750150
Marks MAW, Vennemann T, Siebel W, Markl G (2004) Nd-, O-, and H-isotopic evidence for complex, closed-system fluid evolution of the peralkaline Ilímaussaq intrusion, south Greenland. Geochim Cosmochim Acta 68:3379–3395. doi:10.1016/j.gca.2003.12.008
Marks MAW, Hettmann K, Schilling J, Frost BR, Markl G (2011) The mineralogical diversity of alkaline igneous rocks: critical factors for the transition from miaskitic to agpaitic phase assemblages. J Petrol 52:439–455. doi:10.1093/petrology/egq086
Médard E, Grove TL (2008) The effect of H_2O on the olivine liquidus of basaltic melts: experiments and thermodynamic models. Contrib Miner Petrol 155:417–432. doi:10.1007/s00410-007-0250-4
Metrich N, Rutherford MJ (1992) Experimental study of chlorine behavior in hydrous silicic melts. Geochim Cosmochim Acta 56:607–616. doi:10.1016/0016-7037(92)90085-W
Michael PJ, Schilling J-G (1989) Chlorine in mid-ocean ridge magmas: evidence for assimilation of seawater-influenced components. Geochim Cosmochim Acta 53:3131–3143. doi:10.1016/0016-7037(89)90094-X
Nekvasil H, Burnham CW (eds) (1987) The calculated individual effects of pressure and water content on phase equilibiria in the granite system. Magmatic processes: physicochemical principles. Geochemical Society, University Park, Pennsylvania
Nekvasil H, Dondolini A, Horn J, Filiberto J, Long H, Lindsley DH (2004) The origin and evolution of silica-saturated alkalic suites: an experimental study. J Petrol 45:693–721. doi:10.1093/petrology/egg103
Nicholls J, Carmichael ISE (1969) Peralkaline acid liquids: a petrological study. Contrib Miner Petrol 20:268–294. doi:10.1007/BF00377480
Ohmoto H, Kerrick D (1977) Devolatilization equilibria in graphitic systems. Am J Sci 277:1013–1044. doi:10.2475/ajs.277.8.1013
O'Neill HSC (1987a) The quartz–fayalite–iron and quartz–fayalite–magnetite equilibria and the free energies of formation of fayalite (Fe_2SiO_4) and magnetite (Fe_3O_4). Am Mineral 72:67–75
O'Neill HSC (1987b) The free energies of formation of NiO, CoO, Ni_2SiO_4. Am Mineral 72:280–291
Osborn EF (1959) Role of oxygen pressure in the crystallization and differentiation of basaltic magma. Am J Sci 257:609–647. doi:10.2475/ajs.257.9.609
Piotrowski JM, Edgar AD (1970) Melting relations of undersaturated alkaline rocks from South Greenland. Meddelelser om Grønland 181:62
Poulsen V (1964) The sandstones of the Precambrian Eriksfjord formation in South Greenland. Rapp Grønl Geol Unders 2:16
Ratajeski K, Sisson TW (1999) Loss of iron to gold capsules in rock-melting experiments. Am Mineral 84:1521–1527

Rayleigh FRS (1896) Theoretical considerations respecting the separation of gases by diffusion and similar processes. Philos Mag Ser 5(42):493–498. doi:10.1080/14786449608620944

Scaillet B, MacDonald R (2001) Phase relations of peralkaline silicic magmas and petrogenetic implications. J Petrol 42:825–845. doi:10.1093/petrology/42.4.825

Scaillet B, MacDonald R (2003) Experimental constraints on the relationships between peralkaline rhyolites of the Kenya Rift Valley. J Petrol 44:1867–1894. doi:10.1093/petrology/egg062

Scaillet B, MacDonald R (2006) Experimental constraints on pre-eruption conditions of pantelleritic magmas: evidence from the Eburru complex, Kenya Rift. Lithos 91:95–108. doi:10.1016/j.lithos.2006.03.010

Scaillet B, Pichavant M, Roux J (1995) Experimental crystallization of leucogranite magmas. J Petrol 36:663–705. doi:10.1093/petrology/36.3.663

Scaillet B, Pichavant H, Cioni R (2008) Upward migration of Vesuvius magma chamber over the past 20,000 years. Nature 455:216–219. doi:10.1038/nature07232

Schilling J, Frost BR, Marks MAW, Wenzel T, Markl G (2011) Fe–Ti oxide-silicate (QUIlF-type) equilibria in feldspathoid-bearing systems. Am Mineral 96:100–110. doi:10.2138/am.2011.3596

Schmidt BC, Behrens H (2008) Water solubility in phonolite melts: influence of melt composition and temperature. Chem Geol 256:259–268. doi:10.1016/j.chemgeo.2008.06.043

Schwab RG, Kuestner D (1981) Die Gleichgewichtsfugazitäten geologisch und technologisch wichtiger Sauerstoffpuffer. Neues Jahrbuch der Mineralogie Abhandlungen 140:111–142

Sood MK, Edgar AD (1970) Melting relations of undersaturated alkaline rocks. Meddelelser om Grønland 181:41

Sørensen H (1997) The agpaitic rocks—an overview. Mineral Mag 61:485–498. doi:10.1180/minmag.1997.061.407.02

Sørensen H (2001) The Ilímaussaq alkaline complex, South Greenland: status of mineralogical research with new results. Geol Greenl Surv Bull 190:1–167

Stelling J, Botcharnikov RE, Beermann O, Nowak M (2008) Solubility of H_2O- and chlorine-bearing fluids in basaltic melt of Mount Etna at T = 1050–1250 °C and P = 200 MPa. Chem Geol 256:102–110. doi:10.1016/j.chemgeo.2008.04.009

Thompson RN, Chisholm JE (1969) Synthesis of aenigmatite. Mineral Mag 37:253–255. doi:10.1180/minmag.1969.037.286.15

Toplis MJ, Carroll MR (1995) An experimental-study of the influence of oxygen fugacity on Fe–Ti oxide stability, phase-relations, and mineral-melt equilibria in ferro-basaltic systems. J Petrol 36:1137–1170. doi:10.1093/petrology/36.5.1137

Tuttle OF, Bowen NL (1958) Origin of granite in the light of experimental studies in the system $NaAlSi_3O_8$-$KAlSi_3O_8$-SiO_2-H_2O. Geol Soc Am Mem 74:153

Upton BGJ, Emeleus CH, Heaman LM, Goodenough KM, Finch AA (2003) Magmatism of the mid-Proterozoic Gardar Province, South Greenland: chronology, petrogenesis and geological setting. Lithos 68:43–65. doi:10.1016/S0024-4937(03)00030-6

Villiger S, Ulmer P, Müntener O, Thompson AB (2004) The liquid line of descent of anhydrous, mantle-derived, tholeiitic liquids by fractional and equilibrium crystallization-an experimental study at 1.0 GPa. J Petrol 45:2369–2388. doi:10.1093/petrology/egh042

Wager LR, Deer WA (1939) Geological investigations in east Greenland. Part III. The petrology of the Skaergaard intrusion, Kangerdlugssuaq, East Greenland. Meddelelser om Grønland 105:352

Watson EB (1979) Zircon saturation in felsic liquids: experimental results and applications to trace element geochemistry. Contrib Miner Petrol 70:407–419. doi:10.1007/bf00371047

Webster JD, Holloway JR, Hervig RL (1987) Phase equilibria of a Be, U and F-enriched vitrophyre from Spor Mountain, Utah. Geochim Cosmochim Acta 51:389–402. doi:10.1016/0016-7037(87)90057-3

B. Appendix

Title
An experimental study on the influence of fluorine and chlorine on phase relations in peralkaline phonolitic melts

Authors
Christopher Giehl, Michael A. W. Marks and Marcus Nowak

Status
Published online in *Contributions to Mineralogy and Petrology* 167:977
(doi: 10.1007/s00410-014-0977-7)

Associate Editor
Jochen Hoefs

Reviewer
Renat Almeev, Tom Andersen and Bruno Scaillet

Contributions of the candidate

Scientific ideas	60 %
Experimental work	100 %
Analytical work	90 %
Analysis and interpretation	70 %
Preparation of manuscript	90 %

Contrib Mineral Petrol (2014) 167:977
DOI 10.1007/s00410-014-0977-7

ORIGINAL PAPER

An experimental study on the influence of fluorine and chlorine on phase relations in peralkaline phonolitic melts

Christopher Giehl · Michael A. W. Marks · Marcus Nowak

Received: 2 November 2013 / Accepted: 29 January 2014 / Published online: 25 February 2014

Abstract Fluorine and chlorine affect phase stabilities in magmatic rocks. We present phase equilibrium experiments investigating a peralkaline and iron-rich phonolitic composition with variable F and Cl contents. The starting composition represents a dyke rock, which is a possible parental melt to the peralkaline Ilímaussaq plutonic complex (South Greenland). Experiments were performed at 100 MPa, 1,000–650 °C and low oxygen fugacity adjusted with graphite-lined gold capsules in an internally heated argon pressure vessel and rapid quench cold seal pressure vessels. To cover this large *T* interval, we applied a two-step fractional crystallization strategy where glasses representing residual melt compositions at 800 °C were synthesized as starting material for consecutive experiments at lower *T*. In these experiments, oxidized starting glasses allocate oxygen by reduction of ferric iron and up to 1.2 wt% dissolved OH form through reaction with hydrogen provided by the pressure medium (H_2O) in initially dry experiments. For OH determination, hydrated super-liquidus experiments in Au capsules were performed to calibrate the extinction coefficient for the fundamental OH stretching vibration using infrared spectroscopy ($\varepsilon_{3,415} = 48 \pm 3$ L mol^{-1} cm^{-1}). Observed mineral phases in our experiments are titanomagnetite, fayalitic olivine, clinopyroxene, aenigmatite ($Na_2Fe_5TiSi_6O_{20}$), alkali feldspar and nepheline (±native iron) coexisting with residual melt. Above 1.5 wt% F_{melt} concentrations, fluorite (CaF_2) and hiortdahlite ($Ca_6Zr_2Si_4O_{16}F_4$) are stable in favor of Ca-rich clinopyroxene. Sodalite ($Na_8Al_6Si_6O_{24}Cl_2$) and eudialyte ($Na_{15}Ca_6Fe_3Zr_3Si_{26}O_{73}(OH)_3Cl_2$) form at Cl_{melt} concentrations of 0.2–0.5 wt% (depending on *T*) and $ZrO_{2\ melt}$ concentrations >0.7 wt% are additionally needed to stabilize eudialyte and hiortdahlite. Therefore, F and Cl may become compatible in such systems and have the potential to influence F/Cl melt ratios in evolving magmas.

Keywords Phase equilibrium experiment · Liquid line of descent · Halogens · Phonolite · Ilímaussaq · Agpaitic · Eudialyte · Infrared spectroscopy · Extinction coefficient

Introduction

Peralkaline silicate melts have high solubilities of volatile components like H_2O, CO_2, S, F, Cl and Br (Kogarko 1974; Burnham 1979; Bureau and Métrich 2003; Scaillet and Macdonald 2006). Retention of alkalis and volatiles in these melts induces an unusually large crystallization interval (e.g., Piotrowski and Edgar 1970; Sood and Edgar 1970) and causes high solubilities of highly charged cations like Ti^{4+}, Zr^{4+} and Fe^{3+} (Watson 1979; Dickenson and Hess 1986; Hess 1991; Keppler 1993; Bartels et al. 2010). Silicate melts may contain up to 7 wt% F and 1 wt% Cl (e.g., Carroll and Holloway 1994; Webster and Duffield 1994; Aiuppa et al. 2009). Such elevated concentrations of F and Cl influence phase stabilities, solidus temperatures and viscosities (e.g., Foley et al. 1986; Luth 1988; Carroll 2005; Aiuppa et al. 2009; Filiberto and Treiman 2009; Filiberto et al. 2012; Baasner et al. 2013).

Communicated by J. Hoefs.

Electronic supplementary material The online version of this article (doi:10.1007/s00410-014-0977-7) contains supplementary material, which is available to authorized users.

C. Giehl (✉) · M. A. W. Marks · M. Nowak
Eberhard Karls Universität Tübingen, Wilhelmstr. 56, 72074 Tübingen, Germany
e-mail: christopher.giehl@uni-tuebingen.de
URL: http://www.geo.uni-tuebingen.de/index.php?id=2179

The most common halogen-bearing minerals in magmatic rocks are apatite, mica and amphibole, and less common are titanite, fluorite and topaz (e.g., Price et al. 1996; Marshall et al. 1998; Frindt et al. 2004; Gioncada et al. 2014). In peralkaline rocks, further halogen-bearing minerals such as sodalite, villiaumite, eudialyte and hiortdahlite (see Table 1 for mineral formulae) may occur. Peralkaline rocks are subdivided into miaskitic (with titanite and zircon) and agpaitic varieties, and the latter are characterized by complex Na–Ca–Fe–HFSE silicates such as the above-mentioned ones (Sørensen 1997; Marks et al. 2011). To achieve magma evolution from miaskitic to agpaitic, increasing concentrations of alkalis, H_2O and halogens were suggested to be key factors (Scaillet and Macdonald 2003; Andersen et al. 2010; Marks et al. 2011).

Eudialyte and hiortdahlite are characteristic for agpaitic rocks, and their high concentrations of, e.g., Zr, REEs, U and Th emphasize their economic potential (Sørensen 1992, 1997; Chakhmouradian and Zaitsev 2012). To date, eudialyte is mined in the Lovozero complex (Russia, Kramm and Kogarko 1997; Zakharov et al. 2011) and recent exploration activity rated the agpaitic Ilímaussaq plutonic complex (South Greenland) as a world-class REE and U deposit (e.g., Parsons 2012). As thermodynamic phase stability calculations disregard halogens (e.g., MELTS, Ghiorso and Sack 1995; Aiuppa et al. 2009; Rooney et al. 2012) and stabilities of, e.g., eudialyte and hiortdahlite are mainly unknown, there is a need to investigate such mineral phases experimentally.

The Ilímaussaq complex is a well-studied agpaitic complex (see the recent reviews of Sørensen 2001; Marks and Markl in press). A peralkaline iron-rich phonolitic dyke closely linked to the intrusion shows similar mineral assemblages and mineral chemistry compared with the Ilímaussaq plutonic rocks. These analogies offer convincing evidence that the dyke composition may be similar to the Ilímaussaq parental magma (Larsen and Steenfelt 1974; Marks and Markl 2003). A first set of crystallization experiments using the dyke composition reproduced the phenocryst assemblage (Mag, Ol, Cpx, Afs and Nph) at strongly reducing ($fO_2 \sim \Delta$ log FMQ -3) and nominally dry conditions at 850–800 °C and 100 MPa (Giehl et al. 2013). The concentrations of Cl and F in coexisting melts reached 0.3 and 0.9 wt%, respectively, but no halogen-bearing mineral phases were observed yet. In highly crystallized experiments, the presence of Ae indicated the transition to the agpaitic magmatic stage. However, large-scale equilibration in these runs is questionable because isolated melt pools form independent subsystems. In the present study, we use an experimental step-wise fractional crystallization strategy (Villiger et al. 2004) to overcome this problem. This allows for the experimental investigation of a large T interval of crystallization as is typical for peralkaline melts. We use a starting composition with Cl and F concentrations six times higher compared with the composition of the previous study. Both Cl and F resemble the concentrations of the above-mentioned dyke rock (0.4 wt% Cl and 1.0 wt% F) in order to study the phase relations of observed halogen-bearing phases (Fl, Hio, Sdl, Eud, Table 1).

Table 1 Mineral phases with abbreviations and simplified formulae

Mineral phase	Abbreviation	Formula
Titanomagnetite	Mag	$Fe_2(Fe,Ti)O_4$
Olivine	Ol	$(Fe,Mg)SiO_4$
Clinopyroxene	Cpx	$(Ca,Na)FeSi_2O_6$
Alkali feldspar	Afs	$(Na,K)AlSi_3O_8$
Nepheline	Nph	$Na_3KAl_4Si_4O_{16}$
Aenigmatite	Ae	$Na_2Fe_5TiSi_6O_{20}$
F-bearing phases		
Fluorite	Fl	CaF_2
Hiortdahlite	Hio	$(Ca,Na)_6Zr_2Si_4O_{14–16}F_4$
Apatite-(F)	Ap	$Ca_5(PO_4)_3(OH,F)$
Villiaumite	Vil	NaF
Arfvedsonite	Arf	$Na_3Fe_5Si_8O_{22}(OH,F)_2$
Cl-bearing phases		
Sodalite	Sdl	$Na_8Al_6Si_6O_{24}Cl_2$
Eudialyte	Eud	$Na_{15}Ca_6Fe_3Zr_3Si_{26}O_{73}(OH)_3(Cl,OH)_2$

Mineral phases *in italics* were not synthesized in this study

Experimental methods

Experimental strategy

In the previous study (Giehl et al. 2013), we investigated the phenocryst assemblage (1) of the dyke including Mag, fayalitic Ol, hedenbergite-rich Cpx, Afs and Nph. Experiments with added water (and the concomitant increase in fO_2 as induced by the experimental setup) invariably lead to the crystallization of large amounts of Mag resulting in low FeO*/high SiO_2 liquid lines of descent. In contrast, nominally dry experiments stabilized a phase assemblage matching the phenocrysts of the dyke following a high FeO*/low SiO_2 liquid line of descent. Moreover, mineral phases were generally larger in those experiments.

In this study, we focus on the evolved stage of magma evolution with particular emphasis on the role of Cl and F. In the dyke, the evolved stage is represented by the groundmass assemblage (2) consisting of albite and microcline as separate grains, Nph, aegirine-rich Cpx, Ae, Cl-bearing Sdl and Eud and F-bearing Fl, Hio and Arf (Table 1). This is applicable to the Ilímaussaq plutonic

Table 2 Experimental series and respective starting glasses

Experiment series	Primitive starting glass	Evolved starting glass
Low halogen oxidized	HAF-ox\pr[a]	HAF-ox\ev
Low halogen reduced	HAF-red\pr[a]	HAF-red\ev
High halogen	HAF-hH-red\pr	HAF-hH-red\ev

[a] Giehl et al. (2013)

rocks exhibiting similar phase assemblages in the early augite syenite phase (1) and the agpaitic main phase (2).

For these purposes, the starting glass composition from Giehl et al. (2013) was modified regarding Cl (0.4 wt%) and F (1.0 wt%) concentrations, according to the bulk rock analyses from Larsen and Steenfelt (1974). To follow up the liquid lines of descent, three glasses representing melt compositions from nominally dry phase equilibrium experiments at 800 °C and low fO_2 were synthesized and used as evolved starting compositions. Therefore, three experimental series are distinguished (Tables 2, 3). Starting glasses representing the bulk dyke rock are termed "primitive," and starting glasses representing residual melt compositions of primitive experiments are termed "evolved" for convenience.

In primitive low halogen experiments (oxidized and reduced are similar), the stable phase assemblage at 800 °C represents the complete phenocryst assemblage of the dyke rock. However, reaction textures of these phenocrysts (Mag, Cpx and Ol) in the dyke rock show disequilibrium with groundmass minerals (Ae and Na-rich Cpx, Fig. 3 in Marks and Markl 2003). Therefore, melts coexisting with the phenocryst assemblage were used as evolved starting composition, which is comparable to the withdrawal of phenocrysts from equilibrium with the melt as observed in the dyke rock. Evolved starting glasses are therefore expected to reproduce the dykes' late-magmatic groundmass assemblage in consecutive experiments where H_2O-poor conditions and low fO_2 are maintained. Accordingly, all evolved experiments were conducted under reduced and H_2O-poor conditions using residual melt composition tapped from primitive experiments at 800 °C.

Table 3 Composition of starting glasses in wt% determined with EMP analyses

Data from	Giehl et al. (2013)	This study	Giehl et al. (2013)	This study	This study	This study
T (°C)	900–750	800–650	950–750	800–700	1,000–750	800–700
Exp. series	Low halogen oxidized		Low halogen reduced		High halogen	
Starting gl.	HAF-ox\pr	HAF-ox\ev (residual melt run 94, $T = 800$ °C)	HAF-red\pr	HAF-red\ev (residual melt run 95, $T = 800$ °C)	HAF-hH-red\pr	HAF-hH-red\ev (residual melt run 113, $T = 800$ °C)
#Mg	3	1	3	1	3	3
A. I.	1.5	2.7	1.5	2.2	1.5	2.3
n	18	9	6	9	56	9
SiO_2	54.72(64)	53.15 (40)	53.91(24)	53.62(93)	51.94(57)	50.08(1.11)
TiO_2	0.52(2)	0.91(4)	0.53(2)	0.86(3)	1.05(4)	0.96(5)
ZrO_2	0.65(9)	1.34(11)	0.69(5)	1.17(12)	0.69(7)	0.85(10)
Al_2O_3	14.12(21)	10.00(11)	13.90(18)	11.33(38)	13.79(24)	11.58(17)
FeO*	11.51(29)	15.13(91)	12.23(48)	13.34(70)	12.25(55)	12.92(45)
XFe^{3+}	0.61(1)	0.96(1)	0.45(1)	0.96(1)	0.29(1)	0.94(1)
FeO	4.49	0.61	6.73	0.53	8.70	0.78
Fe_2O_3	7.80	16.13	6.11	14.23	3.95	13.49
MnO	0.46(3)	0.51(7)	0.50(2)	0.37(3)	0.50(5)	0.51(2)
MgO	0.19(2)	0.08(3)	0.20(4)	0.08(3)	0.18(3)	0.20(4)
CaO	2.84(8)	2.04(22)	3.01(20)	1.84(9)	2.98(20)	2.63(10)
Na_2O	9.40(27)	13.54(44)	9.45(32)	12.25(24)	9.52(29)	14.00(33)
K_2O	4.69(11)	4.10(11)	4.92(25)	4.19(10)	4.79(18)	3.72(19)
P_2O_5	0.13(3)	0.36(5)	0.11(4)	0.25(5)	0.16(4)	0.20(3)
Cl	0.06(1)	0.38(2)	0.05(1)	0.49(9)	0.41(4)	0.33(11)
F	0.17(5)	0.79(10)	0.16(6)	0.61(22)	0.98(16)	2.82(46)
Total	99.53(92)	102.32(77)	100.35(38)	100.38(1.12)	99.24(79)	100.80(1.55)

#Mg = Mg * $(Mg + Fe)^{-1}$ * 100; A. I. = (Na + K) * Al^{-1}; n = number of analyses; FeO* indicates total iron analyzed with EMP; XFe^{3+} (Fe^{3+} * (Fe^{2+} + Fe^{3+})$^{-1}$) was determined with Mössbauer spectroscopy, XFe^{3+} is expected to re-equilibrate at experimental conditions; two sigma error is abbreviated as (x) = 0.0 × or (xx) = 0.xx

However, the crystallization of anhydrous mineral phases in primitive experiments accumulates H_2O in the residual melt and the groundmass assemblage of the dyke involves OH-bearing mineral phases (e.g., Eud, Arf). To account for H_2O accumulation in primitive experiments, it is necessary to provide some H_2O in evolved experiments. Therefore, we introduce an alternative source for H_2O using oxidized evolved starting glasses. For the syntheses of these glasses, iron was added as Fe_2O_3 powder, oxidizing conditions were applied during glass syntheses (see below) and Mössbauer analyses confirm an $X\mathrm{Fe}^{3+}$ close to one (Table 3). Low fO_2 prevailing in the experiments allocates oxygen by reducing ferric iron (Fe_2O_3) to ferrous iron (FeO). Hydrogen is provided by the pressure medium (H_2O) and reacts with oxygen to form dissolved OH groups subsequently, still no free fluid phase forms (for details see experimental setup and Giehl et al. 2013). This applies for hydrothermal pressure vessels with a sufficiently high hydrogen fugacity, but is not the case if, e.g., argon is used as pressure medium. To quantify H_2O contents of residual melts, we used Fourier transform infrared (FTIR) spectroscopy on selected experiments. Evolved starting glasses may form up to 1.7 wt% H_2O by complete reduction of 16.8 wt% Fe_2O_3. However, the $X\mathrm{Fe}^{3+}$ of coexisting melts is between 0.1 and 0.3 at Δ log FMQ -4.3 to $+0.8$ (calculated after Kress and Carmichael 1991) in Au capsule experiments of the preceding study. We assume a similar or lower $X\mathrm{Fe}^{3+}$ of the melt in graphite capsule experiments resulting in the formation of up to 1.2–1.5 wt% H_2O. For the applied *P*- and *T*-conditions, we also expect the presence of other C-bearing volatile species (CO_2, CH_4 and CO) and a concomitant lower amount of H_2O formed by the described mechanism.

Starting compositions and glass syntheses

The starting glasses for phase equilibrium experiments were synthesized from oxide and carbonate powders, CaF_2, NaCl and $(NH_4)_2HPO_4$. These mixtures (25 g each) were homogenized and fused followed by rapid quenching in water. During syntheses of the starting glasses for primitive low halogen experiments (Giehl et al. 2013), about 80 % of the initial Cl and F were lost at 1,600 °C and 6 h dwell time. To compensate for this evaporation, Cl and F were added in excess, and synthesis *T* (1,300 °C) and dwell time (2 h) were adjusted to attain target Cl and F concentrations in all other starting glasses (see details of the procedure on eFig. 1).

In the preceding study, electron microprobe (EMP) analyses of Mag were often not possible due to the small crystal size. As Mag incorporates up to 36 wt% TiO_2, the initial TiO_2 concentration of primitive low halogen starting glasses was doubled (1.1 wt%) in the primitive high halogen starting glass in order to facilitate EMP Mag analyses. This starting glass was synthesized in a graphite crucible jacketed with a corundum crucible in a closed high temperature furnace to minimize $X\mathrm{Fe}^{3+}$. The melt was quenched to a glass bead in air, and the exposed oxidized surface was removed to minimize $X\mathrm{Fe}^{3+}$ zonation. Evolved starting glasses were synthesized in a $Pt_{90}Rh_{10}$ crucible in air to maximize $X\mathrm{Fe}^{3+}$ (Table 3). After synthesis, the glasses were ground and a grain size of 300–500 µm was sieved. Compared to smaller grain sizes, this glass powder provides limited nucleation sites on grain boundaries leading to larger mineral phases in phase equilibrium experiments.

Experimental setup

Graphite-lined Au capsules (C capsules) were completely filled with 50–60 mg glass powder to minimize the free volume in the capsule, dried to minimize adsorbed H_2O, welded shut and checked for possible leakage. This type of double-capsule effectively avoids alloying of iron with the capsule material (Holloway et al. 1992) and adjusts reducing conditions (Δ log FMQ -1 to -2.5) within the range of the CCO and the COH oxygen buffer (French and Eugster 1965; French 1966; Jakobsson and Oskarsson 1994). Experiments were carried out at 100 MPa in hydrothermal vertically mounted cold seal rapid quench vessels (CSPV) at 950–650 °C, and one run at 1,000 °C was performed in an internally heated argon pressure vessel (IHPV). The experimental *T* was continuously monitored with K-type (CSPV, ±5 °C) or S-type (IHPV, ±3 °C) thermocouples, respectively. After 24–840 h (usually 336 h), the experiments were terminated by isobaric rapid quenching (ca. 150–200 K s^{-1}, Berndt et al. 2002). For a detailed description of capsule dimensions, capsule preparation and the experimental setup, see Giehl et al. (2013).

Hydrated glasses for FTIR calibration

To quantify H_2O_{melt} concentrations of nominally dry experiments, we complemented EMP glass analyses with FTIR spectroscopy. Hydrated glasses for FTIR calibration were synthesized with 1, 2, 3 and 4 wt% H_2O, respectively, using the evolved low halogen oxidized starting glass. Experiments were conducted in Au capsules using CSPVs at 100 MPa, 850 °C and 24 h run duration. Except for run 179 with 4 wt% H_2O, which contains few Mag crystals (<1 wt%), these hydrated glasses are crystal-free. Glass compositions are homogeneous and within $\pm 2\sigma$ of the starting glass (eTab. 1). However, FeO* is consistently lower compared with the starting glass due to some iron loss to the Au capsule (<5 % relative).

Analytical methods

To check for homogeneity, three to nine glass pieces from top, middle and bottom parts of each experimental capsule were embedded in epoxy resin, polished and carbon coated for EMP analyses. Starting glasses, residual glasses and mineral phases of the experimental products were analyzed with a JEOL 8900 electron microprobe with an acceleration voltage of 15 kV. The beam current was 20 nA for Mag, Ol, Cpx, native iron, Ae, Fl, Hio and Eud, 8–10 nA for Afs, Nph, Sdl and Ap and 4 nA for glasses. The counting times were 16–60 s, depending on element concentrations. Analyses were calibrated against reference materials (diopside, strontium titanate, zirconium dioxide, plagioclase, hematite, rhodonite, albite, sanidine, apatite, tugtupite and topaz), and internal $\phi\rho z$ procedures were used for data reduction (Armstrong 1988). A focused beam was used for Mag, Ol, Cpx, Ae, Fl and Hio. Counting times were kept short, and a defocused beam was used for Afs, Nph, Sdl, Eud, Ap (10 s, 2–10 μm) and glasses (10 s, 10 μm) to avoid beam damage and to ensure a constant sodium signal during analyses.

Starting glasses (ground to <125 μm) were analyzed for $X\mathrm{Fe}^{3+}$ with ^{57}Fe-Mössbauer spectroscopy using a ^{57}Co source in Rh matrix operated at room T. The spectra were calibrated against alpha-Fe(0) foil and interpreted with the RECOIL software package (University of Ottawa, Canada) using Voigt-based fitting methods. Samples were powdered and held in acrylic glass containers.

For FTIR spectroscopy, glass pieces of starting glasses, hydrated glasses and selected phase equilibrium experiments were embedded in epoxy resin enfolded with an alumina ring and polished on both sides to a thickness of 39–97 μm, measured with a digital micrometer (Mitutoyo, accuracy ±3 μm). FTIR analyses were performed using a Bruker Vertex 80v with a Hyperion 3000 microscope in transmission mode using a globar light source and a KBr beam splitter. Samples were analyzed from 550 to 7,500 cm^{-1} with a spectral resolution of 4 cm^{-1} and accumulation of 32–128 scans using a SE-MCT detector. A knife-edge aperture was used to outline 10x10–50x50-μm glass sample, and depending on the amount of mineral phases, air was taken as background reference.

Calculation methods, equilibrium conditions and FTIR calibration

Long run durations lead to the crystallization of sufficiently large mineral phases (shortest axis 4–100 μm), and contamination of EMP analyses with surrounding residual glass or mineral phases was negligible in the majority of analyses. The doubled TiO_2 concentration in the primitive high halogen starting glass resulted in an increase of Mag size and improved quantitative EMP analyses. This allows for mass balance calculations (least squares fit), which were performed using mean values of EMP analyses (normalized to 100 wt%). Quantitative image analysis of BSE images was considered for comparison, but the large number of coexisting mineral phases and their similar shades of gray impede reasonable results. Mineral formulas were calculated using atomic weights from Robie et al. (1979), and for Eud, we used the Excel® calculation spreadsheet from Pfaff et al. (2010). The $X\mathrm{Fe}^{3+}$ in mineral phases was calculated from mineral structural formulae (eTabs. 2–13).

Variable run durations of 168–336 h (compare runs 120 and 157) and repeated experiments (runs 157 and 163) result in identical phase assemblages and similar phase abundances and phase compositions (Table 4). Although mineral phases are not equally distributed on a small scale, the phase assemblages were identical regarding top, middle and bottom of the capsule, and the composition of mineral phases and residual glasses is homogeneous (eTabs. 2–14). This is supported by EMP traverses through residual glasses (runs 127, 139 and 141) with no systematic variations that exceeded statistical inhomogeneities (eTab. 1). Furthermore, low mass balance residuals (s^2) yield reasonable phase abundances, melt fractions and #Mg's of Mag, Ol, Cpx and Ae decrease with decreasing T (Table 4, eFigs. 2 and 3). Exceptions are highly crystallized experiments representing the lowest T's within their experimental series, they are not considered in the following. Long run durations (840 h) for evolved high halogen experiments were found to increase the size of mineral phases (up to 200 μm). Despite long run durations, highly crystallized experiments with less than 30 wt% residual melt do not attain neither textural nor chemical large-scale equilibration due to isolated melt pockets. All experiments were rapidly quenched (ca. 150–200 K s^{-1}), still two low T runs at 700–650 °C (runs 127 and 128) contain few small anhedral dendritic crystals. Based on mixed analyses with residual glass, these dendritic phases are presumably Cpx. They occur frequently as inclusions in euhedral Nph and Sdl and must have crystallized early, probably during rapid heating. Hence, quenching problems can be ruled out. Low viscosity, supported by a high A. I., may favor crystal nucleation over crystal growth, with those crystals being preserved by subsequent overgrowth of Nph and Sdl.

To quantify H_2O in glasses, we calibrated FTIR spectroscopy against Karl Fischer titration (KFT) analyses using nominally dry glass (<0.1 wt% H_2O) and hydrated glasses that were equilibrated with variable amounts of H_2O (1–4 wt%). H_2O contents of hydrated glasses analyzed with KFT are 2.7–5.7 wt%. The additional formation of OH in nominally dry experiments is explained by hydrogen input by diffusion into the capsule in

Table 4 Experimental conditions, run products, phase proportions (in wt%) and mass balance residuals (s^2). All experiments were conducted nominally dry in C capsules at 100 MPa

Run	Run time (h)	T (°C)	[1]fO_2 (Δ log FMQ)	Gl	Mag	Ol	Cpx	Fe	Afs	Nph	Ae	Fl	Hio	Sdl	Eud	s^2
Evolved low halogen oxidized																
119	168	800	−1.7	100	–	–	–	–	–	–	–	–	–	–	<1	0.24
120	168	750	−1.5	79	–	–	4	–	8	3	5	–	–	1	<1	0.18
157	336	750	−1.5	78	–	–	5	–	9	5	2	–	–	1	<1	0.12
163	336	750	−1.5	84	–	–	3	–	5	4	2	–	–	1	1	0.27
127	336	700	−1.4	53	–	–	15	–	14	10	4	–	–	3	1	0.32
128	336	650	−1.2	39	–	–	31	–	17	9	–	–	–	4	<1	0.39
Evolved low halogen reduced																
151	336	800	−1.7	86	–	–	2	–	10	–	1	–	–	1	<1	0.01
130	336	750	−1.5	55	–	–	5	–	26	–	8	–	–	5	1	0.17
141	336	700	−1.4	45	–	–	–	–	27	–	12	–	–	10	6	0.68
Primitive high halogen																
102	24	1,000	−2.2	100	–	–	–	–	–	–	–	–	–	–	–	–
116	336	950	−2.0	100	–	–	–	–	–	–	–	–	–	–	–	–
100	336	925	−2.0	100	<1	<1	–	<1	<1	–	–	–	–	–	–	0.41
98	336	900	−1.9	93	1	3	–	–	3	–	–	–	–	–	–	0.36
97	336	875	−1.9	73	1	6	1	–	19	–	–	–	–	–	–	0.26
96	336	850	−1.8	72	1	6	2	<1	21	–	–	–	–	–	–	0.16
101	336	825	−1.7	49	1	8	1	–	34	<1	–	<1	3	4	–	0.02
113	504	800	−1.7	35	–	11	–	–	39	5	–	<1	5	5	–	0.28
114	504	775	−1.6	29	–	8	–	–	40	7	5	<1	5	6	–	0.11
139	504	750	−1.5	30	–	5	–	–	33	15	7	<1	10	<1	<1	0.38
Evolved high halogen																
166	840	800	−1.7	99	<1	–	–	–	–	–	–	1	–	–	–	1.81
167	840	750	−1.5	70	–	–	–	–	6	12	8	2	–	2	–	0.31
171	840	700	−1.4	55	–	–	–	–	12	17	11	3	–	2	–	0.30

[1] fO_2 is estimated as average between CCO and COH oxygen buffers

combination with liberation of oxygen through reduction of ferric iron. This indicates that 1.7(1) wt% H_2O formed, consistent with initial Fe_2O_3 glass concentrations, through reduction of Fe_2O_3. Three to ten spectra of each glass sample were recorded and found to be identical within error. Representative background-corrected mid-infrared (MIR) spectra are shown on Fig. 1.

Thin samples show sinusoidal modulations caused by interference fringes due to internal reflection (Fig. 1, Tamic et al. 2001). Note fluctuating atmospheric CO_2 represented by a band at 2,350 cm^{-1} (Blank and Brooker 1994). Hydrated glasses show a band at 1,644 cm^{-1} assigned to H_2O bending (Nakamoto 1978) and a broad asymmetric absorption band at 3,415 cm^{-1} due to the fundamental OH stretching vibration (Stolper 1982; Davis and Tomozawa 1996). Increasing absorbance of the 3,415 cm^{-1} band shows a linear relationship (forced through zero) with increasing H_2O glass concentrations analyzed with KFT (eTab. 15, eFig. 4).

Concentrations of H_2O and peak height derived from FTIR spectra of hydrated glasses were used to calculate extinction coefficients using the Beer–Lambert law (eTab. 15, Fig. 1). We used the following formula (Eq. 1, Stolper 1982)

$$\varepsilon = 100 * M * A * d^{-1} * \rho^{-1} * c^{-1} \quad (1)$$

where ε is the extinction coefficient (L mol^{-1} cm^{-1}), M is the molecular weight of H_2O (g mol^{-1}), A is absorbance at 3,415 cm^{-1}, d is glass sample thickness (cm), ρ is density (g L^{-1}) and c is H_2O concentration in wt%. The absorbance of OH bands (A_{3415}) was determined using a linear baseline as illustrated for selected samples on Fig. 1. Glass densities were calculated after Appen (1952) and Kloess (2000) omitting Zr, P, Cl and F; still the sum of all other elements is higher than 97 wt%. The calculated density of evolved oxidized low halogen starting glass (2.68 g L^{-1}) is close to the density determined with an Archimedes balance (2.63(5) g L^{-1}).

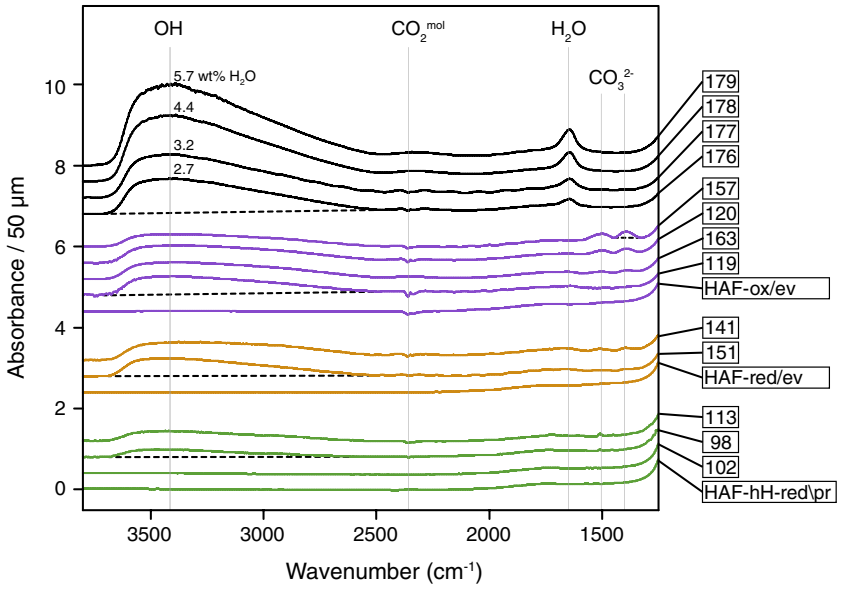

Fig. 1 MIR spectra of starting glasses, hydrated glasses and residual glasses of nominally dry experiments. *Colors* are according to Fig. 2, for experiment conditions see Table 4. CO_2^{mol} represents atmospheric molecular CO_2. Spectra are normalized to 50 µm glass sample thickness and H_2O concentrations for calibration were analyzed with KFT. Spectra are shifted for clarity

The mean ε value of four hydrated glasses (2.7–5.7 wt% H_2O) is $\varepsilon_{3,415} = 48 \pm 3$ L mol^{-1} cm^{-1}), which is significantly lower compared with previously published extinction coefficients for various silicate glass compositions ($\varepsilon_{3,550} = 61$–70 L mol^{-1} cm^{-1}, Pandya et al. 1992; Dixon et al. 1995; Yamashita et al. 1997; Silver and Stolper 1989; Behrens et al. 2009; Shishkina et al. 2010). Mandeville et al. (2002) showed that Fe-bearing andesitic glasses (4.5–7.6 wt% FeO) have lower $\varepsilon_{3,570}$ values compared with Fe-free andesitic glasses (62.3 ± 0.4 and 69.2 ± 0.5, respectively), and the low ε value might therefore be related to the high FeO* content of the analyzed glasses.

The absorbance of carbonate bands (A_{1390}) was determined using a linear baseline as for OH bands (Fig. 1), and carbonate concentrations were calculated using an extinction coefficient for the peak height in basaltic glasses ($\varepsilon_{1,430} = 316 \pm 12$, Shishkina et al. 2010). Near-equilibrium with a C–O–H fluid is indicated by the presence of both OH– and carbonate bands.

Results

Mössbauer spectroscopy

As shown by Giehl et al. (2013), the $X\text{Fe}^{3+}$ of the starting glass constrains fO_2 and may produce secondary H_2O in fluid-absent graphite capsule experiments. Therefore, the primitive high halogen starting glass was synthesized at low fO_2 (red). This starting glass ($X\text{Fe}^{3+} = 0.29$) defines even more reducing fO_2 compared with the low halogen reduced starting glass ($X\text{Fe}^{3+} = 0.45$). This is supported by the observation that native iron is stable in two experiments and Mag and Cpx formula calculations yield $X\text{Fe}^{3+}$ values close to zero (Table 4, eTabs. 2 and 4). In contrast, $X\text{Fe}^{3+}$ of evolved starting glasses is close to 1 in order to produce secondary H_2O and to apply slightly higher fO_2. Keep in mind that the experimental series are termed after the $X\text{Fe}^{3+}$ of the primitive starting glass, so the starting glass, for example, evolved low halogen reduced experiments is oxidized.

Residual melt

MIR spectra of residual glasses from nominally dry C capsule experiments show OH stretching vibrations while molecular H_2O is not observed. Additionally, residual glasses of run 120, 157 and 141 (and possibly run 151, 119 and 163) show a band doublet at 1,500 and 1,390 cm^{-1}, which is attributed to carbonate vibrations (Blank and Brooker 1994; Nowak et al. 2003; Spickenbom et al. 2010). In contrast, spectra of starting glasses and the experiment conducted in an IHPV (run 102) do not show OH, H_2O or carbonate bands. Based on the calibrated extinction coefficient, H_2O concentrations of residual glasses in C capsule experiments are 0.5(1)–1.2(1) wt% (Table 5). In run 157, carbonate was quantified to 0.2(1) wt%, whereas the other experiments yielded values close to the limit of detection. However, these bands offer qualitative evidence for the presence of dissolved carbonate groups. The experiment conducted in an IHPV does not show OH bands or carbonate bands, because H_2 fugacity was too low to yield appreciably H_2O (via the reduction of Fe^{3+}) and hence dissolved OH groups.

Liquid lines of descent of evolved experiments are consecutive to primitive experiments. Averaged EMP glass

Table 5 Glass compositions of hydrated glasses and residual glass compositions of phase equilibrium experiments in wt%

Run	T (°C)	*n*	SiO_2	TiO_2	ZrO_2	Al_2O_3	FeO*	MnO	MgO	CaO	Na_2O	K_2O	P_2O_5	Cl	F	Total[a]	H_2O (wt%)
Hydrated glasses																	
176	850	5	54.14	0.88	1.32	9.47	13.19	0.50	0.09	2.27	12.71	4.01	0.42	0.35	0.65	100	2.7
177	850	4	54.50	0.83	1.32	9.23	13.01	0.49	0.10	2.24	12.80	4.10	0.44	0.36	0.58	100	3.2
178	850	5	54.90	0.83	1.36	9.44	12.63	0.49	0.09	2.17	12.63	4.18	0.30	0.36	0.64	100	4.4
179	850	5	52.33	0.76	1.31	8.95	16.01	0.50	0.08	2.10	12.81	3.83	0.36	0.37	0.59	100	5.7
Residual glasses																	
[b]119	800	9	52.28	0.90	1.25	9.56	14.74	0.52	0.08	2.06	13.42	3.99	0.30	0.32	0.58	100	1.2
[b]120	750	9	51.95	0.63	1.36	8.94	14.83	0.58	0.07	1.72	14.75	3.77	0.26	0.37	0.75	100	1.2
[c]157	750	6	51.42	0.85	1.42	8.52	15.75	0.60	0.07	1.60	14.56	3.77	0.29	0.37	0.79	100	0.9
[b]163	750	5	52.38	0.77	1.31	8.68	15.43	0.58	0.07	1.67	13.97	3.78	0.22	0.36	0.77	100	1.1
127	700	50	52.31	0.77	1.43	6.62	15.03	0.69	0.06	1.26	16.51	3.36	0.40	0.30	1.26	100	na
128	650	9	50.73	0.68	1.47	6.42	13.72	0.92	0.05	1.12	19.22	3.30	0.44	0.19	1.74	100	na
[b]151	800	7	52.32	0.85	1.31	10.68	14.17	0.43	0.07	1.70	13.16	3.92	0.19	0.50	0.71	100	1.2
130	750	9	51.10	0.60	1.30	8.96	15.23	0.50	0.08	1.58	15.69	3.37	0.24	0.35	1.02	100	na
[b]141	700	48	53.40	0.16	0.75	7.94	16.22	0.52	0.10	1.55	16.25	3.05	0.30	0.26	1.27	100	1.2
102	1,000	9	53.69	1.04	0.72	14.47	10.80	0.47	0.16	2.68	9.27	4.99	0.13	0.42	1.14	100	bdl
116	950	9	53.54	1.05	0.73	14.48	10.88	0.51	0.17	2.66	9.60	4.79	0.17	0.36	1.06	100	na
100	925	9	54.05	0.91	0.71	14.58	10.99	0.47	0.19	2.86	9.37	4.60	0.17	0.31	0.78	100	na
98	900	9	53.40	0.88	0.79	14.34	10.80	0.46	0.17	3.16	10.05	4.44	0.12	0.38	1.01	100	0.5
97	875	9	51.38	0.85	1.02	14.10	10.74	0.44	0.14	3.35	11.36	4.21	0.17	0.58	1.66	100	na
96	850	9	51.42	0.92	0.98	14.34	10.59	0.45	0.14	3.35	11.69	4.22	0.16	0.45	1.29	100	na
101	825	9	51.08	0.95	0.87	13.20	11.23	0.42	0.17	2.95	13.18	3.98	0.13	0.33	1.50	100	na
113	800	9	49.98	1.04	0.94	11.78	12.69	0.48	0.18	2.77	13.59	3.87	0.14	0.38	2.16	100	0.7
114	775	9	49.60	0.95	0.90	10.07	14.26	0.58	0.20	2.88	14.18	3.47	0.19	0.36	2.34	100	na
139	750	8	50.27	0.52	1.58	8.01	14.98	0.68	0.22	2.82	14.80	3.18	0.20	0.32	2.41	100	na
166	800	8	51.41	0.92	0.79	10.97	12.87	0.46	0.17	2.10	13.53	3.87	0.18	0.36	2.36	100	na
167	750	8	51.40	0.42	1.02	9.43	13.40	0.61	0.19	1.70	15.15	3.47	0.26	0.37	2.60	100	na
171	700	9	51.70	0.20	1.23	8.07	13.75	0.63	0.21	1.57	16.24	3.06	0.31	0.32	2.71	100	na
Typical error ($\pm 1\sigma$)			0.6	0.05	0.1	0.2	0.4	0.04	0.02	0.15	0.3	0.15	0.04	0.02	0.1		0.1

n is the number of EMP analyses

[a] Total is normalized to 100 wt% anhydrous

[b] Carbonate bands observed, but not quantified

[c] Carbonate band quantified to 0.2 (1) wt%

analyses of hydrated glasses and residual glasses are listed in Table 5 (raw data are provided in the electronic appendix, eTab. 1). Although initial concentrations of TiO_2, Cl and F are different, all three series show very similar liquid lines of descent with decreasing SiO_2, Al_2O_3, K_2O, CaO and increasing Na_2O, A. I. (from 1.5 to 5.5), Na/(Na + K), Na/(Na + Ca), Na/Fe, MnO and P_2O_5 (Fig. 2a–k). Na/Fe generally increases (for 1,000–650 °C), but shifts back to lower Na/Fe around 800 °C (Fig. 2i). In contrast, TiO_2, ZrO_2, Ti/(Ti + Zr), FeO*, MgO, #Mg, Cl, F and Cl/(Cl + F) show considerable variations in different experimental series (Fig. 3a–i). In low halogen experiments, #Mg decreases with decreasing *T*, while #Mg is relatively constant in high halogen experiments. This is due to the limited stability and low abundance of Cpx, which is the mineral phase with the highest #Mg (eFig. 3, eTab. 4). Differences in initial TiO_2 are due to doubled initial concentration in the high halogen starting glass; however, the general trends are similar.

Mineral phases

The observed mineral phases are titanomagnetite, fayalitic olivine, clinopyroxene, native iron, alkali feldspar, nepheline, aenigmatite, fluorite, hiortdahlite, sodalite and eudialyte, coexisting with residual melt (Fig. 4, native iron is not

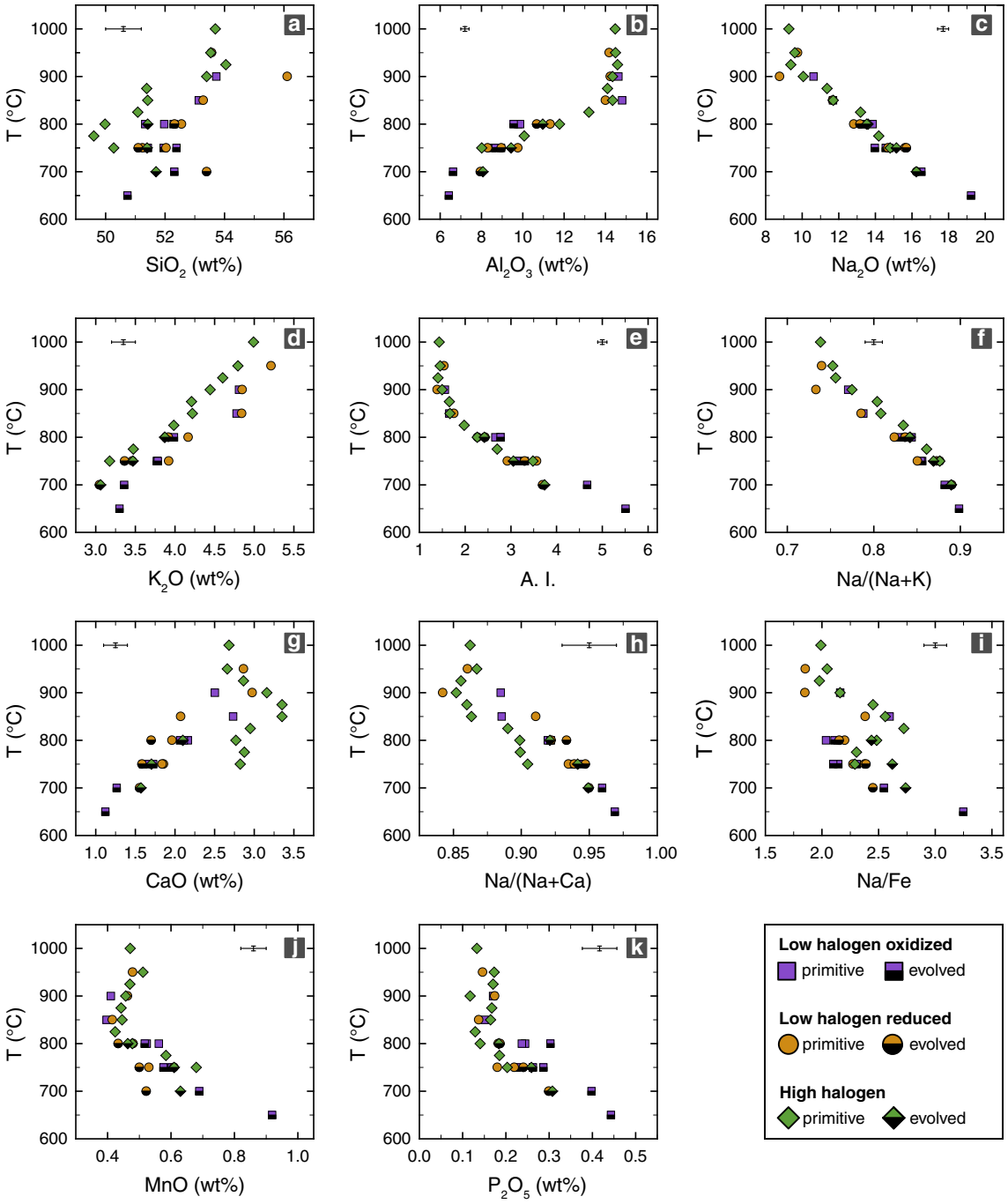

Fig. 2 The compositional trends of residual melts are similar for decreasing SiO_2, Al_2O_3, K_2O, CaO and increasing Na_2O, A. I. (from 1.5 to 5.5), Na/(Na + K), Na/(Na + Ca), Na/Fe, MnO and P_2O_5 (data for primitive low halogen experiments is from Giehl et al. 2013)

shown). Apatite-(F) is only stable in one experiment that failed large-scale equilibration (run 172). In the discussed experiments (Table 4), the $P_2O_{5\ melt}$ concentration increases up to 0.4 wt%; however, no P-bearing mineral phases were observed.

Super-liquidus experiments indicate that the liquidus *T* is between 950 and 925 °C, and the solidus *T* is lower than 650 °C (Table 4). The *T* stabilities of mineral phases are illustrated on Fig. 5, their weight percent proportions are shown in Table 4, coexisting melt compositions are given in Table 5 and compositions and formula calculations of mineral phases can be found in the electronic appendix (eTab. 2–13). Although this paper is focused on mineral stabilities and melt compositions only, we here

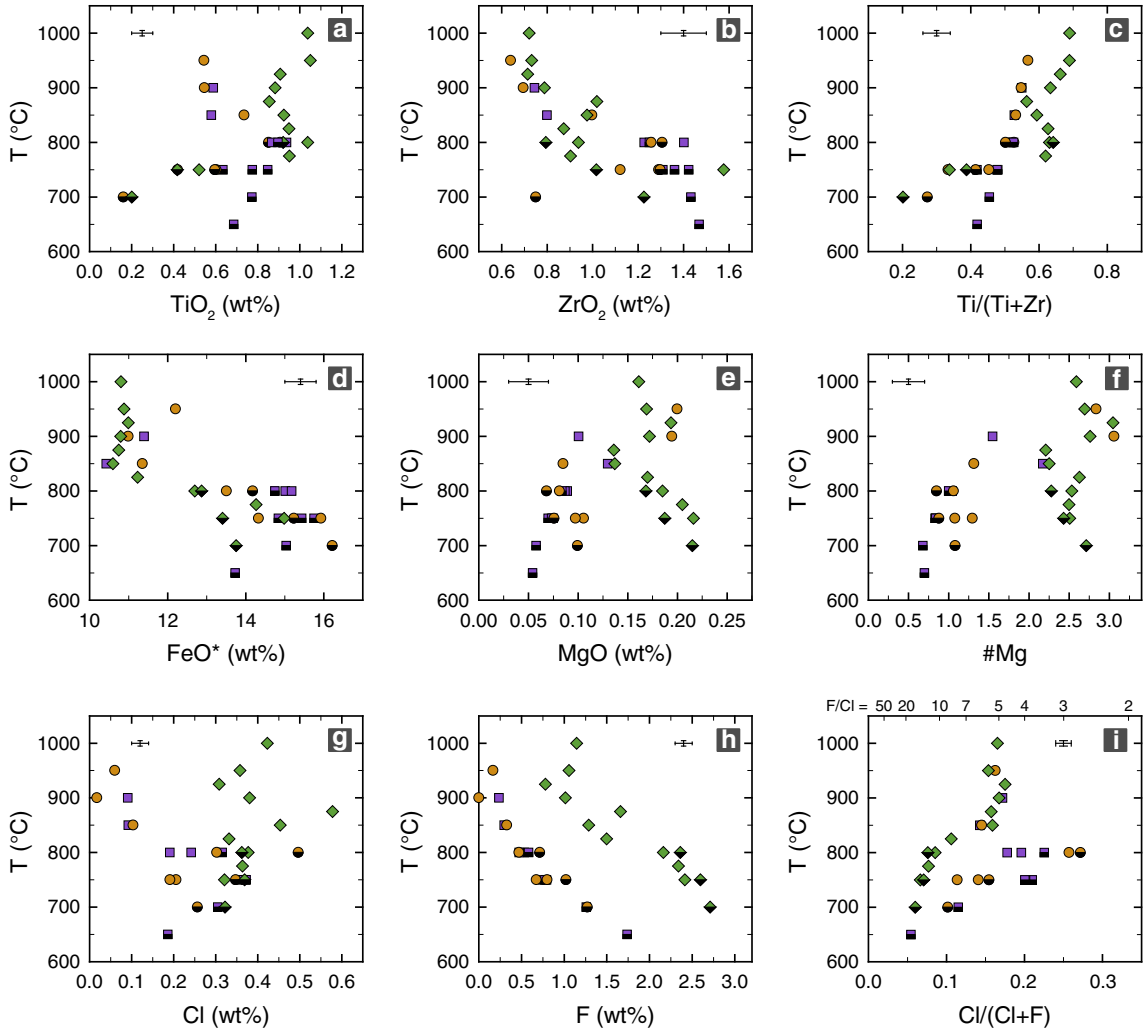

Fig. 3 The compositional trends of residual melts show considerable variations for TiO_2, ZrO_2 (and the Ti/(Ti + Zr) ratio), FeO*, MgO (and the #Mg), Cl, F (and the Cl/(Cl + F) ratio) in different experimental series. For a convenient comparison with literature data, the Cl/(Cl + F) plot includes a second *x*-axis with the widely used F/Cl ratio. *Symbols* and *colors* are according to Fig. 2 (data for primitive low halogen experiments are from Giehl et al. 2013)

report relatively high concentrations of TiO_2 (up to 2.4 wt%) and ZrO_2 (up to 2.1 wt%) in Cpx.

The denotation of the Ca–Zr–F silicate synthesized in this study (eTab. 10) as hiortdahlite is based on its similarity to hiortdahlite originally described by Brøgger (1890) from Langesundsfjord (Norway). However, a pegmatite from Ilímaussaq contains compositionally similar material, with a slightly different crystal structure, and was assigned to hiortdahlite-II (Robles et al. 2001). It is known that minor changes in the composition of cuspidine–wöhlerite group minerals (of which hiortdahlite and hiortdahlite-II are members) may stabilize a new structure. A hiortdahlite-like mineral is also observed in the dyke rock (Larsen and Steenfelt 1974; Marks and Markl 2003), but unfortunately neither EMP nor X-ray diffraction data are available. However, in the present study, we focus on compositional aspects of this mineral phase neglecting structural details. Therefore, we name this phase as hiortdahlite for convenience.

Primitive experiments

In primitive low halogen experiments, the observed mineral phases are Mag, Ol, Cpx, Afs, Nph and, at 750 °C, additionally Ae in the low halogen reduced experiments (Fig. 2 in Giehl et al. 2013). In high halogen experiments, additional F-bearing Fl and Hio are present at 825–750 °C, Sdl is stable between 825 and 775 °C and Eud is observed at 750 °C only (Fig. 4).

In high halogen experiments, Afs and Ol crystallize at higher *T* (950–925 °C) compared with low halogen experiments (900–850 °C, Fig. 5). The *T* interval with Ae

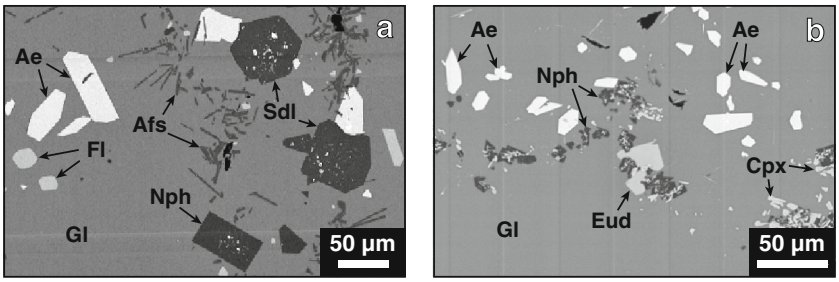

Fig. 4 Back-scattered electron images of evolved phase equilibrium experiments at 750 °C conducted using **a** high halogen (run 167) and **b** low halogen starting glasses (run 120). See Table 1 for mineral phase abbreviations

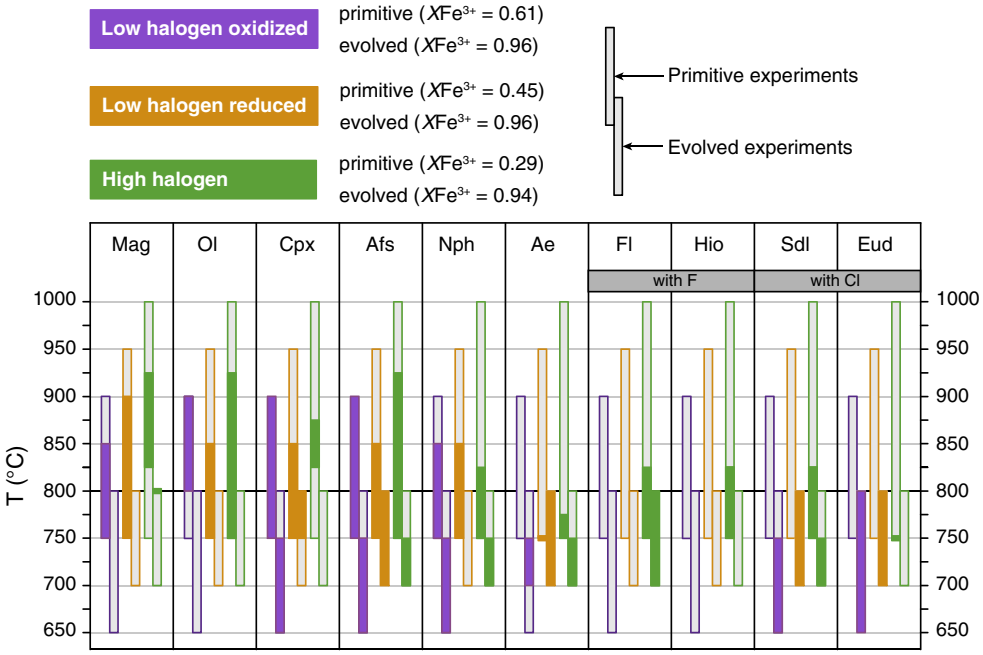

Fig. 5 Mineral phase stabilities with respect to *T*, ordered by experimental series. *Color-filled bars* stable mineral phases for a certain *T* interval (data for primitive low halogen experiments are from Giehl et al. 2013)

present is similar (775–750 °C), but the *T* intervals with Mag (925–825 °C) and Cpx (875–825 °C) present are smaller compared with low halogen experiments.

Evolved experiments

Evolved experiments generally lack Mag, Ol and Hio (the only exception with Mag, run 167, is discussed later). Cpx is present at 750–650 °C in low halogen oxidized experiments, at 800–750 °C in low halogen reduced experiments but absent in high halogen experiments. Afs is stable in almost all runs, except for some near-liquidus experiments at 800 °C (runs 119 and 166). Nph occurs at $T \leq 750$ °C, but is absent in low halogen reduced experiments. In low halogen experiments, Afs is more abundant than Nph, and in high halogen experiments, the opposite is the case. Ae is stable in all experiments at 750–700 °C and in low halogen reduced experiments additionally at 800 °C. In high halogen experiments and low halogen reduced experiments, Ae is more abundant than in low halogen oxidized experiments. Fl is observed in evolved high halogen experiments between 800 and 700 °C. Sdl occurs at and below 750 °C, in low halogen reduced experiments additionally at 800 °C. Eud is stable throughout in evolved low halogen experiments (800–650 °C), but absent in evolved high halogen experiments.

Discussion

Phase relations and liquid lines of descent

Phase equilibrium experiments with oxidized starting glass (runs 151, 141, 119, 163, 120 and 157) have higher H_2O contents compared with experiments with reduced starting glass (runs 98 and 113), even though run 113 is highly crystallized and accumulates H_2O in the residual melt due to crystallization of anhydrous mineral phases. This confirms the higher potential of oxidized starting glasses to form dissolved OH.

Despite many Na-bearing phases (Cpx, Afs, Nph, Ae, Hio, Sdl and Eud), with Afs (+Nph) usually being the most

abundant, Na_2O, the A. I. and the Na/(Na + K) ratio of the residual melts increase with decreasing *T*. Due to a high initial Na_2O concentration, even Na-rich mineral phases lead to increasing Na_2O_{melt}. The A. I. increases with abundant Afs (+Nph) crystallization, because the initial A. I. of the starting glasses is higher than one.

FeO^*_{melt} is rather constant at 1,000–850 °C but increases sharply below 850 °C, and MnO_{melt} shows a similar behavior. This is mainly because of the sharply increasing abundance of Afs (+Nph) below 850 °C, whereas Fe-bearing mineral phases (Mag, Ol and Cpx) are subordinate throughout. In primitive low halogen experiments, Mag, Ol and Cpx coexist between 850 and 750 °C. While Ol stability is similar in primitive high halogen experiments, Mag and Cpx are not observed at $T < 825$ °C. A slightly lower $Na/(Na + Ca)_{melt}$ ratio at $T < 825$ °C may be due to the absence of Ca-rich Cpx. In evolved experiments, FeO^*_{melt} and Na_2O_{melt} continuously increase and Mag and Ol are replaced by Na- and Fe-rich Ae and Eud. This confirms that Mag and Ol are unstable in highly peralkaline melts (e.g., Marsh 1975; Marks et al. 2011).

The two-step fractional crystallization strategy is ideal to avoid reaction textures between evolved residual melt and phenocryst phases, as it is documented by Mag and Ol rimmed by Na–Fe Cpx and Ae in the investigated dyke rock (Marks and Markl 2003). Despite such reaction textures were successfully avoided, the fractionation itself (both experimental and in nature) can be thought as a disequilibrium process. In experiments where ferromagnesian mineral phases like Mag, Ol and Cpx are prevailing, MgO_{melt} decreases. Experiments where ferromagnesian minerals are subordinate or replaced by Ae, Hio or Eud, MgO_{melt} is constant or even slightly increases, and similar trends were identified for $\#Mg_{melt}$.

In primitive experiments, $TiO_{2\ melt}$ and $ZrO_{2\ melt}$ increase; however, the trend is more pronounced for ZrO_2 because TiO_2 is incorporated in Mag, except for high halogen experiments with Hio. Where Ae is stabilized, this trend is inversed and $TiO_{2\ melt}$ decreases. In analogy, $ZrO_{2\ melt}$ decreases where Eud is stable. For evolved experiments, decreasing $ZrO_{2\ melt}$ is observed in low halogen reduced experiments where Eud is abundant; relatively constant $ZrO_{2\ melt}$ is observed in low halogen oxidized experiments with only small amounts of Eud; and increasing $ZrO_{2\ melt}$ is observed in high halogen experiments where Eud is unstable. Therefore, stabilities and abundances of Ae and Eud induce different $Ti/(Ti + Zr)_{melt}$ ratios. The $Ti/(Ti + Zr)_{melt}$ ratio is rather constant if Ae and Eud are absent or have similar abundances, but decreases where Ae dominates over Eud.

In primitive and evolved low halogen experiments, Ca-rich Cpx is stabilized close to the liquidus *T* and induces decreasing CaO_{melt}. In contrast, primitive high halogen experiments show slightly increasing CaO_{melt} before Ca-rich Cpx is stabilized. Due to the low abundance of Cpx, the trend of decreasing CaO_{melt} in the presence of Ca-rich Cpx is less pronounced. At lower *T*, increased F_{melt} stabilizes small amounts of Fl and Hio in favor of Cpx at rather constant CaO_{melt}. In evolved high halogen experiments, however, abundant Fl induces decreasing CaO_{melt}, remarkably similar to evolved low halogen experiments.

Despite both oxidized and reduced evolved low halogen starting glasses have identical XFe^{3+} and very similar compositions (Table 3), slightly different concentrations of FeO*, Na_2O (higher in the evolved oxidized starting glass), Al_2O_3 and Cl (higher in the evolved reduced starting glass) induce modified phase stabilities and abundances. In evolved oxidized experiments, Cpx is more abundant than Ae, whereas in evolved reduced experiments, the opposite is the case.

Cpx adapts to the changing melt composition by shifting its composition from Ca-rich to Na-rich (eTab. 4). Na–Fe-rich Cpx (10 wt% Na_2O, 29 wt% FeO*) is only stable in evolved low halogen oxidized experiments at 700–650 °C. In contrast to evolved low halogen experiments, Cpx is absent in evolved high halogen experiments. However, remarkably similar $Na/(Na + Ca)_{melt}$ (Fig. 2h) and constant fO_2 indicate that, besides FeO* and Na_2O content, different initial halogen concentration influences Cpx stability (see below).

Furthermore, evolved low halogen oxidized experiments have Nph, which is unstable in evolved low halogen reduced experiments. This is probably related to Cl_{melt} concentrations and is discussed in the following.

Stability of halogen-bearing phases

To discuss the stability of halogen-bearing phases, it is necessary to distinguish between halogen super-liquidus solubility of the melt and saturation of melts with halogen-bearing phases. The solubility of F in granitic and rhyolitic melts reaches 8 wt% (e.g., Webster 1990; Webster and Holloway 1990). The Cl solubility in phonolitic melts was reported as 0.6–0.8 wt% and increases with increasing peralkalinity and FeO content, decreasing SiO_2 content and decreasing *P* (e.g., Metrich and Rutherford 1992; Signorelli and Carroll 2000; Signorelli and Carroll 2002).

The H_2O solubility of the starting composition at 100 MPa is about 4.5 wt% (Giehl et al. 2013), similar to results of Schmidt and Behrens (2008) for phonolitic melts (3.5–4.5 wt%). FTIR data imply less than 1.5 wt% of H_2O in residual melts (see above) indicating the absence of a coexisting H_2O-rich fluid phase in our experiments. However, calculations based on the model of Huizenga (2005) suggest a coexisting C–O–H fluid phase with 1–17 % CH_4, 20–65 % CO_2, 1–25 % CO, 13–60 % H_2O and minor

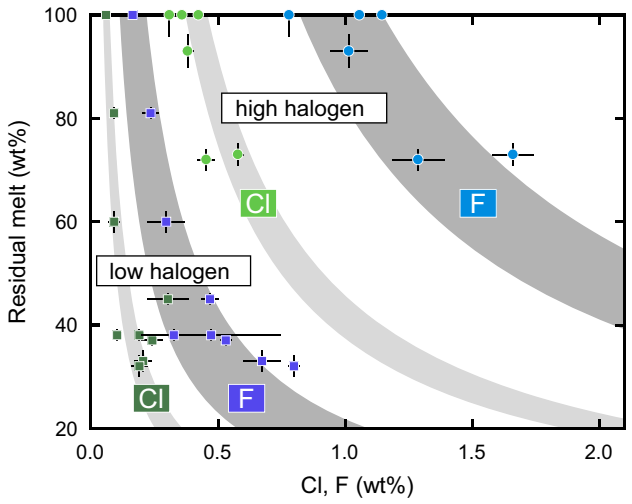

Fig. 6 Calculated rayleigh fractionation is in good agreement with Cl and F melt concentrations (accounting for the analytical uncertainty of starting glass concentrations). Only experiments without Cl- and F-bearing mineral phases are shown (data for primitive low halogen experiments are from Giehl et al. 2013)

amounts of H_2 at our experimental conditions (graphite capsules, Δ log FMQ -2.2 to -1.2). Furthermore, Cl_{melt} and F_{melt} concentrations in our experiments, devoid of Cl- and F-bearing mineral phases (Fig. 6), are consistent with an incompatible behavior of Cl and F, implying that the potential fluid phase has no major effect on Cl and F melt content.

Also, there is no evidence for liquid–liquid immiscibility, and consistent mass balance calculations indicate that no relevant Cl- or F-bearing phase was overlooked. Residual melt concentrations of Cl and F were therefore interpreted regarding saturation of halogen-bearing phases and their impact on liquid lines of descent.

Stability of sodalite

The stability of Sdl with respect to Afs and Nph depends on SiO_2 activity ($aSiO_2$) and NaCl activity (aNaCl) at constant P and T (Eqs. 2–4, Fig. 7a).

$$NaAlSi_3O_8 \leftrightarrow NaAlSiO_4 + 2SiO_2 \quad (2)$$

$$6NaAlSi_3O_8 + 2NaCl \leftrightarrow Na_8Al_6Si_6O_{24}Cl_2 + 12SiO_2 \quad (3)$$

$$6NaAlSiO_4 + 2NaCl \leftrightarrow Na_8Al_6Si_6O_{24}Cl_2 \quad (4)$$

Afs is stable in nearly all sub-liquidus experiment. In primitive low halogen experiments, Nph appears at $T \leq 850$ °C and with falling T, Cl_{melt} increases but is still too low to stabilize Sdl (Fig. 7a, line A–B). In contrast, the higher initial Cl_{melt} concentration in primitive high halogen experiments stabilizes both Nph and Sdl at 825 °C (Figs. 5, 6a, line A′–C). Albeit initial Cl_{melt} concentrations in primitive low halogen experiments are lower, Cl_{melt} at the fractionation T is only slightly lower compared with high halogen experiments because Sdl buffers Cl_{melt}. Most of the evolved experiments are saturated with Sdl but Nph is unstable in evolved low halogen reduced experiments (Figs. 5, 6a, box D). Stormer and Carmichael (1971) showed that at high T, an Afs + Nph assemblage will additionally stabilize Sdl if aNaCl is high enough but at low T, Afs may coexist with Sdl without Nph. Such an Afs + Sdl assemblage is observed in evolved low halogen reduced experiments. Accordingly, Sdl is more abundant (up to 10 wt%) compared with low halogen oxidized experiments (up to 4 wt%) and with evolved high halogen experiments ($\sim$2 wt%). This can be explained by the higher initial Cl concentration (0.49(9) wt%) of evolved low halogen reduced starting glass compared with the evolved low halogen oxidized starting glass (0.37(2) wt%, Eq. 4).

We calculated the invariant point defined by coexisting Afs + Nph + Sdl on a $aSiO_2 - a$NaCl plot (Fig. 7a, box C) using the GEOCALC software (Berman et al. 1987; Lieberman and Petrakakis 1991) and thermodynamic data from Berman (1988) and Sharp et al. (1989). At unit activities of albite, nepheline and sodalite, decreasing T from 825 to 650 °C leads to a slight decrease in $aSiO_2$ from 0.17 to 0.14 while aNaCl is rather constant (0.02). We linked this to our experiments by calculating activities of albite in Afs and nepheline (ss) in Nph from our experiments. For this calculation, Sdl was treated as a pure phase and we used the activity model of Holland and Powell (2003) for Afs and ideal mixing on sites for Nph yielding relatively constant aNaCl = 0.06(1) and slightly decreasing $aSiO_2$ from 0.18 to 0.15 within the same T interval. Sharp et al. (1989) calculated minimum aNaCl for Sdl stability to 0.05–0.13 at 800–1,000 °C, which is reasonable agreement with our data. As previously observed for Nph (Giehl et al. 2013), Sdl is only stable at low H_2O contents since in preliminary experiments using hydrated starting glasses Sdl is absent.

Stability of eudialyte

Eud is typical for agpaitic rocks and experiments on cumulate rocks from Ilímaussaq indicate Eud crystallization T's of 750–800 °C from peralkaline melts with 1.0–1.3 wt% ZrO_2 (Piotrowski and Edgar 1970; Sood and Edgar 1970; Kogarko et al. 1982). In our experiments, Cl-bearing Eud is present at $T \leq 800$ °C in all evolved low halogen experiments and in one primitive high halogen experiment at 750 °C, but is absent in evolved high halogen experiments (Fig. 5). The Cl_{melt} concentrations in Eud-bearing experiments decrease with temperature from 0.5 wt% at 800 °C to 0.2 wt% at 650 °C (Fig. 7b). Also, melts coexisting with Eud have $ZrO_{2\ melt}$ concentration $\geq$1.2 wt%, except for one experiment, where $ZrO_{2\ melt}$ is

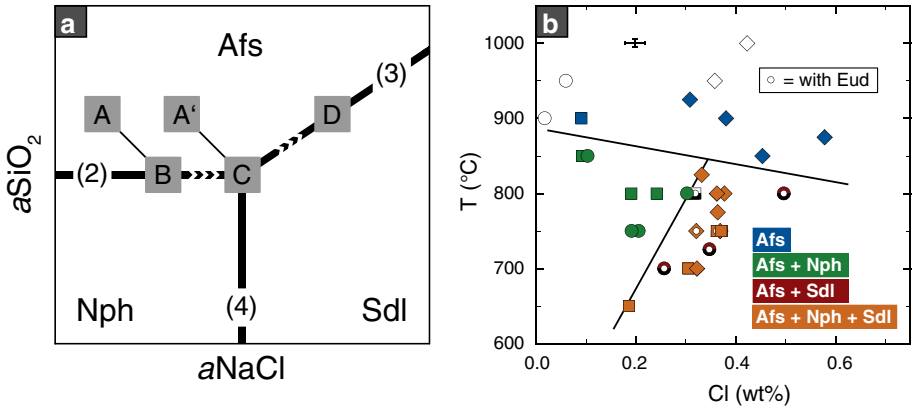

Fig. 7 **a** Stabilities of Afs, Nph and Sdl with respect to *a*NaCl and $aSiO_2$. See Eqs. (2), (3), (4) and text for details. **b** Temperature-dependent stability of Afs, Nph and Sdl related to Cl_{melt}. *Symbols* are according to Fig. 2, and *colors* illustrate stabilities of Afs, Nph and Sdl. *White inner circles* stable Eud

only 0.7 wt% (Fig. 8). However, several experiments with $ZrO_{2\ melt} \geq 1.2$ wt% are Eud-free, while FeO^*_{melt} and A. $I._{melt}$ are similar, but Cl_{melt} is lower than that of Eud-bearing ones at the same *T* (Fig. 7b). Apparently, Eud saturation requires Cl_{melt} concentrations similar to Sdl. These are variable (0.2–0.5 wt% Cl_{melt}) and decrease with decreasing *T* (Fig. 7b). In summary, stable Eud requires sufficiently high melt concentrations of both ZrO_2 and Cl. However, if, e.g., coexisting Ca-rich Cpx is destabilized, Eud is stable coexisting with a melt having 0.7 wt% ZrO_2, and Eud and Ae are then significantly more abundant. Therefore, the absence of Cpx influences the stability of Eud, while Cpx stability is itself controlled by F_{melt} concentration, which is discussed in the following section.

Stability of fluorite and hiortdahlite and their influence on clinopyroxene

In experiments with $T \leq 825$ °C and $F_{melt} \geq 1.5$ wt%, Fl is stable and respective CaO_{melt} concentrations vary from 3.0 to 1.6 wt% (Fig. 9). Despite relatively high F_{melt} (1.3–1.7 wt%) and CaO_{melt} (3.4 wt%), however, Fl is absent in run 96 (850 °C) and 97 (875 °C). This is due to increasing Fl solubility with increasing *T* (e.g., Dolejš and Baker 2006) as Fl can be stable at higher *T* (e.g., 900 °C) as shown by Gabitov et al. (2005).

Hio occurs in Fl-bearing experiments with CaO_{melt} between 3.0 and 2.8 wt% but is absent in Fl-bearing experiments at lower CaO_{melt}, despite similar F_{melt} (Fig. 9) and similar or higher $ZrO_{2\ melt}$ (Fig. 3b). In Fl- and Hio-bearing experiments, Cpx is absent, except for run 101.

In primitive low halogen experiments, CaO_{melt} decreases with decreasing *T* mainly because of abundant Ca-rich Cpx. This trend continues in evolved low halogen experiments, controlled likewise by abundant Ca-rich Cpx and, to some extent, Eud. All other mineral phases incorporate less CaO compared with the melt. In primitive and evolved low halogen experiments, F_{melt} increases with decreasing *T* (up to 1.7 wt%), because F-bearing phases are absent (Figs. 3h, 5).

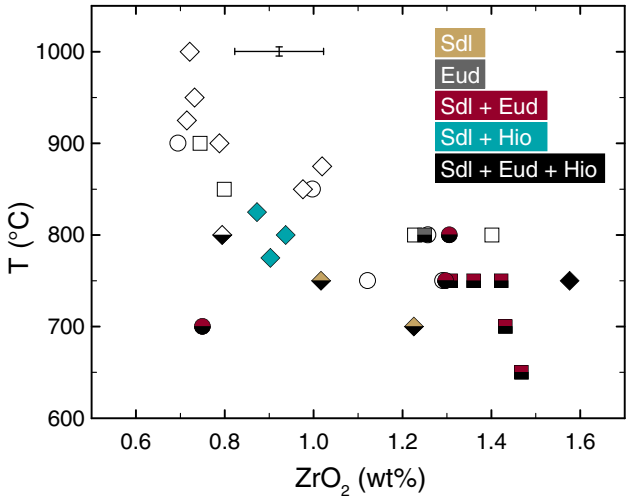

Fig. 8 Stabilities of Sdl, Eud and Hio with respect to $ZrO_{2\ melt}$ content. *Symbols* are according to Fig. 2, and *colors* illustrate stabilities of Sdl, Eud and Hio

In contrast, Ca-rich Cpx in primitive high halogen experiments is limited to 875–825 °C, where Cpx is less abundant and CaO_{melt} slightly increases until Fl and Hio are stabilized at 825 °C (Figs. 2g, 5). The CaO_{melt} content is then relatively constant although Ca-rich Hio and Fl are stable (825–750 °C). However, CaO_{melt} decreases significantly in evolved high halogen experiments by reason of abundant Fl and is remarkably similar to low halogen experiments (Fig. 2g) despite Cpx is not observed. The trend of increasing F_{melt} in primitive and evolved high halogen experiments (up to 2.7 wt%, Fig. 3h) is comparable to low halogen experiments, but displaced to higher F_{melt} concentrations.

High F content combined with low fO_2 favor Fl and Ol over Cpx (Bohlen and Essene 1978; Scaillet and Macdonald 2003, Eq. 5). In our study, Eq. 5 and a similar one

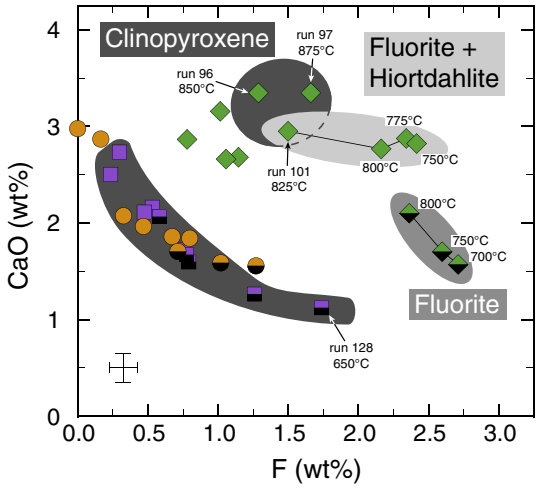

Fig. 9 CaO_{melt} and F_{melt} concentrations related to stabilities of Cpx, Fl and Hio. *Symbols* and *colors* are according to Fig. 2

with Cpx, Fl, Hio and Ol (Eq. 6) explain the observed destabilization of Cpx in favor of Fl and Hio.

$$2CaFeSi_2O_6 + 2F_2O_{-1} \leftrightarrow 2CaF_2 + Fe_2SiO_4 + 3SiO_2 \quad (5)$$

$$6CaFeSi_2O_6 + 6F_2O_{-1} + 4ZrO_2 + 4Na_2O \leftrightarrow 2CaF_2 + 2Ca_2Na_4Zr_2Si_4O_{14}F_4 + 3Fe_2SiO_4 + SiO_2 \quad (6)$$

This is in agreement with higher Ol abundances in experiments with Fl and Hio (Table 4) compared with primitive low halogen experiments (Tab. 3 in Giehl et al. 2013). Similarly, experimental studies on granites demonstrated the (1) destabilization of plagioclase in favor of Fl and topaz (Eq. 7, Dolejš and Baker 2004; Lukkari and Holtz 2007) and (2) the destabilization of titanite in favor of Fl (Eq. 8, Price et al. 1999).

$$CaAl_2Si_2O_8 + 2F_2O_{-1} \leftrightarrow CaF_2 + Al_2SiO_4F_2 + SiO_2 \quad (7)$$

$$CaTiSiO_5 + F_2O_{-1} \leftrightarrow CaF_2 + SiO_2 + TiO_2 \quad (8)$$

As the Na/(Na + Ca) melt ratio increases with decreasing *T* (Fig. 2h), the destabilization of Ca-rich Cpx may be followed by the reoccurrence of Na-rich Cpx at lower *T*. This may result in a compositional gap between Ca- and Na-rich Cpx, frequently reported in nature (e.g., Ferguson 1978; Njonfang and Nono 2003).

Experimental studies on the stability of Fl are limited to SiO_2-oversaturated systems (Webster et al. 1987; Price et al. 1999; Scaillet and Macdonald 2001; Xiong et al. 2002; Scaillet and Macdonald 2003; Gabitov et al. 2005; Dolejš and Baker 2006; Lukkari and Holtz 2007). Magmatic Fl is usually found in CaO-poor (<1 wt%) and F-rich (up to 7 wt%) evolved granites and rhyolites (Price et al. 1996; Marshall et al. 1998).

Scaillet and Macdonald (2004) provided an empirical equation based on *T* and A. $I._{melt}$ to estimate Fl saturation for SiO_2-oversaturated, CaO-poor (<0.5 wt%) magmas. Furthermore, Dolejš and Baker (2006) used granitic compositions to calculate a Fl saturation model based on experiments and confirmed that CaO and F control Fl saturation independently. In the present study, the initial CaO content (3 wt%) is significantly higher compared with the study of Scaillet and Macdonald (2004) and for a given A. $I._{melt}$, Fl saturation is achieved at much lower F_{melt} concentration. For example, at 825 °C, Fl saturation occurs in a melt with A. I. = 2.0 and 1.5 wt% F (Fig. 9), whereas Fl saturation is predicted to occur at 4 wt% F based on the model of Scaillet and Macdonald (2004). This confirms that Fl saturation in granitic and rhyolitic melts requires higher F_{melt} concentration compared with CaO-rich magmas. Unfortunately, calculations using the solubility model of Dolejš and Baker (2006) in experiments with Fl utilizing residual melt composition were unsuccessful. Despite F_{melt} is similar to the calibration experiments, the significantly higher CaO_{melt} probably impedes meaningful results. Despite higher CaO_{melt} and F_{melt} concentrations, the Fl saturation *T* (825 °C) is similar as observed by Scaillet and Macdonald (2004) and Dolejš and Baker (2006).

Evolved high halogen experiments show increasing F_{melt} but decreasing CaO_{melt} and invariably contain Fl as the only Ca-and F-bearing mineral phase. Given that Fl is also stable at significantly lower CaO_{melt}, its stability likely extends by increasing F_{melt} compensating for lower CaO_{melt}. Even though the Dolejš and Baker (2006) model cannot be applied for the compositions used in this study, our data still support the conclusion that the activity product of F and Ca controls Fl stability.

The influence of fluorite and hiortdahlite on eudialyte stability

In contrast to Fl, Hio is not observed in evolved high halogen experiments. Equation 6 shows that the destabilization of Cpx in favor of Hio requires high $ZrO_{2\ melt}$ contents. In primitive high halogen experiments, Hio is stable if $ZrO_{2\ melt}$ concentrations are 0.9 wt% or higher; however, $ZrO_{2\ melt}$ and F_{melt} are similar or higher in evolved high halogen experiments, but Hio is not observed (Figs. 8, 9).

Both Hio and Eud incorporate high concentrations of ZrO_2 (10–13 wt%), but $ZrO_{2\ melt}$ content necessary to stabilize Hio is roughly 0.9 wt% and therefore lower compared with 1.2 wt% for Eud (Fig. 8). However, in one low halogen experiment, Eud is stable coexisting with 0.7 wt% $ZrO_{2\ melt}$, which is probably related to the destabilization of Cpx in this run (discussed in the section on Eud stability). In run 139 with Fl and Hio (750 °C), Eud

is additionally stabilized, which is likely due to the increase in $ZrO_{2\ melt}$ content from 0.9 to 1.6 wt%, as CaO_{melt} and Cl_{melt} are similar to run 114 at 775 °C. Similar to Ca-rich Cpx, Fl is the main Ca-phase in evolved high halogen experiments preventing Eud stability at lower $ZrO_{2\ melt}$. Whereas CaO_{melt} is fairly constant in high halogen experiments with Fl and Hio, low halogen experiments with Eud show decreasing CaO_{melt}. In contrast to Hio, decreasing CaO_{melt} does not limit Eud stability, as Eud is stable coexisting with melts having the lowest CaO_{melt} contents (run 128, Fig. 9). In this experiment, the coexisting melt contains 1.7 wt% F and is therefore comparable to experiments with Hio, but Hio is not observed. This might be explained by Hio incorporating more CaO (34–40 wt%) than Eud (11–12 wt%); we conclude that lower CaO_{melt} is crucial to destabilize Hio.

If Cpx, Fl or both are stable, Hio requires higher CaO_{melt} but lower $ZrO_{2\ melt}$ compared with Eud. If F_{melt} is sufficiently high, Hio is stabilized at higher *T*'s than Eud, as observed in primitive high halogen experiments. In these experiments, $ZrO_{2\ melt}$ is rather constant at ~0.9 wt% between 825 and 750 °C in the presence of Hio. In this *T* interval, $ZrO_{2\ melt}$ concentrations increase to 1.2–1.4 wt% in low halogen experiments, resulting in Eud saturation in consecutive evolved experiments at lower *T* (Fig. 3b). The absence of Eud in evolved high halogen experiments is therefore explained by saturation of Hio and the concomitant delay of increasing $ZrO_{2\ melt}$ concentration. As the trend of increasing $ZrO_{2\ melt}$ is maintained, we expect that saturation of Eud is shifted to lower *T*.

If Hio is not stabilized before Eud at relatively high CaO_{melt} content, this may not happen at lower *T* as CaO_{melt} decreases, and ZrO_2 is then also incorporated in Eud. Still, Fl may be stabilized at any CaO_{melt} concentration if F_{melt} is high enough. As a further consequence of unstable Cpx and Eud in evolved high halogen experiments, the remaining FeO^*_{melt} is incorporated in Mag (800 °C, run 166), which is, except for this experiment, unstable in evolved experiments. At lower *T*, FeO is then incorporated in abundant Ae by reason of increasing peralkalinity.

Factors controlling the behavior of Cl and F in peralkaline systems

Both Cl and F, at least in the absence of fluids, are considered to behave incompatible in silicate melts (e.g., Carroll and Holloway 1994). However, both degassing and fluid exsolution may modify the Cl/(Cl + F) ratio of a melt, as partitioning in favor of a fluid phase is typical for Cl, but not for F. This is supported by analyses of volcanic gases usually having Cl/(Cl + F) ratios from 0.5 to 0.95 (Aiuppa 2009). Fairly constant 0.1–0.2 wt% Cl_{melt} and 0.2–0.3 wt% F_{melt} concentrations were calculated by combining halogen concentrations of amphibole, apatite, mica and mineral–melt distribution coefficients in diorites and gabbros (Zhang et al. 2012). They found that Cl/(Cl + F) decreases close to the solidus *T*, which might indicate fluid exsolution processes. However, both fluid exsolution and degassing processes can only significantly modify the Cl/(Cl + F) ratio if sufficient amounts of fluid are exsolved or degassed (Balcone-Boissard et al. 2010). In both low and high halogen series, the initial Cl/(Cl + F) ratio is 0.15 although initial Cl and Fl concentrations are six times higher in high halogen experiments. However, in both series, Cl_{melt} and F_{melt} increase with decreasing temperature and $Cl/(Cl + F)_{melt}$ is constant until Sdl and Eud form, Cl_{melt} decreases thereafter (Fig. 3i). The ideal incompatible behavior of Cl and F (Fig. 6) is either explained by a fluid consisting mainly of hydrocarbons rather than hydrous species, which would indicate that Cl and F have a low affinity for such hydrocarbon-dominated fluids. Alternatively, a low amount of fluid present and/or a low H_2O activity in such fluids prevent major effects on Cl and F melt concentrations.

At the same time, F_{melt} further increases in low and high halogen experiments although F-bearing mineral phases are present in the latter. This is because CaO_{melt} steadily decreases and F_{melt} is therefore not sufficiently buffered by the precipitation of Ca–F phases. As a consequence, the $Cl/(Cl + F)_{melt}$ ratio strongly decreases down to values of around 0.05.

Primitive high halogen experiments contain Sdl, Fl and Hio (825 °C) at higher *T* due to higher initial Cl_{melt} and F_{melt} concentrations. Presuming sufficient Cl_{melt} contents, Eud saturation is mainly controlled by $ZrO_{2\ melt}$ concentration. Similar to evolved low halogen experiments, Cl_{melt} decreases with decreasing *T* where Sdl (and Eud) are stable. Additionally, Fl and Hio are stable, yet F_{melt} increases. This causes a slightly lower Cl/(Cl + F) of the evolved high halogen starting glass compared with evolved low halogen starting glasses. In evolved high halogen experiments, Sdl is stable, but its abundance is low and Cl_{melt} decreases only slightly compared with evolved low halogen experiments. Fl is stable, F_{melt} slightly increases and $Cl/(Cl + F)_{melt}$ slightly decreases, yet these trends are less pronounced compared with low halogen experiments without F-bearing mineral phases (Fig. 3i).

Our experiments demonstrate the incompatible behavior of Cl and F during crystallization of peralkaline iron-rich phonolitic compositions as Cl_{melt} and F_{melt} increase, whereas $Cl/(Cl + F)_{melt}$ stays constant if no halogen-bearing mineral phases are stable. Consequently, $Cl/(Cl + F)_{melt}$ decreases with stable Cl-bearing mineral phases (evolved low halogen experiments). However, this is also the case with stable Cl- and F-bearing mineral phases (primitive high halogen experiments). Saturation

with halogen-bearing phases occurs at higher T for higher initial Cl and F concentrations, except for Eud. Identical initial Cl/(Cl + F) ratios with different concentrations lead to slightly different trends, still the general trend of decreasing Cl/(Cl + F) is maintained.

Quartz-undersaturated volcanic rocks are typically more Cl-rich than SiO_2-saturated rocks (Aiuppa et al. 2009). In contrast to Sdl, only relatively low concentrations of Cl (<1 wt%, Zhang et al. 2012) can be incorporated in amphibole, apatite and mica. We suggest that the incorporation of Cl in Sdl in line with decreasing Cl_{melt} concentration protracts exsolution of a Cl-rich fluid phase. As already suggested by Stormer and Carmichael (1971), this may contribute to generally higher Cl whole-rock concentrations in SiO_2-undersaturated rocks as we are not aware of a Cl-rich substitute for Sdl in SiO_2-saturated rocks.

Implications for the dyke rock and the Ilímaussaq intrusion

As probably all Ilímaussaq rocks are cumulates and no melt inclusion studies on the Ilímaussaq rocks are available, melt compositions from which these rocks crystallized are unknown. Therefore, we cannot directly compare the extreme increase of Na_2O (up to 19 wt%) and the A. I. (up to 5.5) observed in our experimental residual melts with nature. However, melt inclusions in nephelinites from Oldoinyo Lengai (Tanzania) reach up to 18 wt% Na_2O and A. I.'s up to 13.0 confirming the possible formation of such extreme melt compositions in nature (Mitchell and Dawson 2012). The results of Giehl et al. (2013) and this study show that at low fO_2 and aH_2O a peralkaline melt is capable to initially crystallize a metaluminous phase assemblage (Mag, Ol, Cpx, Afs and Nph). After roughly 60–80 % crystallization (recalculated for the fractionation step, e.g., run 151 and 127, respectively) mineral phases typical for agpaitic rocks (Ae, Hio, Eud) form. This supports the presumption that the dyke rock represents a near-parental melt composition for the Ilímaussaq system capable to crystallize metaluminous and peralkaline agpaitic phase assemblages. The extent of crystallization necessary to form agpaitic assemblages based on our study is similar to previous estimates of 75–99 %, based on a slightly more primitive parental melt composition (Engell 1973; Bailey et al. 1981).

The presence of native iron in the plutonic augite syenite unit (equivalent of the dyke's phenocryst assemblage) of the Ilímaussaq complex has been hypothesized owing to extremely low oxygen fugacities prevailing during formation of these rocks (Δ log FMQ −3 to −5, Marks and Markl 2001). Albeit native iron was most likely oxidized subsequently or consumed due to increasing peralkalinity, our data suggest that crystallization conditions were sufficiently reduced as some experiments show that native iron is stable coexisting with Mag, Ol and Cpx (run 96).

Increasing peralkalinity and increasing FeO^*_{melt} in experiments on peralkaline rhyolites were found to be moderated by Na–Fe-rich Cpx, counteracting the effect of Afs (+Nph, Scaillet and Macdonald 2003). In our experiments, Afs (+Nph) is usually abundant and Ca-rich Cpx coexists with mineral phases that can be attributed to both the phenocryst and the groundmass assemblage of the investigated dyke rock. The transition to Na-rich Cpx occurs in the lowest T experiments (700–650 °C) coexisting with an extremely FeO*-rich (~15 wt%) and highly peralkaline melt (A. I. = 4.7–5.5). The stabilization of Na-rich Cpx is able to inverse the trend of increasing FeO^*_{melt}, but is, in contrast to peralkaline rhyolites, unable to moderate increasing peralkalinity. The late compositional transition from Ca-rich to Na-rich Cpx, likely induced by low fO_2, and also the destabilization of Ca-rich Cpx by high F_{melt} content, may therefore give rise to liquid lines of descent that will form "hyperagpaitic" phase assemblages at even lower T and may result in melt–melt immiscibility (e.g., Khomyakov 1995). Such hyperagpaitic conditions combined with high F_{melt} concentrations may also stabilize Vil. Despite not observed in the experiments, Vil might be stable at experimental conditions, as it is prone to dissolution during preparation of the samples with water.

In the dyke rock, Mag and Ol are typically rimmed by Ae and Na–Fe Cpx. Hio occurs as inclusions in Na–Fe Cpx, Ae and Arf (Fig. 3 in Marks and Markl 2003). This may indicate that Ae and Hio are mineral phases that crystallize at the transition from phenocrysts to groundmass minerals before the peak FeO^*_{melt} content is reached (Ae) and before CaO_{melt} significantly decreases (Hio). In primitive high halogen experiments, Hio crystallizes at higher temperatures than Eud, and Hio and Eud coexist in one experiment (run 139) with a melt having high ZrO_2 (1.6 wt%), CaO (2.8 wt%) and F (2.4 wt%) content. As indicated by 1 wt% F in the bulk dyke rock, our experimental results demonstrate the need for a high F_{melt} content to stabilize Hio. Also, a magma evolution that provides sufficient ZrO_2 and CaO is required. However, it is possible, but not clearly supported by rock textures, that Hio precipitates before Eud.

In Ilímaussaq, the transition from miaskitic (with titanite + zircon) to agpaitic phase assemblages (with Aen + Eud) is controlled by increasing μNa_2O and decreasing μCaO (Marks et al. 2011). Andersen et al. (2012) suggested that low fO_2 may favor the incorporation of Zr in Cpx replacing transitional assemblages as suggested by Marks et al. (2011). In the experiments, neither miaskitic nor transitional assemblages with titanite or zircon were observed, which might be explained by Ti- and Zr-rich Cpx.

The experimental observation that Cl and F do not significantly partition into a hydrocarbon-dominated fluid may allow to explain significant amounts of Cl- and F-bearing minerals in the Ilímaussaq rocks, where primary fluid inclusions are CH_4-dominated and almost devoid of H_2O (e.g., Krumrei et al. 2007). The observed late-stage exsolution of a hydrous fluid phase (e.g.,Konnerup-Madsen et al. 1988; Krumrei et al. 2007; Graser et al. 2008) after crystallization of these phases has then little influence on the halogen budget of the rock.

Conclusions

In this study, we present isobaric two-step fractional crystallization experiments on a peralkaline iron-rich phonolitic composition. The observed mineral phases are titanomagnetite, clinopyroxene, fayalitic olivine, alkali feldspar, nepheline and aenigmatite. High melt concentrations of Cl and F stabilize the halogen-bearing mineral phases fluorite, hiortdahlite, sodalite and eudialyte. With decreasing *T*, increasing melt alkalinity stabilizes Na–Fe clinopyroxene and complex Na–Ca–Fe–Ti–Zr silicates (aenigmatite, eudialyte) at the expense of titanomagnetite and olivine. This is equivalent to the resorption of titanomagnetite and olivine by Na–Fe clinopyroxene as observed in the dyke rock. Aside from halogen melt concentrations, eudialyte and hiortdahlite stabilities are governed by melt concentrations of ZrO_2, and CaO for hiortdahlite. Additionally, high F melt concentrations destabilize Ca-rich clinopyroxene in favor of fluorite and hiortdahlite, which may induce a compositional gap between Ca- and Na-rich clinopyroxene as occasionally observed in nature.

Giehl et al. (2013) concluded that low fO_2 and low H_2O melt content are prerequisites to reproduce the phenocrysts of the dyke rock that resembles the starting material. Based on our experiments, we can extend this conclusion toward the groundmass mineral assemblage. Also, fO_2 might have been low enough to stabilize native iron and apart from amphibole, all major mineral phases were experimentally reproduced.

Acknowledgments Starting glasses were synthesized with the help of Annette Flicker, Fabian Burmann and Tobias Renz, and analyzed with Mössbauer spectroscopy by Christian Schröder. Gold and graphite capsules were issued by Barbara Maier, Holger Marxer assisted in doing IHPV experiments and Indra Gill-Kopp prepared experimental samples for different analytical methods. Harald Behrens (Hannover) analyzed hydrated glasses with Karl Fischer titration. Annette Flicker assisted during infrared spectroscopy and electron microprobe analyses were supported by Thomas Wenzel. Reviews of Renat Almeev, Tom Andersen and Bruno Scaillet refined the manuscript and helped to clarify important details. The Deutsche Forschungsgemeinschaft (Grants MA 2563/4-1 and NO 378/7-1) provided financial support which is thankfully acknowledged.

References

Aiuppa A (2009) Degassing of halogens from basaltic volcanism: insights from volcanic gas observations. Chem Geol 263(1–4):99–109. doi:10.1016/j.chemgeo.2008.08.022

Aiuppa A, Baker DR, Webster JD (2009) Halogens in volcanic systems. Chem Geol 263(1–4):1–18. doi:10.1016/j.chemgeo.2008.10.005

Andersen T, Erambert M, Larsen AO, Selbekk RS (2010) Petrology of nepheline syenite pegmatites in the Oslo Rift, Norway: zirconium silicate mineral assemblages as indicators of alkalinity and volatile Fugacity in mildly agpaitic magma. J Petrol 51(11):2303–2325. doi:10.1093/petrology/egq058

Andersen T, Carr P, Erambert M (2012) Late-magmatic mineral assemblages with siderite and zirconian pyroxene and amphibole in the anorogenic Mt Gibraltar microsyenite, New South Wales, Australia, and their petrological implications. Lithos 151:46–56. doi:10.1016/j.lithos.2011.09.012

Appen AA (1952) Some general features of dependence of the properties of silicate glasses on their composition. Thesis, Leningrad

Armstrong JT (1988) Quantitative analysis of silicate and oxide materials: comparison of Monte Carlo, ZAF and Φ (ρz) procedures. In: Newbury DE (ed) Microbeam analysis—1988. San Francisco Press, San Francisco

Baasner A, Schmidt BC, Webb SL (2013) Compositional dependence of the rheology of halogen (F, Cl) bearing aluminosilicate melts. Chem Geol 346:172–183. doi:10.1016/j.chemgeo.2012.09.020

Bailey JC, Rose-Hansen J, Løvborg L, Sørensen H (1981) Evolution of Th and U whole-rock contents in the Ilimaussaq intrusion. Rapp Grønl Geol Unders 103:87–98

Balcone-Boissard H, Villemant B, Boudon G (2010) Behavior of halogens during the degassing of felsic magmas. Geochem Geophys Geosyst 11(9):Q09005. doi:10.1029/2010gc003028

Bartels A, Holtz F, Linnen RL (2010) Solubility of manganotantalite and manganocolumbite in pegmatitic melts. Am Mineral 95(4):537–544. doi:10.2138/am.2010.3157

Behrens H, Misiti V, Freda C, Vetere F, Botcharnikov RE, Scarlato P (2009) Solubility of H(2)O and CO(2) in ultrapotassic melts at 1200 and 1250 degrees C and pressure from 50 to 500 MPa. Am Mineral 94(1):105–120. doi:10.2138/am.2009.2796

Berman R (1988) Internally consistent thermodynamic data for minerals in the system Na_2O–K_2O–CaOMgO–FeO–Fe_2O_3–Al_2O_3–SiO_2–TiO_2–H_2O–CO_2. J Petrol 29:445–522

Berman R, Brown TH, Perkins EH (1987) Geø-Calc: software for calculation and display of P–T–X phase diagrams. Am Mineral 72:861–862

Berndt J, Liebske C, Holtz F, Freise M, Nowak M, Ziegenbein D, Hurkuck W, Koepke J (2002) A combined rapid-quench and H-2-membrane setup for internally heated pressure vessels: description and application for water solubility in basaltic melts. Am Mineral 87(11–12):1717–1726

Blank JG, Brooker RA (1994) Experimental studies of carbon dioxide in silicate melts: solubility, speciation, and stable carbon isotope behavior. In: Carroll MR, Holloway JR (eds) Volatiles in magmas, vol 30, Reviews in Mineralogy, pp 157–186

Bohlen SR, Essene EJ (1978) The significance of metamorphic fluorite in the Adirondacks. Geochim Cosmochim Acta 42(11):1669–1678. doi:10.1016/0016-7037(78)90255-7

Brøgger WC (1890) Die Mineralien der Syenitpegmatitgänge der südnorwegischen Augit- und Nephelinsyenite. Zeitschrift für Krystallographie und Mineralogie 16:367–377

Bureau H, Métrich N (2003) An experimental study of bromine behaviour in water-saturated silicic melts. Geochim Cosmochim Acta 67(9):1689–1697. doi:10.1016/S0016-7037(02)01339-X

Burnham CW (1979) The importance of volatile constituents. In: Yoder HS (ed) The evolution of the igneous rocks: fiftieth anniversary perspectives. Princeton University Press, Princeton, pp 439–482

Carroll MR (2005) Chlorine solubility in evolved alkaline magmas. Ann Geophys 48(4–5):619–631

Carroll MJ, Holloway JR (eds) (1994) Volatiles in magmas: solubilities of sulfur, noble gases, nitrogen, chlorine, and fluorine in magmas, vol 30. Reviews in mineralogy. Mineralogical Society of America

Chakhmouradian AR, Zaitsev AN (2012) Rare earth mineralization in igneous rocks: sources and processes. Elements 8(5):347–353. doi:10.2113/gselements.8.5.347

Davis KM, Tomozawa M (1996) An infrared spectroscopic study of water-related species in silica glasses. J Non Cryst Solids 201(3):177–198. doi:10.1016/0022-3093(95)00631-1

Dickenson MP, Hess PC (1986) The structural role and homogeneous redox equilibria of iron in peraluminous, metaluminous and peralkaline silicate melts. Contrib Mineral Petrol 92(2):207–217. doi:10.1007/BF00375294

Dixon JE, Stolper EM, Holloway JR (1995) An experimental study of water and carbon dioxide solubilities in mid-ocean ridge basaltic liquids. Part I: calibration and solubility models. J Petrol 36(6):1607–1631

Dolejš D, Baker DR (2004) Thermodynamic analysis of the system Na_2O–K_2O–CaO–Al_2O_3–SiO_2–H_2O–F_2O − 1: stability of fluorine-bearing minerals in felsic igneous suites. Contrib Mineral Petrol 146(6):762–778. doi:10.1007/s00410-003-0533-3

Dolejš D, Baker DR (2006) Fluorite solubility in hydrous haplogranitic melts at 100 MPa. Chem Geol 225(1–2):40–60. doi:10.1016/j.chemgeo.2005.08.007

Engell J (1973) A closed system crystal-fractionation model for the agpaitic Ilímaussaq intrusion, South Greenland, with special reference to the lujavrites. Bull Geol Soc Den 22:354–362

Ferguson AK (1978) The crystallization of pyroxenes and amphiboles in some alkaline rocks and the presence of a pyroxene compositional gap. Contrib Mineral Petrol 67(1):11–15. doi:10.1007/bf00371628

Filiberto J, Treiman AH (2009) The effect of chlorine on the liquidus of basalt: first results and implications for basalt genesis on Mars and Earth. Chem Geol 263:60–68. doi:10.1016/j.chemgeo.2008.08.025

Filiberto J, Wood J, Dasgupta R, Shimizu N, Le L, Treiman AH (2012) Effect of fluorine on near-liquidus phase equilibria of an Fe–Mg rich basalt. Chem Geol 312–313:118–126. doi:10.1016/j.chemgeo.2012.04.015

Foley SF, Taylor WR, Green DH (1986) The effect of fluorine on phase relationships in the system KAlSiO4–Mg2SiO4–SiO2 at 28 kbar and the solution mechanism of fluorine in silicate melts. Contrib Mineral Petrol 93(1):46–55. doi:10.1007/bf00963584

French BM (1966) Some geological implications of equilibrium between graphite and a C–H–O gas phase at high temperatures and pressures. Rev Geophys 4(2):223–253. doi:10.1029/RG004i002p00223

French BM, Eugster HP (1965) Experimental control of oxygen fugacities by graphite-gas equilibriums. J Geophys Res 70(6):1529–1539. doi:10.1029/JZ070i006p01529

Frindt S, Trumbull RB, Romer RL (2004) Petrogenesis of the gross Spitzkoppe topaz granite, central western Namibia: a geochemical and Nd–Sr–Pb isotope study. Chem Geol 206(1–2):43–71. doi:10.1016/j.chemgeo.2004.01.015

Gabitov RI, Price JD, Watson EB (2005) Solubility of fluorite in haplogranitic melt of variable alkalis and alumina content at 800 degrees–1000 degrees C and 100 MPa. Geochem Geophy Geosy 6(3):1–10. doi:10.1029/2004gc000870

Ghiorso MS, Sack RO (1995) Chemical mass transfer in magmatic processes IV. A revised and internally consistent thermodynamic model for the interpolation and extrapolation of liquid–solid equilibria in magmatic systems at elevated temperatures and pressures. Contrib Mineral Petrol 119(2):197–212. doi:10.1007/bf00307281

Giehl C, Marks M, Nowak M (2013) Phase relations and liquid lines of descent of an iron-rich peralkaline phonolitic melt: an experimental study. Contrib Mineral Petrol 165(2):283–304. doi:10.1007/s00410-012-0809-6

Gioncada A, Orlandi P, Vezzoli L, Omarini RH, Mazzuoli R, Lopez-Azarevich V, Sureda R, Azarevich M, Acocella V, Ruch J (2014) Topaz magmatic crystallization in rhyolites of the Central Andes (Chivinar volcanic complex, NW Argentina): constraints from texture, mineralogy and rock chemistry. Lithos 184–187:62–73. doi:10.1016/j.lithos.2013.10.023

Graser G, Potter J, Köhler J, Markl G (2008) Isotope, major, minor and trace element geochemistry of late-magmatic fluids in the peralkaline Ilímaussaq intrusion, South Greenland. Lithos 106(3–4):207–221. doi:10.1016/j.lithos.2008.07.007

Hess PC (1991) The role of high field strength cations in silicate melts. In: Perchuk LL, Kushiro I (eds) Physical chemistry of magmas, vol 9. Springer, New York, pp 152–191. doi:10.1007/978-1-4612-3128-8_5

Holland T, Powell R (2003) Activity-composition relations for phases in petrological calculations: an asymmetric multicomponent formulation. Contrib Mineral Petrol 145(4):492–501. doi:10.1007/s00410-003-0464-z

Holloway JR, Pan V, Gudmundsson G (1992) High-pressure fluid-absent melting experiments in the presence of graphite: oxygen fugacity, ferric/ferrous ratio and dissolved CO_2. Eur J Mineral 4:105–114

Jakobsson S, Oskarsson N (1994) The system C–O in equilibrium with graphite at high pressure and temperature: an experimental study. Geochim Cosmochim Acta 58(1):9–17. doi:10.1016/0016-7037(94)90442-1

Keppler H (1993) Influence of fluorine on the enrichment of high field strength trace elements in granitic rocks. Contrib Mineral Petrol 114(4):479–488. doi:10.1007/bf00321752

Khomyakov AP (1995) Mineralogy of hyperagpaitic alkaline rocks. Oxford Scientific Publications, Clarendon Press, Oxford

Kloess GH (2000) Dichtefluktuationen natürlicher Gläser. Universität Jena, Habil Thesis

Kogarko LN (1974) Role of volatiles. In: Sørensen H (ed) The alkaline rocks. Wiley, London, pp 474–487

Kogarko LN, Lazutkina LN, Romanchev BP (1982) The origin of eudialyte mineralization (translated from Russian). Geokhimiya 10:1415–1432

Konnerup-Madsen J, Kreulen R, Rose-Hansen J (1988) Stable isotope characteristics of hydrocarbon gases in the alkaline Ilímaussaq complex, South Greenland. Bull Minéral 102:642–653

Kramm U, Kogarko LN (1997) Nd and Sr isotope signatures of the Khibina and Lovozero agpaitic centres, Kola Alkaline province, Russia. Lithos 32(3–4):225–242

Kress VC, Carmichael ISE (1991) The compressibility of silicate liquids containing Fe_2O_3 and the effect of composition, temperature, oxygen fugacity and pressure on their redox states. Contrib Mineral Petrol 108(1–2):82–92. doi:10.1007/BF00307328

Krumrei TV, Pernicka E, Kaliwoda M, Markl G (2007) Volatiles in a peralkaline system: abiogenic hydrocarbons and F–Cl–Br systematics in the naujaite of the Ilímaussaq intrusion, South Greenland. Lithos 95:298–314. doi:10.1016/j.lithos.2006.08.003

Larsen LM, Steenfelt A (1974) Alkali loss and retention in an iron-rich peralkaline phonolite dyke from the Gardar province, south Greenland. Lithos 7:81–90. doi:10.1016/0024-4937(74)90021-8

Lieberman J, Petrakakis K (1991) TWEEQU thermobarometry: analysis of uncertainties and applications to granulites from western Alaska and Austria. Can Mineral 29(4):857–887

Lukkari S, Holtz F (2007) Phase relations of a F-enriched peraluminous granite: an experimental study of the Kymi topaz granite stock, southern Finland. Contrib Mineral Petrol 153(3):273–288. doi:10.1007/s00410-006-0146-8

Luth RW (1988) Effects of F on phase equilibria and liquid structure in the system $NaAlSiO_4$–$CaMgSi_2O_6$–SiO_2. Am Mineral 73(3–4):306–312

Mandeville CW, Webster JD, Rutherford MJ, Taylor BE, Timbal A, Faure K (2002) Determination of molar absorptivities for infrared absorption bands of H_2O in andesitic glasses. Am Mineral 87(7):813–821

Marks M, Markl G (2001) Fractionation and assimilation processes in the alkaline augite syenite unit of the Ilimaussaq intrusion, South Greenland, as deduced from phase equilibria. J Petrol 42(10):1947–1969. doi:10.1093/petrology/42.10.1947

Marks M, Markl G (2003) Ilímaussaq 'en miniature': closed-system fractionation in an agpaitic dyke rock from the Gardar Province, South Greenland (contribution to the mineralogy of Ilímaussaq no. 117). Mineral Mag 67(5):893–919. doi:10.1180/0026461036750150

Marks MAW, Hettmann K, Schilling J, Frost BR, Markl G (2011) The mineralogical diversity of alkaline igneous rocks: critical factors for the transition from miaskitic to agpaitic phase assemblages. J Petrol 52(3):439–455. doi:10.1093/petrology/egq086

Marsh JS (1975) Aenigmatite stability in silica-undersaturated rocks. Contrib Mineral Petrol 50:135–144

Marshall AS, Hinton RW, Macdonald R (1998) Phenocrystic fluorite in peralkaline rhyolites, Olkaria, Kenya Rift Valley. Mineral Mag 62(4):477–486

Metrich N, Rutherford MJ (1992) Experimental study of chlorine behavior in hydrous silicic melts. Geochim Cosmochim Acta 56:607–616. doi:10.1016/0016-7037(92)90085-W

Mitchell RH, Dawson JB (2012) Carbonate–silicate immiscibility and extremely peralkaline silicate glasses from Nasira cone and recent eruptions at Oldoinyo Lengai Volcano, Tanzania. Lithos 152:40–46. doi:10.1016/j.lithos.2012.01.006

Nakamoto K (1978) Infrared and Raman spectra of inorganic and coordination compounds, 3rd edn. John Wiley & Sons Inc., New York

Njonfang E, Nono A (2003) Clinopyroxene from some felsic alkaline rocks of the Cameroon Line, central Africa: petrological implications. Eur J Mineral 15(3):527–542. doi:10.1127/0935-1221/2003/0015-0527

Nowak M, Porbatzki D, Spickenbom K, Diedrich O (2003) Carbon dioxide speciation in silicate melts: a restart. Earth Planet Sci Lett 207(1–4):131–139

Pandya N, Muenow DW, Sharma SK (1992) The effect of bulk composition on the speciation of water in submarine volcanic glasses. Geochim Cosmochim Acta 56(5):1875–1883. doi:10.1016/0016-7037(92)90317-C

Parsons I (2012) Full stop for mother earth. Elements 8:396–398

Pfaff K, Wenzel T, Schilling J, Marks MAW, Markl G (2010) A fast and easy-to-use approach to cation site assignment for eudialyte-group minerals. Neues Jahrbuch der Mineralogie Abhandlungen 187(1):69–81

Piotrowski JM, Edgar AD (1970) Melting relations of undersaturated alkaline rocks from South Greenland. Meddelelser om Grønland 181:62

Price JD, Hogan JP, Gilbert MC (1996) Rapakivi texture in the Mount Scott Granite, Wichita Mountains, Oklahoma. Eur J Mineral 8(2):435–451

Price JD, Hogan JP, Gilbert MC, London D, Morgan GB (1999) Experimental study of titanite–fluorite equilibria in the A-type Mount Scott Granite: implications for assessing F contents of felsic magma. Geology 27(10):951–954. doi:10.1130/0091-7613(1999)027<0951:esotfe>2.3.co;2

Robie RA, Hemingway BS, Fisher JR (1979) Thermodynamic properties of minerals and related at 298.15 K and 1 Bar (10^5 Pascals) pressure and at higher temperatures. US Geol Surv Bull 1452:456

Robles ER, Fontan F, Monchoux P, Sørensen H, de Parseval P (2001) Hiortdahlite II from the lllmaussaq alkaline complex, South Greenland, the Tamazeght complex, Morocco, and the Iles de Los, Guinea. Geol Greenl Surv Bull 190:131–137

Rooney T, Hart W, Hall C, Ayalew D, Ghiorso M, Hidalgo P, Yirgu G (2012) Peralkaline magma evolution and the tephra record in the Ethiopian Rift. Contrib Mineral Petrol 164(3):407–426. doi:10.1007/s00410-012-0744-6

Scaillet B, Macdonald R (2001) Phase relations of peralkaline silicic magmas and petrogenetic implications. J Petrol 42(4):825–845. doi:10.1093/petrology/42.4.825

Scaillet B, Macdonald R (2003) Experimental constraints on the relationships between peralkaline rhyolites of the Kenya Rift Valley. J Petrol 44(10):1867–1894. doi:10.1093/petrology/egg062

Scaillet B, Macdonald R (2004) Fluorite stability in silicic magmas. Contrib Mineral Petrol 147(3):319–329. doi:10.1007/s00410-004-0559-1

Scaillet B, Macdonald R (2006) Experimental and Thermodynamic constraints on the sulphur yield of peralkaline and metaluminous silicic flood eruptions. J Petrol 47(7):1413–1437. doi:10.1093/petrology/egl016

Schmidt BC, Behrens H (2008) Water solubility in phonolite melts: influence of melt composition and temperature. Chem Geol 256(3–4):259–268. doi:10.1016/j.chemgeo.2008.06.043

Sharp ZD, Helffrich GR, Bohlen SR, Essene EJ (1989) The stability of sodalite in the system NaAlSiO4–NaCl. Geochim Cosmochim Acta 53(8):1943–1954. doi:10.1016/0016-7037(89)90315-3

Shishkina TA, Botcharnikov RE, Holtz F, Almeev RR, Portnyagin MV (2010) Solubility of H_2O- and CO_2-bearing fluids in tholeiitic basalts at pressures up to 500 MPa. Chem Geol 277(1–2):115–125. doi:10.1016/j.chemgeo.2010.07.014

Signorelli S, Carroll MR (2000) Solubility and fluid-melt partitioning of Cl in hydrous phonolitic melts. Geochim Cosmochim Acta 64(16):2851–2862. doi:10.1016/s0016-7037(00)00386-0

Signorelli S, Carroll M (2002) Experimental study of Cl solubility in hydrous alkaline melts: constraints on the theoretical maximum amount of Cl in trachytic and phonolitic melts. Contrib Mineral Petrol 143(2):209–218. doi:10.1007/s00410-001-0320-y

Silver L, Stolper E (1989) Water in albitic glasses. J Petrol 30(3):667–709. doi:10.1093/petrology/30.3.667

Sood MK, Edgar AD (1970) Melting relations of undersaturated alkaline rocks from the Ilímaussaq intrusion and Grønnedal-Ika Complex South Greenland, under water vapour and controlled partial oxygen pressure. Meddelelser om Grønland 181(12):41

Sørensen H (1992) Agpaitic nepheline syenites: a potential source of rare elements. Appl Geochem 7(5):417–427

Sørensen H (1997) The agpaitic rocks—an overview. Mineral Mag 61(4):485–498. doi:10.1180/minmag.1997.061.407.02

Sørensen H (2001) The Ilímaussaq alkaline complex, South Greenland: status of mineralogical research with new results. Geol Greenl Surv Bull 190:1–167

Spickenbom K, Sierralta M, Nowak M (2010) Carbon dioxide and Argon diffusion in silicate melts: insights into the CO_2 speciation in magmas. Geochim Cosmochim Acta 74(22):6541–6564

Stolper E (1982) Water in silicate glasses: an infrared spectroscopic study. Contrib Mineral Petrol 81(1):1–17. doi:10.1007/bf00371154

Stormer JC, Carmichael ISE (1971) The free energy of sodalite and the behavior of chloride, fluoride and sulfate in silicate magmas. Am Mineral 56:292–306

Tamic N, Behrens H, Holtz F (2001) The solubility of H2O and CO2 in rhyolitic melts in equilibrium with a mixed CO2–H2O fluid phase. Chem Geol 174(1–3):333–347. doi:10.1016/S0009-2541(00)00324-7

Villiger S, Ulmer P, Müntener O, Thompson AB (2004) The liquid line of descent of anhydrous, mantle-derived, tholeiitic liquids by fractional and equilibrium crystallization—an experimental study at 1.0 GPa. J Petrol 45(12):2369–2388. doi:10.1093/petrology/egh042

Watson EB (1979) Zircon saturation in felsic liquids: experimental results and applications to trace element geochemistry. Contrib Mineal Petrol 70(4):407–419. doi:10.1007/bf00371047

Webster JD (1990) Partitioning of F between H2O and CO2 fluids and topaz rhyolite melt. Contrib Mineral Petrol 104(4):424–438. doi:10.1007/bf01575620

Webster JD, Duffield WA (1994) Extreme halogen abundances in tin-rich magma of the Taylor Creek Rhyolite, New Mexico. Econ Geol 89(4):840–850. doi:10.2113/gsecongeo.89.4.840

Webster JD, Holloway JR (1990) Partitioning of F and Cl between magmatic hydrothermal fluids and highly evolved granitic magmas. Geol Soc Am Spec Pap 246:21–34. doi:10.1130/SPE246-p21

Webster JD, Holloway JR, Hervig RL (1987) Phase equilibria of a Be, U and F-enriched vitrophyre from Spor Mountain, Utah. Geochim Cosmochim Acta 51(3):389–402. doi:10.1016/0016-7037(87)90057-3

Xiong X-L, Rao B, Chen F-R, Zhu J-C, Zhao Z-H (2002) Crystallization and melting experiments of a fluorine-rich leucogranite from the Xianghualing Pluton, South China, at 150 MPa and H2O-saturated conditions. J Asian Earth Sci 21:175–188

Yamashita S, Kitamura T, Kusakabe M (1997) Infrared spectroscopy of hydrous glasses of arc magma compositions. Geochem J 31(3):169–174

Zakharov V, Maiorov D, Alishkin A, Matveev V (2011) Causes of insufficient recovery of zirconium during acidic processing of lovozero eudialyte concentrate. Russ J Non Ferr Met 52(5):423–428. doi:10.3103/s1067821211050129

Zhang C, Holtz F, Ma C, Wolff PE, Li X (2012) Tracing the evolution and distribution of F and Cl in plutonic systems from volatile-bearing minerals: a case study from the Liujiawa pluton (Dabie orogen, China). Contrib Mineral Petrol 164(5):859–879. doi:10.1007/s00410-012-0778-9

C. Appendix

Title
Development of potential new geothermometers for (per-) alkaline phonolitic systems

Authors
Christopher Giehl, Michael A.W. Marks and Marcus Nowak

Status
In preparation

Contributions of the candidate

Scientific ideas	70 %
Experimental work	100 %
Analytical work	90 %
Analysis and interpretation	80 %
Preparation of manuscript	90 %

Development of potential new geothermometers for (per–) alkaline phonolitic systems

Abstract

Geothermometry in highly evolved peralkaline rocks is often difficult as Fe-Ti oxides, olivine and Ca-rich clinopyroxene are unstable, instead complex Na-Fe-Ti-Zr silicates like eudialyte and aenigmatite occur. Therefore, most available geothermometers are not applicable and only few other approaches to calculate crystallization *T*´s are available for such rocks. In this study, existing geothermometers were tested using experimental data from phase equilibrium experiments (1000 – 650 °C) on an iron-rich peralkaline phonolitic composition. Stable mineral phases within this *T* interval are titanomagnetite, fayalitic olivine, Ca-Na-Fe clinopyroxene, alkali feldspar, nepheline, aenigmatite, sodalite, eudialyte, fluorite and hiortdahlite coexisting with melt. Both olivine – clinopyroxene - Fe-Ti oxide equilibria and clinopyroxene/melt element partitioning yield large deviations compared with experimental *T*`s, confirming serious problems of these thermometers in highly peralkaline systems.

Therefore, we provide calibration for the following potential geothermometers based on Mn mineral/mineral partitioning:

$\log K_d$ (*c*Mn,eudialyte/clinopyroxene) = 0.376*(10000/*T* (K)) - 3.858 (n=7,r^2=0.94,T_{int}=800–650°C)

$\log K_d$ (*c*Mn,aenigmatite/clinopyroxene) = 0.292*(10000/*T* (K)) - 2.715 (n=6,r^2=0.87,T_{int}=800–700°C)

with Mn (wt%) *T* being temperature in K, n is the number of calibration experiments, r^2 the coefficient of determination and T_{int} the *T* interval were calibration experiments were conducted. Furthermore, of two thermometers based on mineral/melt partitioning were calibrated:

$\log K_d$ (*c*Mn,clinopyroxene/melt) = -0.310*(10000/*T* (K)) + 3.139 (n=16,r^2=0.95,T_{int}=900-650°C)

$\log K_D$ (Na/(Na+Ca),clinopyroxene/melt) = 0.472*(10000/*T* (K)) - 5.063 (n=16;r^2=0.94,T_{int}=900-650°C)

Our experiments also demonstrate that high F melt concentrations destabilize Ca-rich clinopyroxene and fluorite and hiortdahlite are stable instead. This induces a compositional gap between Ca- and Na-rich clinopyroxene as occasionally observed in nature. Elevated concentations of Ti and Zr in clinopyroxene are influenced by oxygen fugacity and the presence or absence of Ti-Zr silicates. Experimental data reveals complex trends for Ti and Zr in clinopyroxene and further work is needed to evaluate the potential of these element ratios.

Introduction

Phase equillibrium experiments at high *P* and *T* provide knowledge on mineral stabilities, the compositional evolution of minerals and the influence of volatile components and oxygen fugacity in magmatic systems. Therefore, they allow for the reconstruction of the crystallization sequence, liquid lines of descent and pre-eruptive conditions and provide calibrations for geothermometers based on mineral-mineral and mineral-melt partitioning of specific elements. Numerous thermometers for magmatic systems utilize element partitioning between Fe-Mg(-Ca)-bearing mineral phases (olivine, biotite, clinopyroxene and orthopyroxene, e. g. Ellis and Green 1979; Lindsley 1983; Lee and Ganguly 1988; Perkins and Vielzeuf 1992), Fe-Ti oxides (e. g. Buddington and Lindsley 1964), pyroxene-melt partitioning (Putirka et al. 1996), Ol-Cpx(-Fe-Ti oxide) equilibria (Andersen et al. 1993) and feldspathoid-bearing Ol-Fe-Ti oxide equilibria (Schilling et al. 2011b).

Agpaitic rocks are a subgroup of peralkaline (A. I. = (Na+K)/Al > 1) rocks and represent some of the most evolved magmatic rocks known with a crystallization interval > 300 °C (e. g. Sood and Edgar 1970; Giehl et al. 2013; 2014) and typically high concentrations of HFSE (e. g. Zr), Cl and F (Bailey et al. 2001). In such rocks, geothermometry is difficult because #Mg`s are close to zero and Fe-Mg(-Ca) silicates are often absent, instead complex Na-Fe-Ti-Zr silicates like eudialyte and aenigmatite are stable (**Tab. 1**, Marks and Markl 2013; Giehl et al. 2014). Therefore, few alternative possibilities are applicable to calculate crystallization *T*`s, for example Nph and Afs compositions (Hamilton 1961; Fuhrman and Lindsley 1988), Na-K partitioning among Nph and Afs (Powell and Powell 1977) and activities of Na-Al components in Cpx, Afs and Nph (e. g. Markl et al. 2001).

In this study, the reliability of selected geothermometers based on Ol-Cpx(-Fe-Ti oxide) equilibria and Cpx-melt equilibria was tested using data from isobaric, H_2O-poor phase equilibrium experiments on a peralkaline iron-rich phonolitic composition with variable Cl and F content (Giehl et al. 2013; Giehl et al. 2014). In these experiments, titanomagnetite, fayalitic olivine, calcic clinopyroxene, alkali feldspar and nepheline are stable at 850 – 800 °C. At lower *T*, Mag and Ol are unstable, but sodic clinopyroxene, aenigmatite, sodalite and eudialyte occur, and F_{melt} concentrations > 1.5 wt% additionally stabilize fluorite and hiortdahlite (see **Tab. 1** for mineral abbreviations). Also, in these experiments Cpx shows high concentrations of TiO_2 (up to 2.1 wt%) and ZrO_2 (up to 2.4 wt%).

Concentrations of TiO_2 in Cpx of metaluminous rocks are usually less than 1 wt%, but may reach elevated concentrations up to 9.4 wt% TiO_2 (up to 0.3 apfu) in peralkaline rocks (Ferguson 1977). Concentrations of ZrO_2 are usually lower and are not even routinely analyzed (e. g. Watson and Ryerson 1986; Deer et al. 1992). In highly evolved rocks, however, Cpx may incorporate significant amounts of ZrO_2 (Sabine 1950), exemplified by Cpx in syenites, phonolites and trachytes (up to 14.5 wt%, Sabine 1950; Gomes et al. 1970; Larsen 1976; Nielsen 1979; Jones and Peckett 1981; Duggan 1987; Mann et al. 2006; Andersen et al. 2012).

There is no clear correlation of Zr between host rock and Zr_{Cpx} (Duggan 1987), but increasing fractionation parallels increasing Zr in Cpx (Gomes et al. 1970; Larsen 1976). A study on a ZrO_2-rich (0.5 wt%) syenite from Mt Gibraltar revealed that at extremely low fO_2 Zr is rather incorporated in Cpx than forming distinct Zr-silicates (Andersen et al. 2012). In Ilímaussaq, increasing Zr_{Cpx} is reversed when saturation of Zr-silicates (e. g. eudialyte) occurs (Markl et al. 2001).

In this study, we present compositional trends in minerals and mineral-melt element partitioning for a peralkaline agpaitic phonolitic system with focus on complex Na-Ca-Fe-Mn-Ti-Zr silicates and Ti- and Zr-rich Cpx. In addition, we show that Ol-Cpx(-Fe-Ti oxide) and Cpx-melt thermometry cannot be reliably applied in such systems and propose potential geothermometers based on Mn partitioning between eudialyte/clinopyroxene, aenigmatite/clinopyroxene and clinopyroxene/melt, and Na/(Na+Ca) clinopyroxene/melt partitioning. Due to the frequent occurence of these minerals, these thermometers are particularly suitable for peralkaline agpaitic rocks.

Experimental and analytical methods

This paper discusses data generated in phase equilibrium experiments on an iron-rich peralkaline phonolitic composition (Giehl et al. 2013; Giehl et al. 2014). In the following a brief summary of the experimental and analytical methods is given. The starting composition represents a peralkaline dyke rock that is a potential parental melt of the Ilímaussaq plutonic complex (South Greenland, Larsen and Steenfelt 1974; Marks and Markl 2003; Giehl et al. 2013; 2014). Three starting glasses with variable F and Cl contents were synthesized. Isobaric experiments (100 MPa) were conducted in an internally heated argon pressure vessel (IHPV, 1000 °C) and hydrothermal cold seal pressure vessels (CSPV, 950 - 650 °C) for 336 - 840 h in graphite-lined gold capsules, followed by rapid quench. To cover the large *T* interval, a two-step fractional crystallization strategy was applied. Therefore, residual melt compositions from experiments at 800 °C were resynthesized as starting material for subsequent experiments at lower *T*. All experimental products were analyzed with electron microprobe (EMP) analyses and some selected with fourier-transform infrared spectroscopy (FTIR) for analyzing H_2O_{melt} content. Attainment of equilibrium was demonstrated by systematic changes of #Mg and melt fractions, homogeneous mineral phase and residual glass compositions within one experiment and by comparison of repeated experiments. More details on experimental and analytical methods are given in Giehl et al. (2013; 2014).

Table 1 Mineral phases with simplified formulae and compositional variations

Mineral phase	Abbr.	Formula	Cl/ (Cl+OH) #Cl	Na/ (Na+-Ca) *X*Na	100*Mg/ (Fe^{2+}+Mn+Mg) #Mg	Ti/ (Ti+Zr) *X*Ti
Olivine	Ol	$(Fe,Mn,Mg)SiO_4$			X	
Clinopyroxene	Cpx	$(Ca,Na)(Fe,Mn,Mg,Ti,Zr)Si_2O_6$		X	X	X
Aenigmatite	Ae	$Na_2(Fe,Mn,Mg)_5(Ti,Zr)Si_6O_{20}$		X	X	X
Eudialyte	Eud	$Na_{15}Ca_6Fe_3(Zr,Ti)_3Si_{26}O_{73}(OH)_3(Cl,OH)_2$	X	X	X	X
Hiortdahlite	Hio	$Ca_4(Ca,Na)_2(Zr,Ti)_2Si_4O_{15\text{-}16}F_4$		X		X

Results

Phase relations and compositional trends of the coexisting melt are briefly summarized. Residual melts in all three experimental series show decreasing SiO_2, Al_2O_3, K_2O, CaO, increasing Na_2O, MnO and P_2O_5 and resulting increasing A.I., Na/(Na+K), Na/(Na+Ca) and Na/Fe. In contrast, variable liquid lines of descent are observed for TiO_2, ZrO_2, Ti/(Ti+Zr), FeO*, MgO, #Mg, Cl, F and Cl/(Cl+F) (as discussed in detail in Giehl et al. 2014). FTIR spectroscopy on selected experiments confirms low H_2O_{melt} concentrations of ≤1.2 wt%.

Mineral phases present are Mag, Cpx, Ol, Afs, Nph and Ae. Roughly 1.5 wt% F_{melt} stabilize Fl and Hio while Cpx is destabilized; and Sdl and Eud crystallization require a coexisting melt with 0.2 – 0.5 wt% Cl, Hio and Eud additionally require > 0.7 wt% $ZrO_{2\ melt}$. Experiments with highly peralkaline residual melts lack Fe-Ti oxide, Ol and Hio while Afs, Nph, Sdl and Ae are stable. Details on phase stabilities are given in Giehl et al. (2014).

Compositional trends and mineral-melt partitioning

Systematic variations of several element ratios are observed for Ol, Cpx, Ae, Eud and Hio as given in **Table. 1**.

Cl-OH ratios in eudialyte and the coexisting melt

With decreasing *T,* $\#Cl_{melt}$ and $\#Cl_{Eud}$ decrease (**Fig. 1a** and **b,** data from Giehl et al. 2014,). However, in one primitive experiment using primitive starting composition $\#Cl_{Eud}$ is significantly lower compared to experiments using evolved starting composition at 750 °C. Determination of cH_2O_{melt} (and therefore calculation of $\#Cl_{melt}$ for the experiment) by FTIR failed due to the low residual melt fraction. However, lower $\#Cl_{Eud}$ can be explained by the extent of accumulated H_2O through different residual melt fractions of ~34 wt% and ~80 wt%, respectively, and a resulting lower $\#Cl_{melt}$ (**Fig. 1a**).

Na-Ca systematics

Na/(Na+Ca) ratios (*X*Na) of Cpx, Hio, Eud and the coexisting melt versus *T* are shown on **Fig. 2a**. Whilst XNa_{Eud} (0.66 – 0.71) is fairly constant, XNa_{melt} (0.84 – 0.97) and XNa_{Hio} (0.18 – 0.26) slightly increases with decreasing *T* (**Fig. 2a**). In contrast,

142 $X\mathrm{Na}_{Cpx}$ (0.10 – 0.79) is highly variable, increases with decreasing *T* and is positively
143 correlated with $X\mathrm{Na}_{melt}$ (**Fig. 2a** and **b**).

144 ## Fe-Mn(-Mg) systematics

145 With decreasing *T*, #Mg`s (Mg/(Fe^{2+}+Mn+Mg)) of Ol (5-2) and Ae (3-1) decrease
146 (**Fig. 3**). In contrast, $\#\mathrm{Mg}_{Cpx}$ decrease (12-5) at 900 – 750 °C, however, at 750 -
147 650 °C $\#\mathrm{Mg}_{Cpx}$ increases as $Fe^{3+}/(Fe^{3+}+Fe^{2+})$ of Cpx ($X\mathrm{Fe}^{3+}$) strongly increases. Both
148 Ol and Ae have higher #Mg for a given *T* in experiments with halogen-rich starting
149 compositions (**Fig. 3a** and **c)**. With decreasing *T*, MnO in Ae, Eud and the coexisting
150 melt increase. In contrast, MnO in Cpx decreases with decreasing *T* (**Fig. 4a**). The
151 comparison with MnO_{melt} shows similar trends, MnO in Ae and Eud increase with
152 increasing MnO_{melt}, in contrast MnO_{Cpx} decreases (**Fig. 4b**).

153 ## Ti-Zr systematics

154 Ae is Ti-rich and incorporates minor amounts of Zr, Hio and Eud are Zr-rich and
155 incorporate minor amounts of Ti (Giehl et al. 2014). The $X\mathrm{Ti}_{Ae}$ (0.99 – 0.97) and
156 $X\mathrm{Ti}_{Hio}$ (0.26-0.25) are fairly constant, in one experiment were Hio coexists with Eud,
157 $X\mathrm{Ti}_{Hio}$ is significantly lower (0.16). With decreasing *T,* $X\mathrm{Ti}_{Eud}$ increases from 0.03 to
158 0.25 (**Fig. 5a**), while two possible trends are observed when plotted against $X\mathrm{Ti}_{melt}$
159 (**Fig. 5b**) In contrast to Ae, Hio and Eud, Cpx contains minor amounts of TiO_2 and
160 ZrO_2, $X\mathrm{Ti}_{Cpx}$ shows a complex trend with *T* and $X\mathrm{Ti}_{melt}$ (**Fig. 5a** and **b**). The coexisting
161 melt shows a poorly defined trend of decreasing *X*Ti with decreasing *T* (**Fig. 5a**).

162 # Discussion

163 ## Geothermometry in (per-)alkaline rocks

164 Both Ol-Cpx(-Fe-Ti oxide) and Cpx-melt thermometers (Andersen et al. 1993; Putirka
165 2008; Masotta et al. 2013) show reasonable agreement (±50 °C) with experimental
166 *T*`s where Cpx is Na-poor (< 0.15 apfu). However, large deviations are observed with
167 increasing Na content in Cpx (**Fig. 6**). This confirms that high Na content in Cpx
168 introduces serious problems for such thermometers (e. g. Essene 1982; Lindsley
169 1983; Marks and Markl 2001). Relatively large uncertainties of 75 - 130 °C were
170 reported for thermometers utilizing Nph and Afs compositions (Perchuk and
171 Ryabchikov 1968; Putirka 2008), however, QUILF calculations are more accurate but
172 require Ol or Fe-Ti oxides, which are often unstable in highly peralkaline melts

(Marks et al. 2011; Giehl et al. 2014). Cpx-melt thermometers from Putirka (2008) were recalibrated with new experimental data by Masotta et al. (2013). In this work, the precision of Cpx-melt thermometers was improved and the extended experimental dataset covers phonolitic, tephri-phonolitic and trachytic compositions. However, this kind of thermometer is only applicable if melt compositions are known.

Mineral phase compositions of Ol and Cpx (and Mag) from experiments at 100 MPa and 900 – 800 °C were used to test the reliability of *T* calculations with the QUILF95 software (Ver. 6.42, Andersen et al. 1993). The difference between calculated *T*`s and experiment *T*`s (Δ*T*) plotted against Na_{Cpx} (apfu) of the corresponding experiment is shown on **Fig. 6**. For Cpx with <0.15 Na (apfu) Δ*T* is ±35 °C, however, in experiments with Na-rich Cpx (0.19 – 0.24 apfu) *T* is underestimated by more than 100 °C. In experiments where Na is even higher (0.22 – 0.81 apfu) *T* estimates are not possible because Ol (and Fe-Ti oxides) are unstable. QUILF calculations using Cpx with Na > 0.1 apfu were previously found to yield unexpectedly low *T* and $aSiO_2$ (sample GM1223, Marks and Markl 2001). Our experiments confirm the underestimation of *T* by QUILF and we suggest not to use Na-rich Cpx (>0.15 Na apfu) for such calculations.

We further tested seven Cpx-melt thermometers calibrated with Cpx-melt pairs from phonolites, tephri-phonolites and trachytes (Putirka et al. 1996; Putirka 2008; Masotta et al. 2013). Two thermometers (T2, Putirka et al. 1996 and TALK33, Masotta et al. 2013) reproduce the experimental *T*´s within 50 °C for Cpx with <0.4 and <0.25 apfu Na, respectively. However, all models yield strong negative correlations of Δ*T* with Na_{Cpx} (apfu). The calibration data of e. g. TALK2012 (Masotta et al. 2013) is limited to Cpx with Na < 0.2 apfu, except for data published by Andújar et al. (2008, Na_{Cpx} = 0.25 – 0.42 apfu). The comparison with our experimental data shows that the model is only reasonably accurate for Na-poor Cpx (<0.15 apfu, Δ*T* < 50 °C) as Cpx with higher Na (apfu) are underrepresented in the dataset used for calibration. Not only this confirms that the model should not be used beyond the calibrated range, but limits the applicability to Cpx with Na <0.15 apfu, although Cpx used for calibration is more Na-rich (up to 0.42 apfu). We conclude that *T* calculation with both Ol-Cpx(-Fe-Ti oxide) equilibria and Cpx-melt equilibria with Na-rich Cpx yield erronous results. Therefore extension of the calibration dataset would be necessary to improve the accuracy for (per-)alkaline systems. However, extremely low #Mg`s in such systems

206 principally pose the question if other element ratios, e. g. the Fe/Mn ratio or the
207 Na/Ca ratio are more suitable for such rocks.

208 ## New potential thermometers for peralkaline rocks

209 During early-, late- and post-magmatic stages Eud occurs and is therefore ideal to
210 trace geochemical and petrological processes (e. g. Mitchell and Liferovich 2006;
211 Schilling et al. 2009; Mitchell and Chakrabarty 2012). The composition of naturally
212 occuring eudialyte is highly variable, however, few constraints on stability and
213 compositional trends of eudialyte are known. Schilling et al. (2011a) found that Fe/Mn
214 ratios of Eud decrease with fractionation. However, Ratschbacher et al. (2011)
215 showed that Fe/Mn ratios in Eud are influenced by coexisting amphibole and Cpx
216 and suggested REE+Y vs. Cl as a suitable fractionation indicator.

217 In the present study, Cpx shows increasing Fe/Mn ratios, whereas Ae and Eud show
218 decreasing Fe/Mn ratios with decreasing *T*, confirming the abovementioned
219 observations in natural rocks. The absence of Cpx in one experiment at 700 °C (run
220 141, Giehl et al. 2014) induces higher Fe/Mn in Eud, confirming an effect of
221 coexisting Cpx on Fe/Mn ratios for Eud.

222 The Mn distribution coefficients for Eud/Cpx (log K_d (*c*Mn, Eud/Cpx)), Ae/Cpx (log K_d
223 (*c*Mn, Ae/Cpx)) and Cpx/melt (log K_d (*c*Mn, Cpx/melt)), provide linear relationships
224 when plotted against inverse *T* (**Figs. 7** and **8).** Linear regressions of the
225 experimental data yield the following equations:

226 log K_d (*c*Mn,Eud/Cpx) = 0.376*(10000/*T* (K)) - 3.858 (n=7, r^2=0.94, T_{int}=800–650 °C)
227 (Eq. 4)

228 log K_d (*c*Mn,Ae/Cpx) = 0.292*(10000/*T* (K)) - 2.715 (n=6, r^2=0.87, T_{int}=800–700 °C)
229 (Eq. 5)

230 log K_d (*c*Mn,Cpx/melt) = -0.310*(10000/*T* (K)) + 3.139 (n=16, r^2=0.95, T_{int}=900-
231 650 °C) (Eq. 6)

232 with Mn in wt%, *T* in K, r^2 is the coefficient of determination, n is the number of
233 calibration experiments and T_{int} is the interval covered by calibration experiments.
234 High coefficients of determination emphasize their potential as geothermometers.

Due to highly variable $X\mathrm{Na}_{Cpx}$ it is tempting to suspect a correlation with $X\mathrm{Na}_{melt}$ (**Fig. 9**), similar to the abovementioned Mn thermometers, a correlation with inverse T is found for log K_D(XNa, Cpx/melt):

$$\log K_d\ (X\mathrm{Na,Cpx/melt}) = 0.472*(10000/T\ (\mathrm{K})) - 5.063\ (n=16;\ r^2=0.94,\ T_{int}=900\text{-}650\ ^\circ\mathrm{C})\quad \text{(Eq. 7)}$$

Comparison with previous experimental data

To our knowledge, no phase equilibrium experiments with Eud are available and coexisting Cpx and Ae were only reported once in an experimental study on peralkaline rhyolites (Di Carlo et al. 2010). In contrast to our study, these experiments were performed at highly variable H_2O_{melt} content (0.7 to 4.6 wt%) and $f\mathrm{O}_2$ (Δ log FMQ -1.2 to -3.5). This dataset was used to test Ae/Cpx (Mn) and Cpx/melt (Mn) calibrations by comparing calculated T`s with known experimental T´s (ΔT). For Ae/Cpx (Mn), some data points show good agreement, while others deviate significantly **(Fig. 10)**. Experiments conducted at similar and lower $f\mathrm{O}_2$ (Δ log FMQ -2.8 to -0.7) compared to calibration experiments (Δ log FMQ -1.8 to -1.2) show reasonable agreement (ΔT < 50 °C). In contrast, slightly higher $f\mathrm{O}_2$ (Δ log FMQ -0.8 to -0.4) leads to increasing ΔT (80 – 90 °C). The correlation of ΔT with $f\mathrm{O}_2$ implies applicability within or below the calibrated $f\mathrm{O}_2$ range. To include the $f\mathrm{O}_2$ effect into the calibration, this would require calibration data at variable $f\mathrm{O}_2$ conditions.

To test the Cpx/melt(XNa) thermometer experiments of this study were compared with data from experimental studies on phonolites (Berndt et al. 2001; Freise et al. 2003; Andújar et al. 2010; Masotta et al. 2013). Most of the experiments are in reasonable agreement with Equation 7, suggesting the potential use as a geothermometer between 900 – 650 °C.

Application to nature

So far, crystallization T`s of the dykes` groundmass assemblage were estimated from Nph thermometry and Ab-Jd-Ne equilibria (<775 °C and 600 – 450 °C, respectively, Marks and Markl 2003). Upper and lower limits of log K_d (Mn) were calculated for one dyke rock sample (GM 1849) using min-max values from Eud (**Tab. 2**), Ae and Cpx analyses (Marks and Markl 2003). Calculations yield 625 – 530 °C (Eud/Cpx) and 615 – 500 °C (Ae/Cpx), which is outside the calibrated T interval, but reasonably close to previous estimates (**Fig. 7**). Also, similar equilibration T´s for both Eud/Cpx and Ae/Cpx thermometers coincide with the textural observation that Eud and Ae

coexist in this sample. The application of Cpx/melt thermometers requires knowledge on melt compositions. Such information can be obtained from melt inclusion data, which is currently unavailable for the Ilímaussaq rocks.

Table 2 Eudialyte EMP analyses from sample GM1849 (wt%, Marks and Markl 2003)

SiO_2	47.33	46.77
TiO_2	0.09	0.04
ZrO_2	8.64	9.09
Al_2O_3	0.17	0.14
FeO	6.18	6.30
MnO	0.73	0.69
CaO	11.02	10.87
Na_2O	14.87	15.01
K_2O	0.33	0.33
Cl	1.33	1.39
HfO_2	0.13	0.20
Nb_2O_5	0.66	0.54
Nd_2O_3	0.03	0.04
Ce_2O_3	0.06	0.06
Y_2O_3	0.41	0.43
La_2O_3	0.03	0.02
SrO	0.00	0.00
Total	92.00	91.92

Another rock type suited to apply the Eud/Cpx thermometer are the lujavrites of Ilímaussaq where crystallization *T*`s were estimated to 500 – 450 °C (Markl et al. 2001). Application of the Eud/Cpx thermometer with data from Ratschbacher et al. (2011) yields 550 – 430 °C.

In the agpaitic nepheline syenites of Tamazeght (Morocco) Eud occurs during late- and post-magmatic stages (Schilling et al. 2009). Constraints on *T* from Nph thermometry indicate 900 – 800 °C during early magmatic conditions and 500 – 400 °C for post-magmatic hydrothermal veins (Marks et al. 2008). The Eud/Cpx thermometer yields between 670 and 550 °C, consistent with textural observations (Schilling et al. 2009). Similarly, in SiO_2-undersaturated syenites of the Agua de Pau volcano (Sao Miguel, Azores Islands) Eud represents the latest stages of crystallization and is interpreted to coexist with aegirine-augite (Ridolfi et al. 2003). Here, Eud/Cpx Mn thermometry yields reasonable 620°C.

Limitations of of the model

We here emphasize that calibration experiments were conducted at 100 MPa, H_2O_{melt} ≤ 1.2 wt% and Δ log FMQ -1.8(5) to -1.2(5). Experiments from Di Carlo et al. (2010) imply the influence of variable H_2O_{melt} and fO_2 conditions on Mn distribution between Ae and Cpx. Such effects need further experimental investigations at variable fO_2 conditions.

Investigations on interdiffusion of (Fe,Mn)-Mg and Fe-Mg in diopside show that Cpx compositions record and retain peak *T* conditions of formation (Dimanov and Wiedenbeck 2006; Müller et al. 2013). However, such diffusion data for Ae and Eud are unavailable. Application tonature was only possible in rocks were Eud is relatively late in the crystallization sequence. Therefore, the applicability at higher *T*´s needs to be demonstrated.

References

Andersen DJ, Lindsley DH, Davidson PM (1993) QUILF - A PASCAL program to assess equilibria among Fe-Mg-Mn-Ti Oxides, Pyroxenes, Olivine and Quartz. Computers & Geosciences 19 (9):1333-1350. doi:10.1016/0098-3004(93)90033-2

Andersen T, Carr P, Erambert M (2012) Late-magmatic mineral assemblages with siderite and zirconian pyroxene and amphibole in the anorogenic Mt Gibraltar microsyenite, New South Wales, Australia, and their petrological implications. Lithos 151:46-56. doi:10.1016/j.lithos.2011.09.012

Andújar J, Costa F, Martí J (2010) Magma storage conditions of the last eruption of Teide volcano (Canary Islands, Spain). Bulletin of Volcanology 72 (4):381-395. doi:10.1007/s00445-009-0325-3

Andújar J, Costa F, Marti J, Wolff JA, Carroll MR (2008) Experimental constraints on pre-eruptive conditions of phonolitic magma from the caldera-forming El Abrigo eruption, Tenerife (Canary Islands). Chemical Geology 257 (3-4):173-191. doi:10.1016/j.chemgeo.2008.08.012

Bailey JC, Gwozdz R, Rose-Hansen J, Sørensen H (2001) Geochemical overview of the Ilimaussaq alkaline complex, South Greenland. Geology of Greenland Survey Bulletin 190:35-53

Berndt J, Holtz F, Koepke J (2001) Experimental constraints on storage conditions in the chemically zoned phonolitic magma chamber of the Laacher See volcano. Contributions to Mineralogy and Petrology 140 (4):469-486. doi:10.1007/PL00007674

Buddington AF, Lindsley DH (1964) Iron-Titanium Oxide Minerals and Synthetic Equivalents. Journal of Petrology 5 (2):310-357. doi:10.1093/petrology/5.2.310

Deer WA, Howie RA, Zussman J (1992) An Introduction to the Rock Forming Minerals. 2nd edn. Prentice Hall, Harlow, England

Di Carlo I, Rotolo SG, Scaillet B, Buccheri V, Pichavant M (2010) Phase Equilibrium Constraints on Pre-eruptive Conditions of Recent Felsic Explosive Volcanism at

Pantelleria Island, Italy. Journal of Petrology 51 (11):2245-2276. doi:10.1093/petrology/egq055

Dimanov A, Wiedenbeck M (2006) (Fe,Mn)-Mg interdiffusion in natural diopside: effect of pO₂. Eur J Mineral 18 (6):705-718. doi:10.1127/0935-1221/2006/0018-0705

Duggan MB (1987) Zirconium-rich sodic pyroxenes in felsic volcanics from the Warrumbungle Volcano, Central New South Wales, Australia. Mineralogical Magazine 52:491-496

Ellis DJ, Green DH (1979) An experimental study of the effect of Ca upon garnet-clinopyroxene Fe-Mg exchange equilibria. Contributions to Mineralogy and Petrology 71 (1):13-22. doi:10.1007/bf00371878

Essene EJ (ed) (1982) Characterization of Metamorphism trough Mineral Equilibria: Geologic thermometry and barometry, vol 10. Reviews in Mineralogy. Mineralogical Society of America, Washington, D.C.

Ferguson AK (1977) The natural occurrence of aegirine—neptunite solid solution. Contributions to Mineralogy and Petrology 60 (3):247-253. doi:10.1007/bf01166799

Freise M, Holtz F, Koepke J, Scoates J, Leyrit H (2003) Experimental constraints on the storage conditions of phonolites from the Kerguelen Archipelago. Contributions to Mineralogy and Petrology 145 (6):659-672. doi:10.1007/s00410-003-0453-2

Fuhrman ML, Lindsley DH (1988) Ternary-Feldspar Modeling and Thermometry. American Mineralogist 73 (3-4):201-215

Giehl C, Marks M, Nowak M (2013) Phase relations and liquid lines of descent of an iron-rich peralkaline phonolitic melt: an experimental study. Contributions to Mineralogy and Petrology 165 (2):283-304. doi:10.1007/s00410-012-0809-6

Giehl C, Marks MAW, Nowak M (2014) An experimental study on the influence of fluorine and chlorine on phase relations in peralkaline phonolitic melts. Contributions to Mineralogy and Petrology. doi:10.1007/s00410-014-0977-7

Gomes CdB, Moro SI, Dutra CV (1970) Pyroxenes from the alkaline rocks of Itiriparapua, Sao Paolo, Brasil. American Mineralogist 55:224-230

Hamilton DL (1961) Nephelines as crystallization temperature indicators. The Journal of Geology 69:321-329

Jones AP, Peckett A (1981) Zirconium-bearing aegirines from Motzfeldt, South Greenland. Contributions to Mineralogy and Petrology 75 (3):251-255. doi:10.1007/bf01166764

Larsen LM (1976) Clinopyroxenes and Coexisting Mafic Minerals from the Alkaline Ilímaussaq Intrusion, South Greenland. Journal of Petrology 17 (2):258-290. doi:10.1093/petrology/17.2.258

Larsen LM, Steenfelt A (1974) Alkali loss and retention in an iron-rich peralkaline phonolite dyke from the Gardar province, south Greenland. Lithos 7 (2):81-90. doi:10.1016/0024-4937(74)90021-8

Lee HY, Ganguly J (1988) Equilibrium Compositions of Coexisting Garnet and Orthopyroxene: Experimental Determinations in the System FeO-MgO-Al2O3-SiO2, and Applications. Journal of Petrology 29 (1):93-113. doi:10.1093/petrology/29.1.93

Lindsley DH (1983) Pyroxene thermometry. American Mineralogist 68 (5-6):477-493

Mann U, Marks M, Markl G (2006) Influence of the oxygen fugacity on mineral compositions in peralkaline melts: The Katzenbuckel volcano, Southwest Germany. Lithos 91:262-285. doi:10.1016/j.lithos.2005.09.004

370 Markl G, Marks M, Schwinn G, Sommer H (2001) Phase equilibrium constraints on intensive
371 crystallization parameters of the Ilimaussaq complex, South Greenland. Journal of
372 Petrology 42 (12):2231-2258. doi:10.1093/petrology/42.12.2231
373 Marks M, Markl G (2001) Fractionation and assimilation processes in the alkaline augite
374 syenite unit of the Ilimaussaq intrusion, South Greenland, as deduced from phase
375 equilibria. Journal of Petrology 42 (10):1947-1969. doi:10.1093/petrology/42.10.1947
376 Marks M, Markl G (2003) Ilímaussaq 'en miniature': closed-system fractionation in an
377 agpaitic dyke rock from the Gardar Province, South Greenland (contribution to the
378 mineralogy of Ilímaussaq no. 117) Mineralogical Magazine 67 (5):893-919.
379 doi:10.1180/0026461036750150
380 Marks M, Markl G (2013) The Ilímaussaq alkaline complex (South Greenland). In: Charlier B,
381 Namur O, Latypov R, Tegner C (eds) Layered Intrusions. Springer, Dordrecht,
382 Marks MAW, Hettmann K, Schilling J, Frost BR, Markl G (2011) The Mineralogical Diversity of
383 Alkaline Igneous Rocks: Critical Factors for the Transition from Miaskitic to Agpaitic
384 Phase Assemblages. Journal of Petrology 52 (3):439-455.
385 doi:10.1093/petrology/egq086
386 Marks MAW, Schilling J, Coulson IM, Wenzel T, Markl G (2008) The Alkaline-Peralkaline
387 Tamazeght Complex, High Atlas Mountains, Morocco: Mineral Chemistry and
388 Petrological Constraints for Derivation from a Compositionally Heterogeneous
389 Mantle Source. Journal of Petrology 49 (6):1097-1131
390 Masotta M, Mollo S, Freda C, Gaeta M, Moore G (2013) Clinopyroxene–liquid thermometers
391 and barometers specific to alkaline differentiated magmas. Contributions to
392 Mineralogy and Petrology 166 (6):1545-1561. doi:10.1007/s00410-013-0927-9
393 Mitchell RH, Chakrabarty A (2012) Paragenesis and decomposition assemblage of a Mn-rich
394 eudialyte from the Sushina peralkaline nepheline syenite gneiss, Paschim Banga,
395 India. Lithos 152:218-226. doi:10.1016/j.lithos.2012.02.003
396 Mitchell RH, Liferovich RP (2006) Subsolidus deuteric/hydrothermal alteration of eudialyte in
397 lujavrite from the Pilansberg alkaline complex, South Africa. Lithos 91 (1–4):352-372.
398 doi:10.1016/j.lithos.2006.03.025
399 Müller T, Dohmen R, Becker HW, Heege J, Chakraborty S (2013) Fe–Mg interdiffusion rates in
400 clinopyroxene: experimental data and implications for Fe–Mg exchange
401 geothermometers. Contributions to Mineralogy and Petrology 166 (6):1563-1576.
402 doi:10.1007/s00410-013-0941-y
403 Nielsen TFD (1979) The occurrence and formation of Ti-Aegirines in peralkaline syenites.
404 Contributions to Mineralogy and Petrology 69 (3):235-244. doi:10.1007/bf00372325
405 Perchuk LL, Ryabchikov ID (1968) Mineral Equilibria in the System Nepheline-Alkali Feldspar-
406 Plagioclase and their Petrological Significance. Journal of Petrology 9 (1):123-167.
407 doi:10.1093/petrology/9.1.123
408 Perkins D, Vielzeuf D (1992) Experimental investigation of Fe-Mg distribution between
409 olivine and clinopyroxene: Implications for mixing properties of Fe-Mg in
410 clinopyroxene and garnet-clinopyroxene thermometry. American Mineralogist
411 77:774-783
412 Powell M, Powell R (1977) A nepheline-alkali feldspar geothermometer. Contributions to
413 Mineralogy and Petrology 62 (2):193-204. doi:10.1007/bf00372877
414 Putirka K (2008) Thermometers and barometers for volcanic systems. In: Putirka K, Tepley F
415 (eds) Reviews in Mineralogy and Geochemistry: Minerals, inclusions and volcanic
416 processes, vol 69. Mineralogical Society of America, pp 61-120

417 Putirka K, Johnson M, Kinzler R, Longhi J, Walker D (1996) Thermobarometry of mafic
418 igneous rocks based on clinopyroxene-liquid equilibria, 0–30 kbar. Contributions to
419 Mineralogy and Petrology 123 (1):92-108. doi:10.1007/s004100050145
420 Ratschbacher B, Marks MAW, Pfaff K, Markl G Mineral Compositions Indicate Magma
421 Recharge Processes in the Ilímaussaq Complex, Greenland. In: Goldschmidt, Prague,
422 Czech Republic, 14th - 19th August 2011. Mineralogical Magazine 75(3), p 1698
423 Ridolfi F, Renzulli A, Santi P, Upton BGJ (2003) Evolutionary stages of crystallization of weakly
424 peralkaline syenites: evidence from ejecta in the plinian deposits of Agua de Pau
425 volcano (São Miguel, Azores Islands). Mineralogical Magazine 67 (4):749-767.
426 doi:10.1180/0026461036740131
427 Sabine PA (1950) The Optical Properties and Composition of the Acmitic Pyroxenes.
428 Mineralogical Magazine 29:113-125. doi:10.1180/minmag.1950.029.209.03
429 Schilling J, Frost BR, Marks MAW, Wenzel T, Markl G (2011b) Fe-Ti oxide-silicate (QUIlF-type)
430 equilibria in feldspathoid-bearing systems. American Mineralogist 96 (1):100-110.
431 doi:10.2138/am.2011.3596
432 Schilling J, Marks MAW, Wenzel T, Markl G (2009) Reconstruction of magmatic to subsolidus
433 processes in an agpaitic system using eudialyte textures and composition: a case
434 study. The Canadian Mineralogist 47 (2):351-365. doi:10.3749/canmin.47.2.351
435 Schilling J, Wu FY, McCammon C, Wenzel T, Marks MAW, Pfaff K, Jacob DE, Markl G (2011a)
436 The compositional variability of eudialyte-group minerals. Mineralogical Magazine 75
437 (1):87-115. doi:10.1180/minmag.2011.075.1.87
438 Sood MK, Edgar AD (1970) Melting relations of undersaturated alkaline rocks from the
439 Ilímaussaq intrusion and Grønnedal-Ika Complex South Greenland, under Water
440 Vapour and controlled Partial Oxygen Pressure. Meddelelser om Grønland 181
441 (12):41
442 Watson EB, Ryerson FJ (1986) Partitioning of zirconium between clinopyroxene and
443 magmatic liquids of intermediate composition. Geochimica et Cosmochimica Acta 50
444 (11):2523-2526. doi:10.1016/0016-7037(86)90035-9

445

446

Figures and captions

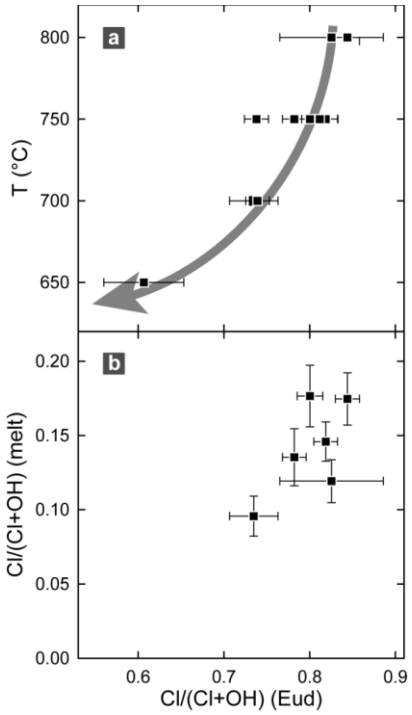

Fig. 1 #Cl in Eud versus (a) *T* and (b) $\#Cl_{melt}$. Figure b only contains data points were H_2O melt concentrations are available. The trends are guide to the eyes

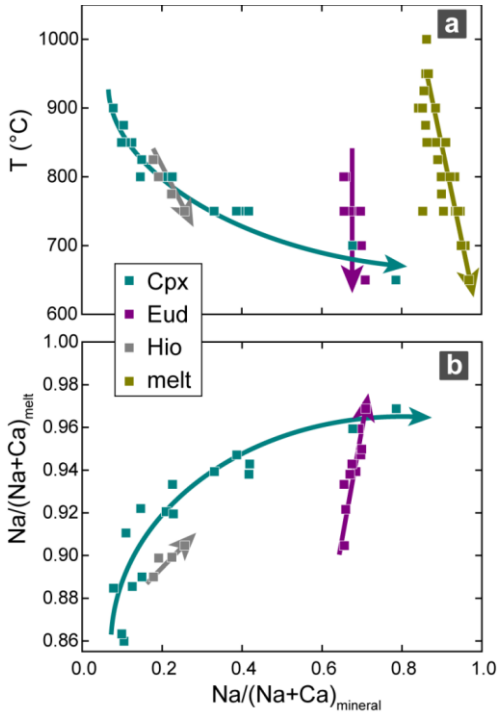

Fig. 2 Na/(Na+Ca) ratios of mineral phases with respect to (a) *T* and (b) the coexisting melt (trends are guide to the eyes, Ae is not shown)

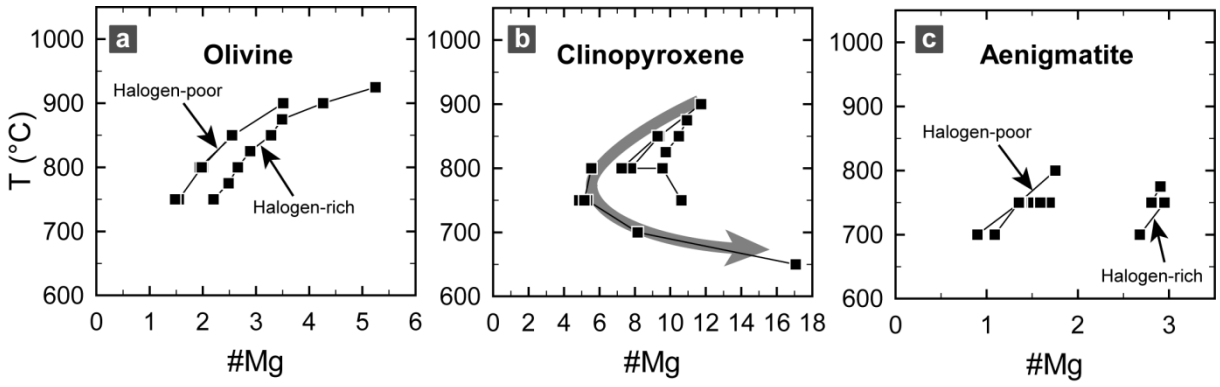

Fig. 3 Magnesium number (#Mg = Mg*(Fe+Mn+Mg)$^{-1}$*100) of (a) Ol, (b) Cpx and (c) Ae (calculated with data from Giehl et al. 2014, electronic supplement eTables 3, 4 and 8)

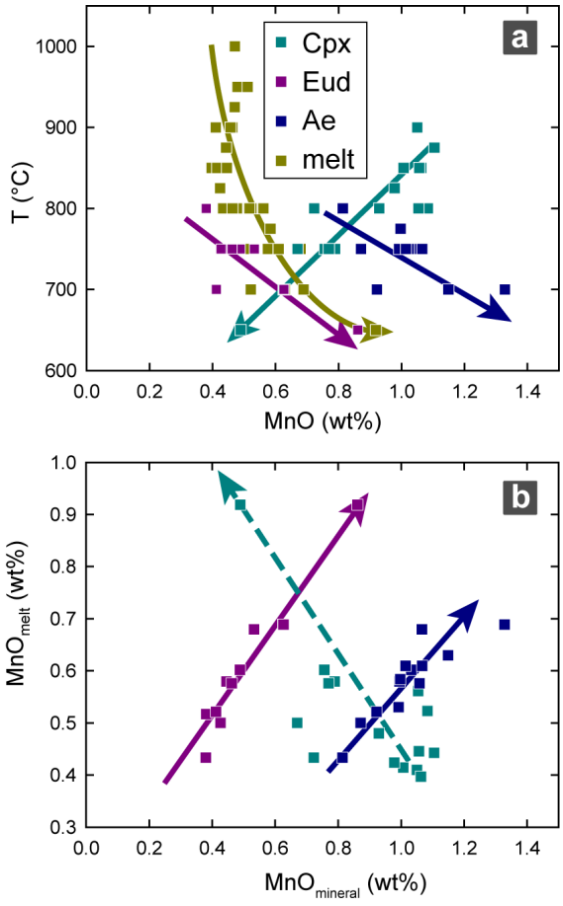

Fig. 4 MnO concentrations of Cpx, Ae, Eud and melt versus *T* (trends are guide to the eyes, Mag, Ol and Hio are not shown)

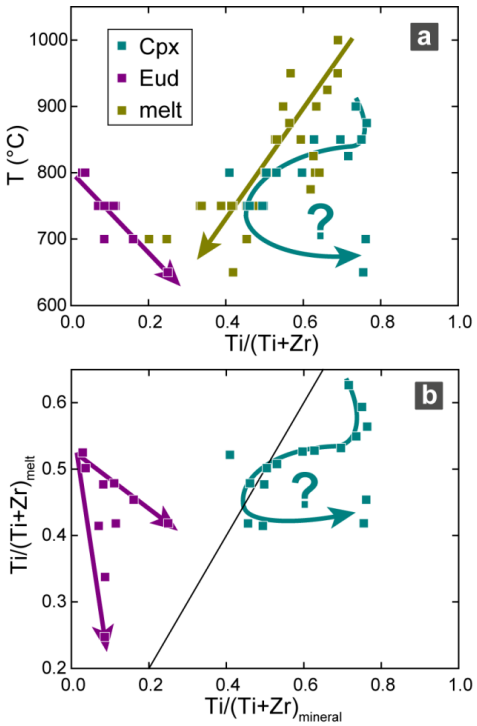

462

463 **Fig. 5** Ti/(Ti+Zr) of Cpx, Eud and melt versus (a) T and (b) Cpx and Eud versus
464 $X\mathrm{Ti}_{\mathrm{melt}}$ (trends are guide to the eyes, Ae and Hio are not shown)

465

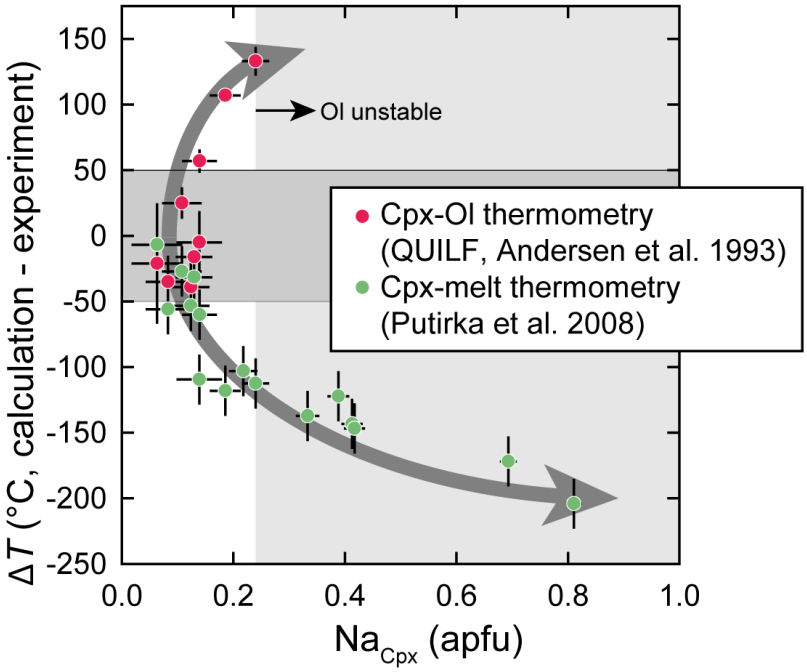

466

467 **Fig. 6** Comparison of experimental *T*´s and fO_2`s with geothermometers based on
468 Cpx-melt partitioning (Putirka 2008) and Ol-Cpx(-Mag) equilibria (QUILF type,
469 Andersen et al. 1993). Calculations with Na-poor Cpx (<0.15 apfu) match
470 experimental *T*´s within 50 °C, higher Na content leads to increasing deviations. The
471 trends are guide to the eyes

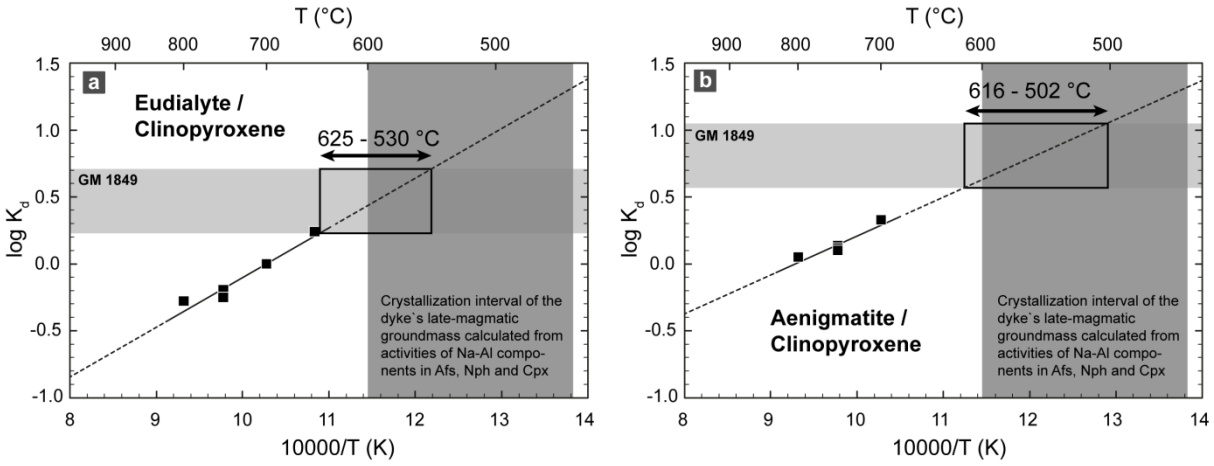

472

473 **Fig. 7** Mn distribution between (a) Eud and Cpx and between (b) Ae and Cpx as a
474 function of inverse *T*. For comparison, we present K_d (Mn) Eud/Cpx and K_d (Mn)
475 Ae/Cpx from dyke rock sample GM1849 (Marks and Markl 2003). Also, Eud of the
476 investigated dyke rock (sample GM1849, Marks and Markl 2003) was analyzed with
477 EMP, analysis conditions were according to Pfaff et al. (2010).

478

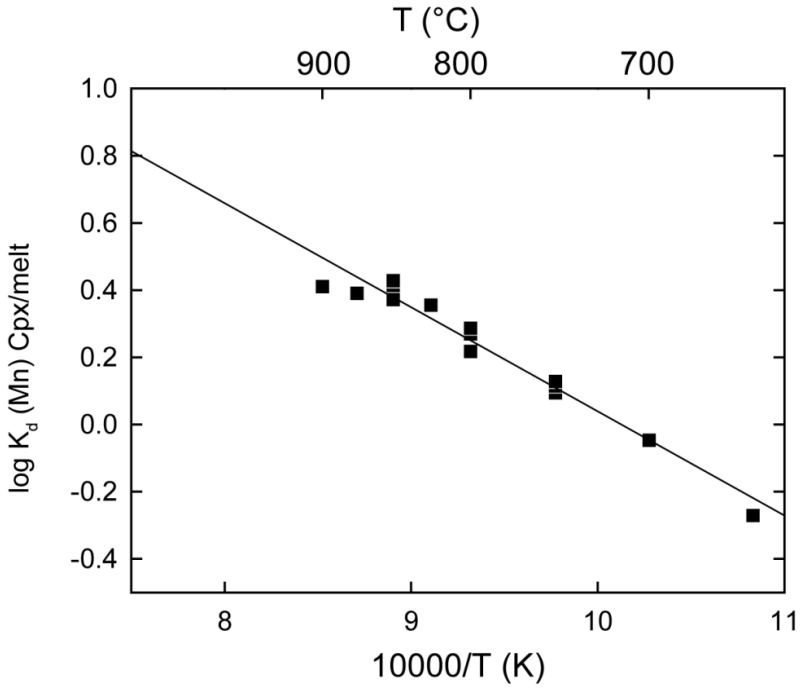

479

480 **Fig. 8** Calibration for Cpx/melt (Mn) partitioning versus experimental *T* using
481 experimental data

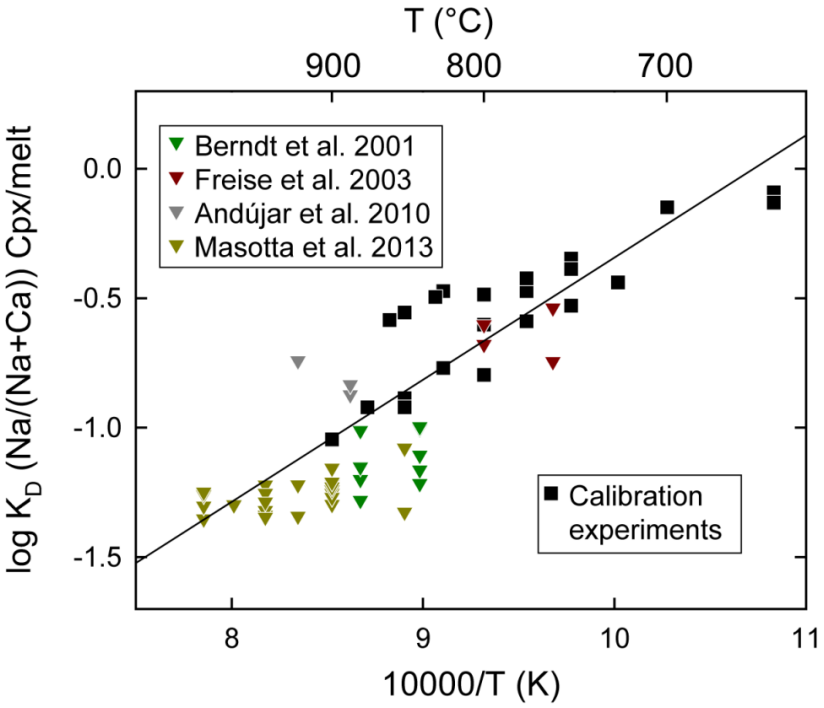

Fig. 9 Comparison of Cpx/melt (*X*Na) partitioning versus experimental *T* using experimental data (Berndt et al. 2001; Freise et al. 2003; Masotta et al. 2013)

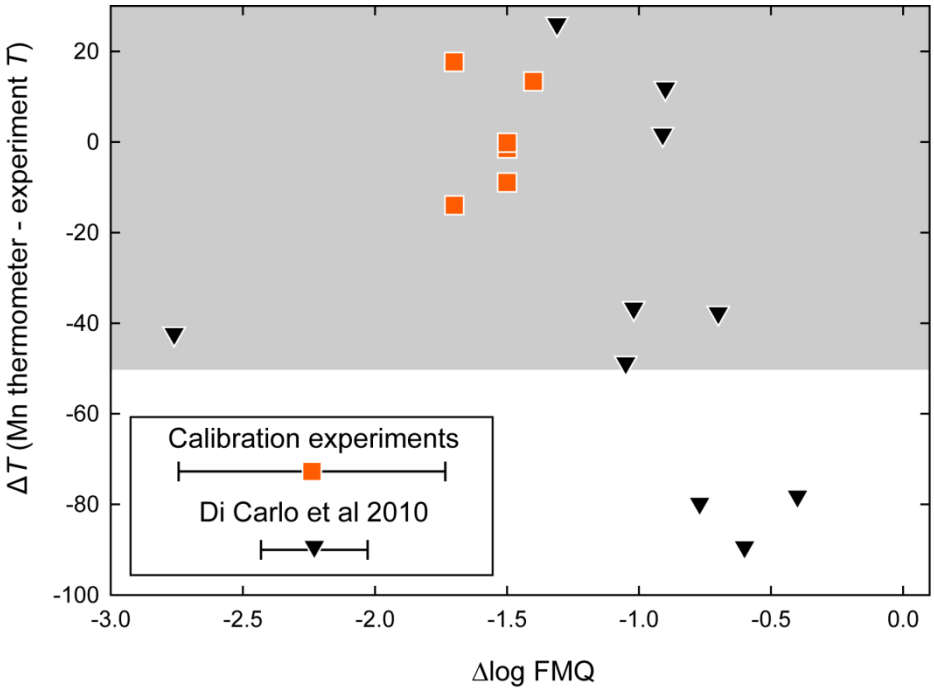

Fig. 10 Comparison of the Mn-Ae/Cpx thermometer with data from experiments on peralkaline rhyolites (Di Carlo et al. 2010). For calibration experiments, fO_2 error estimations are based on upper and lower limits defined by the CCO and COH oxygen buffers. For the experiments on peralkaline rhyolites a typical error given in Di Carlo et al. (2010) is used